Azotobacter vinelandii NITROGENASE : ROLE OF THE MoFe PROTEIN α-SUBUNIT HISTIDINE-195 RESIDUE IN CATALYSIS

by

ChulHwan Kim

Dissertation submitted to the faculty of the
Virginia Polytechnic Institute and State University
in partial fulfillment of the requirements for the degree of

DOCTOR OF PHILOSOPHY

in

Biochemistry and Anaerobic Microbiology

APPROVED:

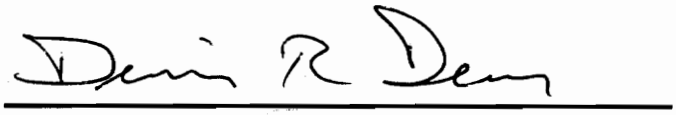

D. R. Dean, Chairman

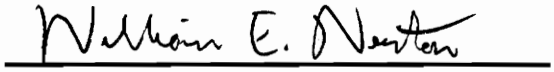

W. E. Newton

J. S. Chen

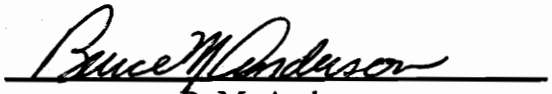

B. M. Anderson

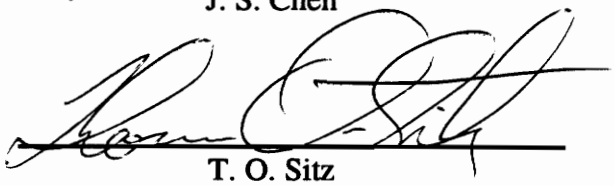

T. O. Sitz

June, 1994

Blacksburg, Virginia

Azotobacter vinelandii NITROGENASE : ROLE OF THE MoFe PROTEIN α-SUBUNIT HISTIDINE-195 RESIDUE IN CATALYSIS

by

ChulHwan Kim

Committee Chairman: Dennis R. Dean
Biochemistry and Anaerobic Microbiology

(ABSTRACT)

Site-directed mutagenesis and gene replacement procedures were used to isolate mutant strains of *Azotobacter vinelandii* that produce altered MoFe proteins where the α-subunit residue-195 position, normally occupied by a histidine residue, was individually substituted by a variety of other amino acids. Structural studies have revealed that this histidine residue is associated with the FeMo-cofactor binding domain and probably provides an NH→S hydrogen bond to a central bridging sulfide located within FeMo-cofactor. The present study investigates the role of the α-histidine-195 residue in nitrogenase catalysis by examining the altered MoFe proteins.

Comparisons of the catalytic and spectroscopic properties of altered MoFe proteins produced by the *A.vinelandii* mutant strains suggest that the α-histidine-195 residue has a structural role which serves to keep the FeMo-cofactor attached to the MoFe protein and to correctly position the FeMo-cofactor within the polypeptide matrix such that N_2 binding is accommodated. Substitution of the α-His-195 residue by a glutamine residue results in an altered MoFe protein that binds but does not reduce N_2, the physiological substrate. Stopped-flow spectroscopic analyses indicate that the α-195^{Gln} MoFe protein is unable to reduce N_2 even though the altered MoFe protein can reach the redox state necessary for N_2

reduction. Although, N_2 is not a substrate for the altered MoFe protein, it is an inhibitor of both acetylene and proton reduction, both of which are otherwise effectively reduced by the altered MoFe protein. This result provides evidence that N_2 inhibits proton and acetylene reduction by simple occupancy of the active site. The α-195^{gln} MoFe protein catalyzes HD formation in the presence of N_2 and D_2. Moreover, N_2 binding at the active site of the altered MoFe protein is inhibited by the addition of D_2. These observations indicate that binding of nitrogen to the enzyme is necessary but its reduction is not required for the formation of HD. N_2 uncouples MgATP from proton reduction catalyzed by the α-195^{gln} MoFe protein, but does so without lowering the overall rate of MgATP hydrolysis. Thus, the quasi-unidirectional flow of electrons from the Fe protein to the MoFe protein that occurs during nitrogenase turnover is controlled, in part, by the substrate serving as an effective electron sink. N_2-induced uncoupling of ATP hydrolysis from substrate reduction by the α-195^{gln} MoFe protein is reversed by the addition of H_2 (D_2) in the assay atmosphere. This observation can successfully be explained if it is assumed that the altered MoFe protein has a much greater binding affinity for H_2 (D_2) than for N_2. Substitution of the α-histidine-195 residue by glutamine also imparts hypersensitivity of acetylene reduction and N_2 binding to inhibition by CO, indicating that the imidazole group of the α-histidine-195 residue might protect an Fe contained within FeMo-cofactor from attack by CO.

ACKNOWLEDGMENTS

I would like to thank my father and my mother for always being with me in spirit during the course of my study. My love and passion toward them would never surpass theirs for me. I would not have accomplished this without my parent's support.

I thank Dr. Dennis Dean for his support and patience with me during my research. His guidance and scientific input were the major ingredients for my success. I am appreciative of Dr. William Newton for his advice and care; numerous discussions with him were a main ingredient for my accomplishment. I am pleased that Dr. Jiann-Shin Chen has been a member of my committee. Thanks to him for providing both academic and personal advice. I thank to Dr. Bruce Anderson and Dr. Thomas Sitz for their support and encourgement. I also thank former members of my committee, Dr. Timothy Larson and Dr. Dennis Bazylinski for their help. Thanks also to my Master's program adviser Dr. Edwin Bunce who encouraged my early interest in science.

I would like to express my special thanks to Mrs. Constance Anderson for editing my dissertation. I would also like to give my special thanks to Dr. Karl Fisher for helping me understand and write on the mechanism of nitrogenase catalysis. Thanks also go to mass spectrometry scientist Mr. Kim Harich for helping me obtain data.

Thanks to my former and present colleagues in Dr. Dean's lab and Dr. Newton's lab for being such good friends; John Peters, Richard Jack, Valerie Cash, Limin Zheng, Marty Jacobson, John Cantwell, Joan Shen, Karl Fisher, Tamaki Kurusu, Krissie Thrasher, Mark Sadler, and Christie Dapper.

Also thanks to my Korean buddies, Cheulho Lee, Younghwan Han, Changkyun Kim,

Sukbin Cha, Yongjoon Lee, Insuk Jang, Minho Cho, Sungho Park, Sangkeon Lee, Raehak Yoo, Seungbum Ahn, Jaeguen Yang, Myungsoo Moon, as well as Dr. Sangbeom Choi for their support.

Finally, I thank my sister Hyunkyung Kim for her love and support. Her delightful letters have been a powerful battery to recharge my energy.

TABLE OF CONTENTS

LIST OF ILLUSTRATIONS

LIST OF TABLES

Introduction

In our universal ecological system, the reduction of dinitrogen to ammonia, a process called nitrogen fixation, is an essential part of the global nitrogen cycle. Although commercial fertilizer manufacturers use the Haber-Bosch chemical process to produce fixed nitrogen, the major N-input into the global system is contributed by many microorganisms that are capable of this process. Many free-living bacteria, or symbiotic ones that are associated with plants, can perform this nitrogen fixation reaction. Studying the biological nitrogen fixation not only permits the understanding of the chemical nature of this reaction but also has practical merit concerning the nutrition and health of the global community. For example, a complete elucidation of the molecular mechanism of this reaction might permit the design of synthetic catalysts, while a genetic approach can create agronomically more efficient nitrogen-fixing organisms.

The nitrogenase enzyme is the catalytic component of biological nitrogen fixation. Among the three genetically distinct nitrogenases recognized so far, only molybdenum-containing nitrogenase is discussed. The enzyme is composed of two component proteins called Fe protein and MoFe protein (reviewed by Dean and Jacobson, 1992). The Fe protein is a homodimer with an M_r of about 60,000 and acts as a specific one-electron reductant of the MoFe protein. The MoFe protein is an $\alpha_2\beta_2$ tetramer with an M_r of about 230,000 and provides the N_2 binding and reduction site. The reaction catalyzed by nitrogenase also requires MgATP as an energy source (McNary and Burris, 1962) and

$$N_2 + 8\ e^- + 8\ H^+ + 16\ MgATP \rightarrow 2\ NH_3 + H_2 + 16\ MgADP + 16\ Pi$$

reduced ferredoxin or flavodoxin as a source of reducing equivalents (Mortenson, 1963; Benemann et al., 1969). Dithionite may serve as an artificial reductant *in vitro* (Burns and Bulen, 1965). In addition to reducing its physiological substrate, nitrogenase can reduce other small molecules. In the absence of the reducible substrates, nitrogenase can reduce protons which are derived from water, to produce hydrogen. During catalysis, electrons are delivered one at a time from the Fe protein to the MoFe protein with a concomitant hydrolysis of at least two MgATP molecules for each electron transfer, followed by dissociation and reassociation of the component proteins. Two different types of prosthetic groups are present in the MoFe protein : P-clusters and FeMo-cofactors. The major functions of these metal centers are believed to be the acceptance, storage, and internal transfer of electrons in the MoFe protein and substrate reduction (Dean et al., 1993). The polypeptide environment surrounding these metal centers might also be important for the individual functions of the metal centers. Direct information regarding the structures of the individual metal centers, as well as their polypeptide environment, is now available from the recent X-ray crystallographic studies of the MoFe protein (Kim and Rees, 1992a,b; Bolin et al., 1993).

Prior to the X-ray crystal structure determination, site-directed mutagenesis studies have been underway to elucidate the functions of particular amino acid residues within the metal center polypeptide environments. A working model (Dean et al., 1990a, b; Dean and Jacobson, 1992; Scott et al., 1992) which assigned the polypeptide regions for the P-cluster and the FeMo-cofactor binding within the MoFe protein has been used for selecting amino acid residues as targets for substitution. A proposed FeMo-cofactor binding domain within the MoFe protein α-subunit including 17 amino acid residues (Av-α-

183CEGFRGVSQSLGHHIAN199, Domain IV) was the author's interest to investigate. Selection of particular amino acid residues as targets for substitution and as choices for substituting amino acid in this polypeptide region has been previously described in detail (Dean et al., 1990a; Scott et al., 1990). Biophysical, spectroscopic and biochemical alterations in the mutant strains and altered MoFe proteins resulting from some amino acid substitutions have also been reported (Newton and Dean, 1993; Scott et al., 1990; Scott et al, 1992; Thomann et al., 1991).

The MoFe protein α-His-195 residue is considered to be important in catalytic properties of the MoFe protein. This proposal came from the suggestion that the MoFe protein residues not duplicated in the corresponding position within the FeMo-cofactor biosynthetic gene product, such as the α-His-195 residue, might have some functional significance for the catalytic properties of the MoFe protein. A substitution which replaced the α-His-195 residue with the corresponding NifE residue, Asn, results in the disturbance in the FeMo-cofactor polypeptide environment and changes in EPR signal and substrate reduction patterns. These observations indicate a potential role of the α-His-195 residue in the structural and/or catalytic properties of the MoFe protein. The structural importance of the α-His-195 residue was also suggested by Thomann et al. (1991) based on their studies of the electron spin echo envelope modulation (ESEEM) analysis. They showed that the α-His-195 residue was required for the N-coordination of the FeMo-cofactor within the MoFe protein either by being directly ligated to FeMo-cofactor or by exerting its effect on N-coordination

elsewhere. Recent model on MoFe protein structure based on X-ray crystallography showed that the α-His-442 residue is the only N-ligand to FeMo-cofactor. However, the

α-His-195 residue, although not a direct ligand to the FeMo–cofactor, is the N-donor of the putative hydrogen bonding to one of the central bridging sulfides of the FeMo-cofactor. Therefore, the α-His-195 residue may have its essential role on N-coordination between the FeMo-cofactor and the MoFe protein via this interaction.

The focus of this thesis research was to further determine the role of the α-His-195 residue on nitrogenase catalysis by examining the mutant strains of *A. vinelandii* which have single amino acid substitutions at the α-195-His position. In this dissertation, major work of the author's research on the nitrogenase MoFe protein was presented in Chapter I and Chapter II, which will be published in separate journals in the near future. A work on the pre-steady state analysis of the MoFe protein was described in Chapter III. Chapter IV and Chapter V represent two separate, already published works in which the author has contributed in connection with side projects or additional research. Literature review section provides the background information necessary for the understanding of the individual chapters. Experimental procedure section includes research methods, which the candidate has developed or made a significant contribution in development, as well as detailed description of the general assay techniques.

Literature review

This review chapter covers information on molybdenum-containing nitrogenase system which is relevant to the author's research. Recent reviews on vanadium-nitrogenase system and a third nitrogenase system can be found elsewhere (Bishop and Premakumar, 1992).

Genetic organizations of *nif* genes

Initial genetic studies on the molybdenum-based nitrogenase system centered mainly on the facultative anaerobe *Klebsiella pneumoniae* (Roberts et al., 1978). All 20 *nif* genes in *K. pneumoniae* were identified and sequenced by many laboratories: *nifJ*, *nifH*, *nifD*, *nifK*, *nifT*, *nifY*, *nifE*, *nifN*, *nifX*, *nifU*, *nifS*, *nifV*, *nifW*, *nifZ*, *nifM*, *nifF*, *nifL*, *nifA*, *nifB*, and *nifQ* (see reference Arnold et al., 1988 for entire sequence). These genes are clustered within a single region of the chromosome and are organized into eight transcriptional units. Comparative analyses of the *nif* genes from *K. pneumoniae* and other diazotrophs, including *A. vinelandii*, *Rhodobacter capsulatus*, *Bradyrhizobium japonicum*, and *Clostridium pasteurianum*, also identified the *nif* gene organization in these organizms (reviewed by Dean and Jacobson, 1992). In *A. vinelandii*, the *nif* genes are clustered into two different linkage groups and organized into 12 transcriptional units. In contrast to *K. pneumoniae*, there are many additional open reading frames in the *A. vinelandii* sequence which may also be under the control of *nif* gene regulation (Dean and Jacobson, 1992; Jacobson et al., 1989). Physical organizations of *nif* genes in *K. pneumoniae* and *A. vinelandii* are shown in Figure 1. The known functions of the *nif* genes are the production

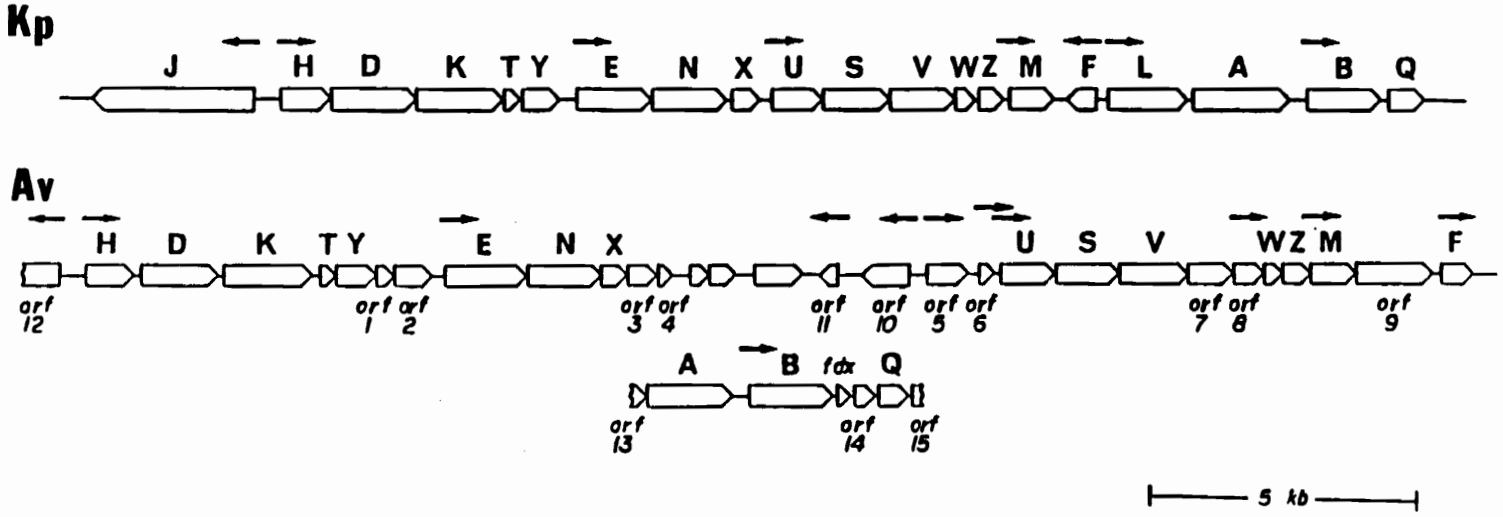

Figure 1. Comparison of the physical organizations of the *nif* genes from *A. vinelandii* with that of *K. pneumoniae*. Arrows indicate the position and direction for known or proposed transcription initiation sites. The numbering of the orfs is arbitrary. For information concerning the development of the *K. pneumoniae* gene map see Arnold et al. (1988) and references cited therein. For information concerning development of the *A. vinelandii* gene map see Jacobson et al. (1989), Bennett et al. (1988), and Joerger and Bishop (1988) and references cited therein (from Dean and Jacobson, 1992).

Table I. Recognized or proposed functions of the *nif* gene products.

Gene	Recognized or proposed functions of *nif* gene products
nifH	Fe protein subunit, FeMo-co biosynthesis
nifD	MoFe protein α-subunit
nifK	MoFe protein β-subunit
nifF	Flavodoxin, Electron transfer to Fe protein
nifJ	Pyruvate-flavodoxin oxidoreductase, Electron transfer to flavodoxin
nifM	Activation of Fe protein
nifU	Stabilization of Fe protein, might provide iron required for nitrogenase metallocluster formation
nifS	Cysteine desulfurase, provides the inorganic sulfide required for nitrogenase metallocluster formation
nifV	Homocitrate synthase, Synthesize the organic component of FeMo-co
nifE	Required for FeMo-co biosynthesis, Forms $\alpha_2\beta_2$ tetramer with the *nifN* gene product
nifN	Required for FeMo-co biosynthesis, Forms $\alpha_2\beta_2$ tetramer with the *nifE* gene product
nifB	Required for FeMo-co biosynthesis
nifQ	Involved in FeMo-co biosynthesis
nifW	Function not known
nifZ	Function not known
nifA	Positive regulatory element
nifL	Negative regulatory element
nifX	probably a negative regulatory element
nifT	Function not known
nifY	Function not known

of the structural nitrogenase component proteins, maturation of the component proteins, metallocluster processing and insertion, electron transport, and regulation. Recognized or proposed functions of the *nif* gene products are summarized in Table I (reviewed by Dean and Jacobson, 1992).

Nitrogenase component proteins and their prosthetic groups

The MoFe protein is a tetramer with an M_r of about 230,000. Sodium dodecyl sulfate-polyacrylamide gel electrophoresis and tryptic peptide analyses showed that the MoFe protein is composed of two non-identical subunits (Kennedy et al., 1976). These subunits were later isolated by ion exchange chromatography and characterized as the α-subunit (M_r = 55,000) and the β-subunit (M_r = 60,000) (Lundell and Howard, 1978; Swisher et al., 1977). The MoFe protein contains 2 molybdenum atoms, 30 iron atoms and 34 non-protein sulfur atoms per molecule. These atoms are organized into two distinct metallocluster types called P-clusters and FeMo-cofactors. Sixteen iron atoms and 16 sulfur atoms constitute two P-clusters and can be extruded from the MoFe protein as [4Fe-4S] clusters by treating the native protein with thiols in a denaturing organic solvent (Kurtz et al., 1979). The remaining iron, sulfur and molybdenum atoms constitute two FeMo-cofactors. The FeMo-cofactors can also be extruded from the native MoFe protein by an acid-base treatment followed by extraction into N-methylformamide (NMF) (Shah and Brill, 1977). The Fe protein is a dimer of two identical subunits with an M_r of about 60,000. The redox active center of the Fe protein is a single [4Fe-4S] cluster which bridges two subunits. The crystallographic structure of the Fe protein and its metal center has been described previously (Georgiadis et al., 1992) and will not be reviewed here.

Aspects of Fe protein study

The Fe protein is a obligate electron donor to the MoFe protein. During catalysis, electrons are delivered one at a time from the Fe protein to the MoFe protein with the concomitant hydrolysis of at least two MgATP molecules per each electron transfer, in a process involving the association and dissociation of the component proteins (reviewed by Dean et al., 1993). Intermolecular electron transfer probably involves the Fe-S centers of the Fe protein (Fe_4S_4 cluster) and the MoFe protein (P-cluster). In order for the electron transfer to occur, the two component proteins are brought together in a specific manner such that the Fe protein Fe_4S_4 cluster is located near the MoFe protein P-cluster. A component protein docking model has been proposed based on site-directed mutagenesis studies, chemical cross linking experiments, and X-ray crystal structures of the nitrogenase component proteins (Howard, 1993; Kim et al., 1992; Kim and Rees, 1992; Lowery et al., 1989; Wolle et al., 1992; Willing et al., 1989). This model demonstrates the ionic interaction between the component proteins for the formation of the functional nitrogenase complex. For example, the Fe protein Arg-100 residue and the MoFe protein Asp-161 residue are believed to be involved in the ionic interaction and the intermolecular electron transfer. This proposal is supported by the observation that certain amino acid substitutions for the Arg-100 or α-Asp-161 residue result in hypersensitivity of nitrogenase activity to salt and/or uncoupling MgATP hydrolysis from electron transfer (Kim et al., 1992; Lowery et al., 1989; Wolle et al., 1992). Another important aspect of the nitrogenase Fe protein study is the role of the MgATP molecule on catalysis. Several biochemical and biophysical features of the Fe protein are altered upon the binding of MgATP: 1) lowered redox potential; 2) more axial EPR spectra; 3) alterations in circular

dichroism spectra; and 4) increased susceptibility of the Fe-S cluster iron molecules to removal by chelation (reviewed by Dean and Jacobson, 1992). These Fe protein features indicate that MgATP binding causes a conformational change and lowers the redox potential of the Fe-S cluster, necessary for the component protein docking and electron transfer process.

In addition to the mechanistic role in the nitrogenase reaction, the Fe protein also has one or more non-catalytic roles. The observation that the NifH- strain produces neither the functional Fe protein nor the FeMo-cofactor but produces a FeMo-cofactor-deficient apo-MoFe protein, suggested the role of the Fe protein in the FeMo-cofactor biosynthesis (Filler et al., 1986; Robinson et al., 1986). It appears that a catalytically competent Fe protein is not required for FeMo-cofactor biosynthesis because a non-catalytic Fe protein with the intact Fe-S cluster remains capable of supporting this role (Gavini and Burgess, 1992). The Fe protein is also thought to be involved in the insertion of the preformed FeMo-cofactor into the apo-MoFe protein (Robinson et al., 1989).

Nitrogenase activity is regulated in some diazotrophic organisms at the posttranslational level by reversible ADP-ribosylation of the Fe protein. This system has been studied primarily in *Rhodospirillum rubrum* (reviewed by Roberts and Ludden, 1992). This regulation occurs by two different enzyme activities: ADP-ribosyltransferase and ADP-ribose glycohydrolase, both purified from *R. rubrum* and characterized (Lowery and Ludden, 1988; Saari et al., 1984). Although the *A. vinelandii* nitrogenase system appears to lack this regulation, the isolated Fe protein from this organism can be ADP-ribosylated *in vitro* by treatment with purified ADP-ribosyltransferase (Lowery and Ludden, 1988). The Arg-100 residue of the Fe protein is the site of the ADP-ribosylation. This residue is

located on the same surface of the Fe protein as the Fe_4S_4 cluster and believed to be involved in the ionic interaction between the Fe protein and the MoFe protein.. Thus, ADP-ribosylation probably regulates the nitrogenase activity by interfering with the component protein interaction.

Electron transfer and MgATP hydrolysis

The electron transfer process for nitrogenase catalysis can be divided into individual steps: 1) the electron transport from pyruvate to the Fe protein's Fe_4S_4 cluster via the *nif*-specific flavodoxin-pyruvate: flavodoxin oxidoreductase system; 2) intermolecular transfer of an electron from the Fe protein Fe_4S_4 cluster to the MoFe protein P-cluster; and 3) intramolecular delivery of electrons within the MoFe protein from the P-cluster to the FeMo-cofactor which provides the substrate reduction site. During the catalysis, the Fe protein binds two MgATP molecules. The two component proteins dock each other in a specific manner such that the Fe_4S_4 cluster of the Fe protein is located in close proximity to the P-cluster of the MoFe protein. An electron is then transferred with concomitant hydrolysis of two MgATP molecules, and the Fe-MoFe protein complex is dissociated. Therefore, at least two MgATP molecules are utilized per each electron transfer. There is, however, many conditions where the electron transfer is uncoupled from MgATP hydrolysis and high ATP/2e$^-$ ratios are observed. For example, the following conditions can result in high ATP/2e$^-$ ratios: 1) conditions of high or low pH (< 6.4 or > 8.5); 2) conditions of high or low temperature ($< 20°C$ or $> 30°C$); 3) low electron flux resulting from a large excess of MoFe protein over Fe protein; 4) hybrid nitrogenase complexes formed from components from different species; 5) certain amino

acid substitutions that alter component protein interaction; 6) *nifV*(-) nitrogenase in the presence of CO; and 7) some alternative substrates such as CN^- and CH_3NC. These phenomena have been explained as manifestations of futile cycling of MgATP hydrolysis where transferred electrons within the MoFe protein are redonated back to the oxidized Fe protein without being utilized for substrate reduction.

FeMo-cofactor is the substrate reduction site

FeMo-cofactor is responsible for the unique S=3/2 EPR signal of the native MoFe protein and is generally believed to be the substrate reduction site. This conclusion is based on the spectroscopic and catalytic properties of the wild type MoFe protein and some aspects of altered MoFe proteins produced by certain mutant strains (reviewed by Newton and Dean, 1993). Mutant strains (*nifE*, *nifN*, or *nifB* mutants) which produce cofactorless MoFe proteins exhibit neither the characteristic S=3/2 EPR signal nor catalytic activity. When the FeMo-cofactor extracted from the native MoFe protein is inserted into the cofactorless apo MoFe protein from each mutant strain, both EPR signal and catalytic activity are restored (Brigle et al., 1987; Nagatani et al., 1974; Paustian et al; 1990; Shah and Brill, 1977). The association of the FeMo-cofactor with both the spectroscopic and catalytic features of the MoFe protein indicated that the FeMo-cofactor is the substrate reduction site. Other compelling evidence has come from the study of NifV- mutants of *K. pneumoniae* (Hawkes et al., 1984; Liang et al., 1990; McLean and Dixon, 1981). The NifV- mutant produces the MoFe protein having homocitrate replaced by citrate. Such altered MoFe protein reduces N_2 at a lower rate and its proton reduction (H_2 evolution) is inhibited by carbon monoxide. FeMo-cofactors extracted from either wild type or NifV-

mutant were incubated with the partially-purified apo MoFe protein from the NifB- mutant in the presence of Fe protein. The reconstituted MoFe proteins (either by wild type FeMo-cofactor or by NifV- FeMo-cofactor) exhibited catalytic properties characteristic of the MoFe protein used as a source of FeMo-cofactor. The paralleled observations of EPR and catalytic properties of the mutant strains with amino acid substitutions in the FeMo-cofactor binding environment also support that FeMo-cofactor is the substrate reduction site (Scott et al., 1990).

Metal centers and their polypeptide environments within the MoFe protein

Recent efforts to elucidate the organization, structure, and biosynthesis of the nitrogenase metalloclusters and to determine their functions, have been the major part of the nitrogen fixation research. A direct approach using the isolated metalloclusters to determine their structure and function was not successful. The reasons for this are: 1) the unusual and complex nature of the clusters; 2) the extreme O_2 lability of the MoFe protein and its metalloclusters; and 3) chemical instability of N-methylformamide used for cluster extraction. However, the analytical and spectroscopic information obtained from such an approach was valuable in developing structural models for the FeMo-cofactor and P-cluster based on X-ray crystallographic analyses of *A. vinelandii* and *C. pasteurianum* MoFe protein.

Interactions of the polypeptide environments with the metalloclusters are important in the respective structure and function of these metalloclusters within the MoFe protein. When the individual metalloclusters are isolated from the native MoFe protein, they have different chemical and spectroscopic features from those of the protein-bound metal

centers. Examples of differences between the isolated and protein-bound metalloclusters include: 1) P-clusters (8 Fe centers within MoFe protein) are extruded in the form of [4Fe-4S] clusters (Kurtz et al., 1979) and 2) FeMo-cofactor extracted from its polypeptide matrix exhibits a broader S=3/2 EPR signal and does not reduce N_2 (Rawlings et al., 1978). The importance of the metallocluster polypeptide environments within the MoFe protein is also indicated by the demonstration that a nitrogenase reconstituted from apo-MoFe protein and the iron-vanadium cofactor exhibited substrate reduction patterns different from either molybdenum-nitrogenase or vanadium-nitrogenase (Smith et al., 1988).

Biochemical-genetic studies have been initiated to gain insight into the contribution of the polypeptide environment to the structure and function of the metalloclusters (Brigle et al., 1987a; Kent et al., 1989; Kent et al., 1990; Scott et al., 1990; Scott et al., 1992). These studies include the site-specific substitutions of amino acid residues targeted as direct ligands to individual metallocluster types or located in the vicinity. Additional studies include biochemical and/or spectroscopic characterizations of the mutant strains or the altered MoFe proteins that arise from such substitutions. The basic rationale of the approach that has been used to provide information concerning the FeMo-cofactor environments is described below.

Nitrogen ligation and cysteinyl mercaptide ligation to FeMo-cofactor were suggested by data obtained from cluster extrusion and spectroscopy. Extrusion of FeMo-cofactor into *N*-methylformamide (NMF) and electron spin echo envelope modulation (ESEEM) experiments on *A. vinelandii* MoFe protein indicated histidine as a possible N-donor ligand to the FeMo-cofactor (Shah and Brill, 1977; Thomann et al., 1987). The reaction of

isolated FeMo-cofactor with a thiol in a 1:1 stoichiometry also indicated that one cysteinyl residue could provide a ligand to the FeMo-cofactor (Burgess et al., 1980).

Deduced amino acid sequences of MoFe protein α-subunit from different microorganisms have been compared in order to look for the conserved cysteine and histidine residues, with the hope that amino acid residues assigned as FeMo-cofactor ligands would be conserved among the species. MoFe protein primary sequences from *A. vinelandii*, *K. pneumoniae*, *Anabaena 7120*, *B. japonicum*, and *C. pasteurianum* are shown in Figure 2. There are five cysteine residues conserved among the α-subunit sequences and three cysteine residues conserved among the β-subunit sequences: α-Cys-62, α-Cys-88, α-Cys-154, α-Cys-183, α-Cys-275 and β-Cys-70, β-Cys-95, β-Cys-153 (the numbering refers to the *A. vinelandii* sequence). Primary sequences of MoFe protein α- and β-subunits were also compared to one another. The three interspecifically conserved Cys residues and their respective regions in the α-subunit show both spatial and amino acid sequence identity when compared to the corresponding regions surrounding the three conserved β-subunit Cys residues (α-Cys-62, α-Cys-88, α-Cys-154 and β-Cys-70, β-Cys-95, β-Cys-153, Fig. 3). These regions which are conserved at both the interspecies and intersubunit levels were assigned as potential P-cluster binding sites based on the suggestion that P-clusters are bound to the α- and β-subunit domains that share sequence identity to each other (Dean and Jacobson, 1992). Regions surrounding the remaining conserved Cys residues (α-Cys-183, α-Cys-275, Fig. 3) were considered to be potential FeMo-cofactor environments. This assignment came from the suggestion that FeMo-cofactor is not physically associated with the P-clusters and their amino acid environments (Hawkes and Smith, 1983; Kurtz et al., 1979; McLean et al., 1987; Paustian et al., 1989;

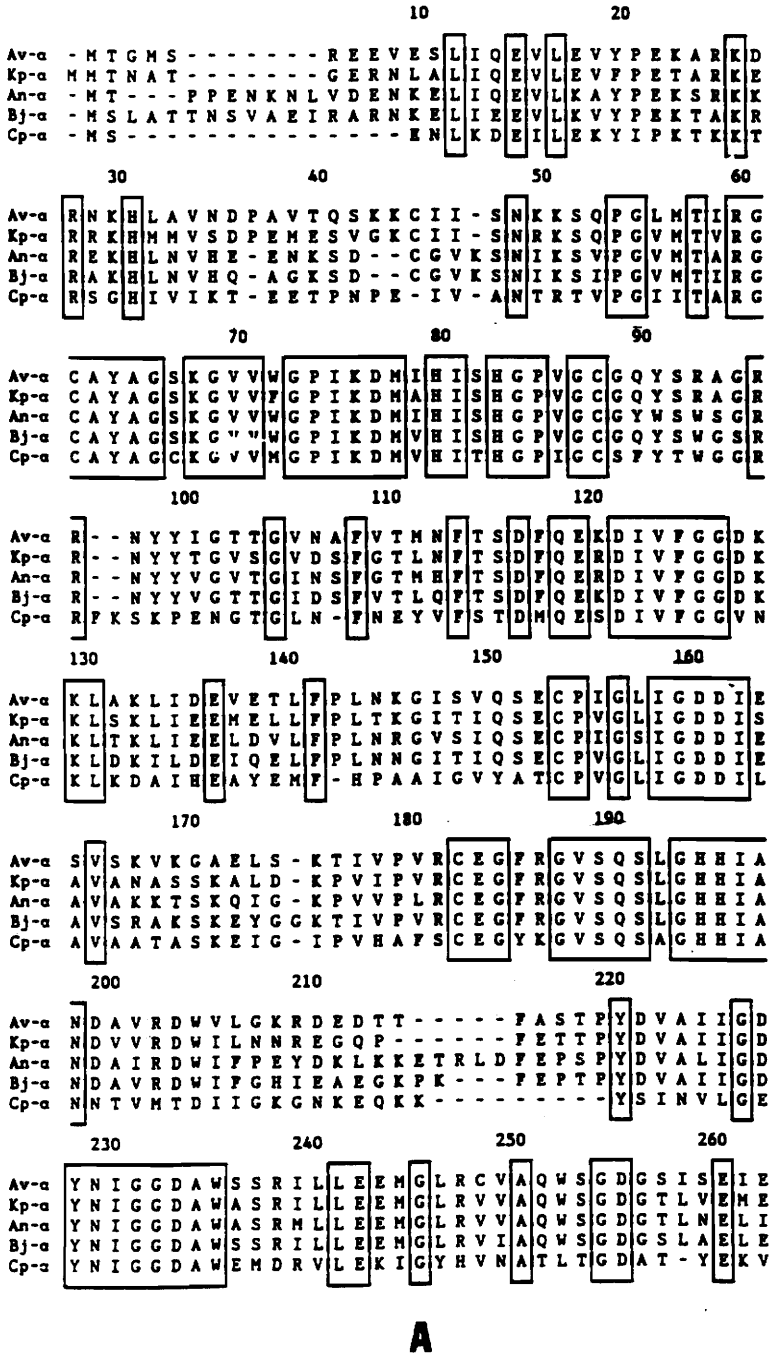

Figure 2. Alignment of MoFe protein primary sequences. (A) MoFe protein α-subunit alignments; (B) MoFe protein β-subunit alignments. Av, *A. vinelandii*; Kp, *K. pneumoniae*; An, *Anabaena* 7120; Bj, *B. japonicum*; Cp, *C. pasteurianum*. numbering is according to the *A. vinelandii* sequence. Residues conserved in all sequences shown are boxed (from Dean and Jacobson, 1992).

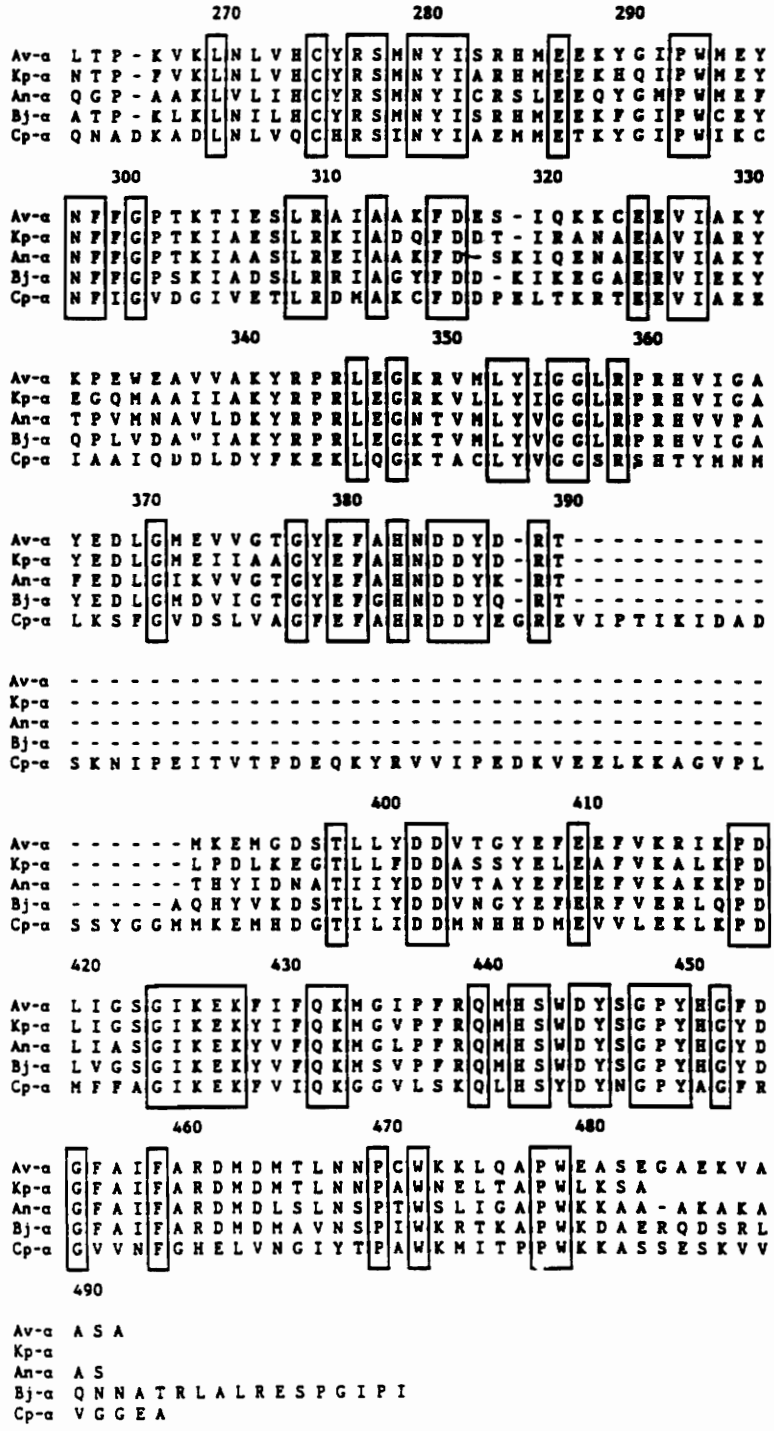
270 280 290
Av-α L T P - K V K L N L V H C Y R S M N Y I S R H M E E K Y G I P W M E Y
Kp-α N T P - F V K L N L V H C Y R S M N Y I A R H M E E K H Q I P W M E Y
An-α Q G P - A A K L V L I H C Y R S M N Y I C R S L E E Q Y G M P W M E F
Bj-α A T P - K L K L N I L H C Y R S M N Y I S R H M E E K F G I P W C E Y
Cp-α Q N A D K A D L N L V Q C H R S I N Y I A E H M E T K Y G I P W I K C
300 310 320 330
Av-α N F F G P T K T I E S L R A I A A K F D E S - I Q K K C E E V I A K Y
Kp-α N F F G P T K I A E S L R K I A D Q F D D T - I R A N A E A V I A R Y
An-α N F F G P T K I A A S L R E I A A K F D - S K I Q E N A E K V I A K Y
Bj-α N F F G P S K I A D S L R R I A G Y F D D - K I K E G A E R V I E K Y
Cp-α N F I G V D G I V E T L R D M A K C F D D P E L T K R T E E V I A E K
340 350 360
Av-α K P E W E A V V A K Y R P R L E G K R V M L Y I G G L R P R H V I G A
Kp-α E G Q M A A I I A K Y R P R L E G R K V L L Y I G G L R P R H V I G A
An-α T P V M N A V L D K Y R P R L E G N T V M L Y V G G L R P R H V V P A
Bj-α Q P L V D A V I A K Y R P R L E G K T V M L Y V G G L R P R H V I G A
Cp-α I A A I Q D D L D Y F K E K L Q G K T A C L Y V G G S R S H T Y M N M
370 380 390
Av-α Y E D L G M E V V G T G Y E F A H N D D Y D - R T - - - - - - - - - -
Kp-α Y E D L G M E I I A A G Y E F A H N D D Y D - R T - - - - - - - - - -
An-α F E D L G I K V V G T G Y E F A H N D D Y K - R T - - - - - - - - - -
Bj-α Y E D L G M D V I G T G Y E F G H N D D Y Q - R T - - - - - - - - - -
Cp-α L K S F G V D S L V A G F E F A H R D D Y E G R E V I P T I K I D A D
Av-α -
Kp-α -
An-α -
Bj-α -
Cp-α S K N I P E I T V T P D E Q K Y R V V I P E D K V E E L K K A G V P L
400 410
Av-α - - - - - - M K E M G D S T L L Y D D V T G Y E F E E F V K R I K P D
Kp-α - - - - - - L P D L K E G T L L F D D A S S Y E L E A F V K A L K P D
An-α - - - - - - T H Y I D N A T I I Y D D V T A Y E F E E F V K A K K P D
Bj-α - - - - - A Q H Y V K D S T L I Y D D V N G Y E F E R F V E R L Q P D
Cp-α S S Y G G M M K E M H D G T I L I D D M N H H D M E V V L E K L K P D
420 430 440 450
Av-α L I G S G I K E K F I F Q K M G I P F R Q M H S W D Y S G P Y H G F D
Kp-α L I G S G I K E K Y I F Q K M G V P F R Q M H S W D Y S G P Y H G Y D
An-α L I A S G I K E K Y V F Q K M G L P F R Q M H S W D Y S G P Y H G Y D
Bj-α L V G S G I K E K Y V F Q K M S V P F R Q M H S W D Y S G P Y H G Y D
Cp-α M F F A G I K E K F V I Q K G G V L S K Q L H S Y D Y N G P Y A G F R
460 470 480
Av-α G F A I F A R D M D M T L N N P C W K K L Q A P W E A S E G A E K V A
Kp-α G F A I F A R D M D M T L N N P A W N E L T A P W L K S A
An-α G F A I F A R D M D L S L N S P T W S L I G A P W K K A A - A K A K A
Bj-α G F A I F A R D M D M A V N S P I W K R T K A P W K D A E R Q D S R L
Cp-α G V V N F G H E L V N G I Y T P A W K M I T P P W K K A S S E S K V V
490
Av-α A S A
Kp-α
An-α A S
Bj-α Q N N A T R L A L R E S P G I P I
Cp-α V G G E A

A

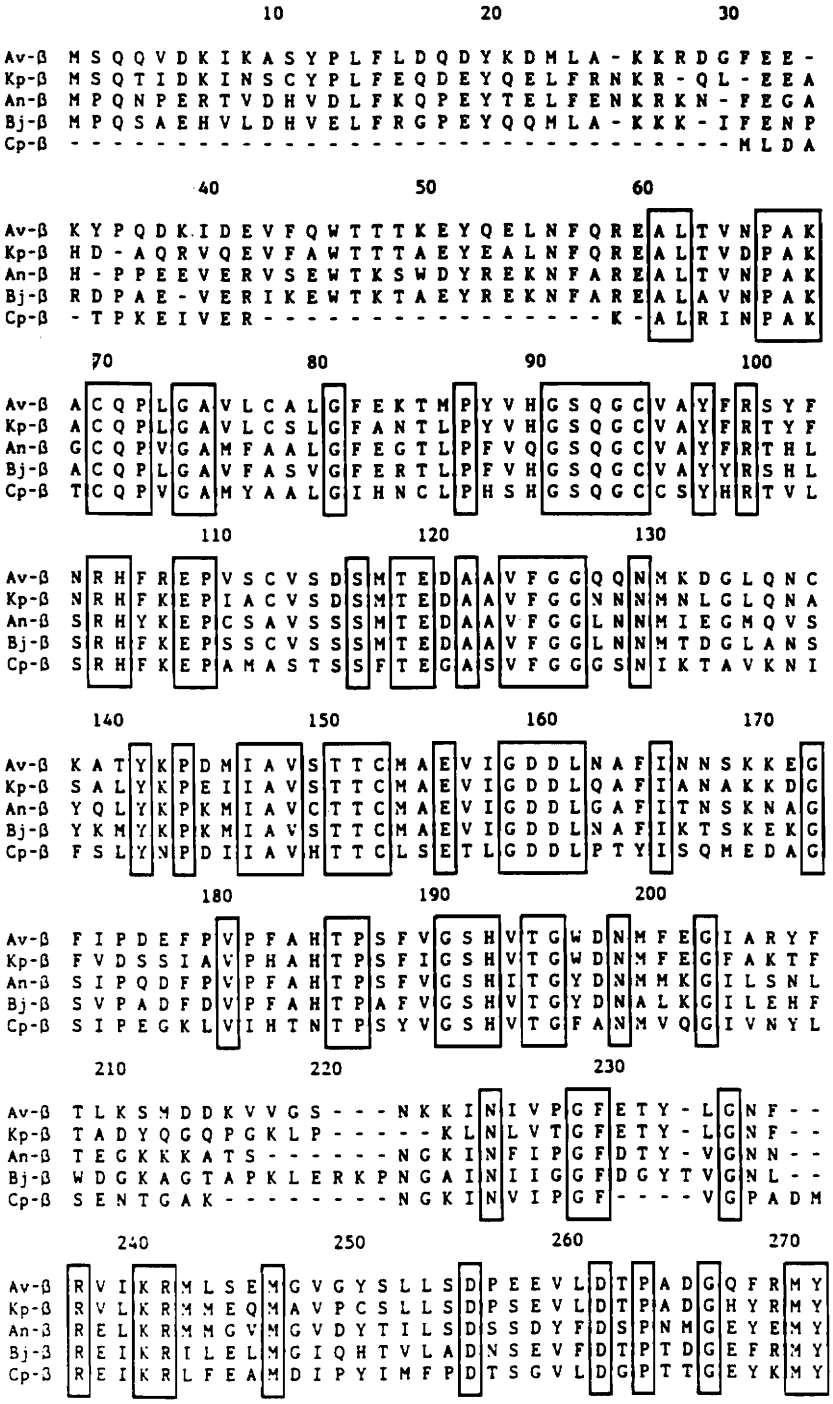
10 20 30
Av-β M S Q Q V D K I K A S Y P L F L D Q D Y K D M L A - K K R D G F E E -
Kp-β M S Q T I D K I N S C Y P L F E Q D E Y Q E L F R N K R - Q L - E E A
An-β M P Q N P E R T V D H V D L F K Q P E Y T E L F E N K R K N - F E G A
Bj-β M P Q S A E H V L D H V E L F R G P E Y Q Q M L A - K K K - I F E N P
Cp-β - M L D A
40 50 60
Av-β K Y P Q D K I D E V F Q W T T T K E Y Q E L N F Q R E A L T V N P A K
Kp-β H D - A Q R V Q E V F A W T T T A E Y E A L N F Q R E A L T V D P A K
An-β H - P P E E V E R V S E W T K S W D Y R E K N F A R E A L T V N P A K
Bj-β R D P A E - V E R I K E W T K T A E Y R E K N F A R E A L A V N P A K
Cp-β - T P K E I V E R - - - - - - - - - - - - - - - - K - A L R I N P A K
70 80 90 100
Av-β A C Q P L G A V L C A L G F E K T M P Y V H G S Q G C V A Y F R S Y F
Kp-β A C Q P L G A V L C S L G F A N T L P Y V H G S Q G C V A Y F R T Y F
An-β G C Q P V G A M F A A L G F E G T L P F V Q G S Q G C V A Y F R T H L
Bj-β A C Q P L G A V F A S V G F E R T L P F V H G S Q G C V A Y Y R S H L
Cp-β T C Q P V G A M Y A A L G I H N C L P H S H G S Q G C C S Y H R T V L
110 120 130
Av-β N R H F R E P V S C V S D S M T E D A A V F G G Q Q N M K D G L Q N C
Kp-β N R H F K E P I A C V S D S M T E D A A V F G G N N N M N L G L Q N A
An-β S R H Y K E P C S A V S S S M T E D A A V F G G L N N M I E G M Q V S
Bj-β S R H F K E P S S C V S S S M T E D A A V F G G L N N M T D G L A N S
Cp-β S R H F K E P A M A S T S S F T E G A S V F G G G S N I K T A V K N I
140 150 160 170
Av-β K A T Y K P D M I A V S T T C M A E V I G D D L N A F I N N S K K E G
Kp-β S A L Y K P E I I A V S T T C M A E V I G D D L Q A F I A N A K K D G
An-β Y Q L Y K P K M I A V C T T C M A E V I G D D L G A F I T N S K N A G
Bj-β Y K M Y K P K M I A V S T T C M A E V I G D D L N A F I K T S K E K G
Cp-β F S L Y N P D I I A V H T T C L S E T L G D D L P T Y I S Q M E D A G
180 190 200
Av-β F I P D E F P V P F A H T P S F V G S H V T G W D N M F E G I A R Y F
Kp-β F V D S S I A V P H A H T P S F I G S H V T G W D N M F E G F A K T F
An-β S I P Q D F P V P F A H T P S F V G S H I T G Y D N M M K G I L S N L
Bj-β S V P A D F D V P F A H T P A F V G S H V T G Y D N A L K G I L E H F
Cp-β S I P E G K L V I H T N T P S Y V G S H V T G F A N M V Q G I V N Y L
210 220 230
Av-β T L K S M D D K V V G S - - - N K K I N I V P G F E T Y - L G N F - -
Kp-β T A D Y Q G Q P G K L P - - - - - K L N L V T G F E T Y - L G N F - -
An-β T E G K K K A T S - - - - - - N G K I N F I P G F D T Y - V G N N - -
Bj-β W D G K A G T A P K L E R K P N G A I N I I G G F D G Y T V G N L - -
Cp-β S E N T G A K - - - - - - - - N G K I N V I P G F - - - - V G P A D M
240 250 260 270
Av-β R V I K R M L S E M G V G Y S L L S D P E E V L D T P A D G Q F R M Y
Kp-β R V L K R M M E Q M A V P C S L L S D P S E V L D T P A D G H Y R M Y
An-β R E L K R M M G V M G V D Y T I L S D S S D Y F D S P N M G E Y E M Y
Bj-β R E I K R I L E L M G I Q H T V L A D N S E V F D T P T D G E F R M Y
Cp-β R E I K R L F E A M D I P Y I M F P D T S G V L D G P T T G E Y K M Y

B

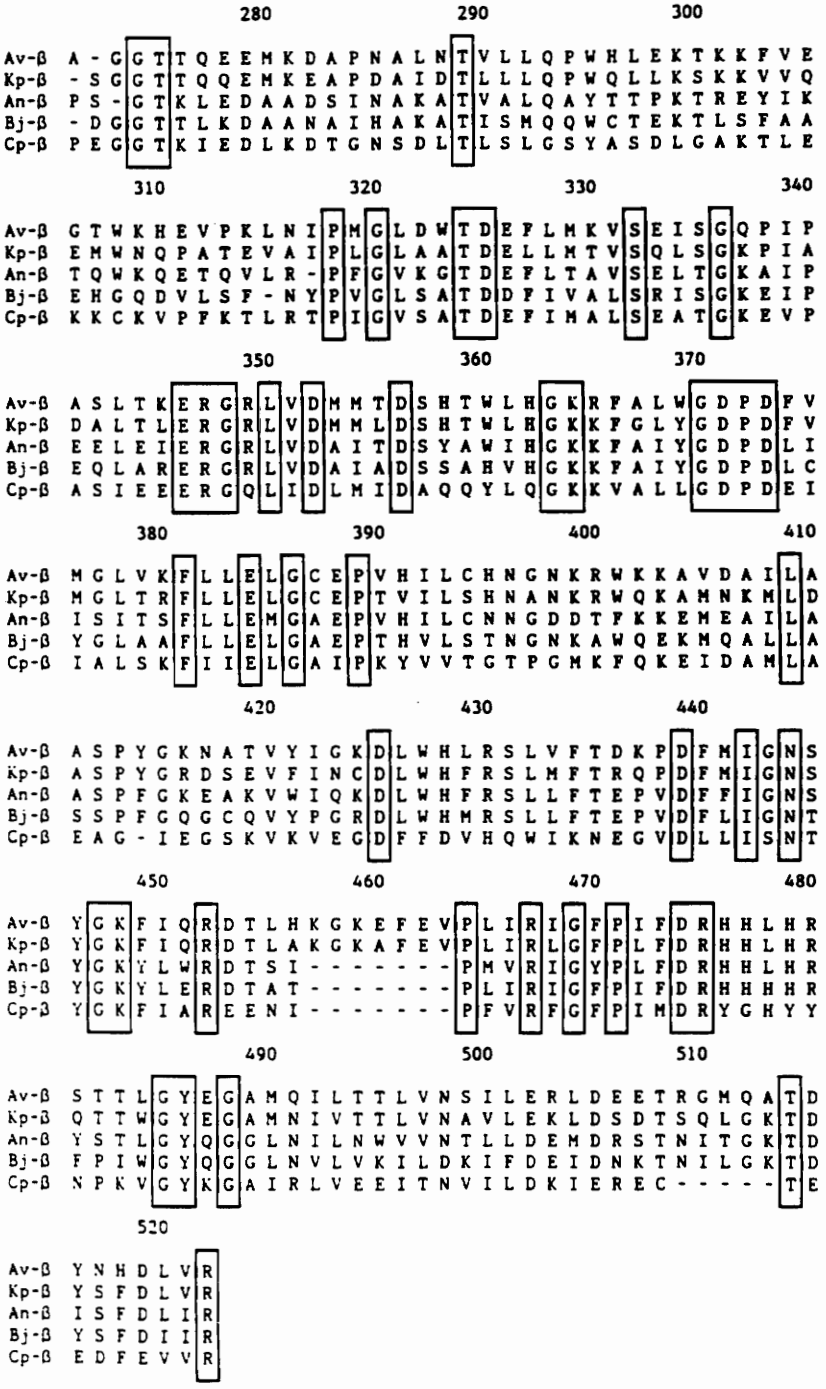
280 290 300
Av-β A - G G T T Q E E M K D A P N A L N T V L L Q P W H L E K T K K F V E
Kp-β - S G G T T Q Q E M K E A P D A I D T L L L Q P W Q L L K S K K V V Q
An-β P S - G T K L E D A A D S I N A K A T V A L Q A Y T T P K T R E Y I K
Bj-β - D G G T T L K D A A N A I H A K A T I S M Q Q W C T E K T L S F A A
Cp-β P E G G T K I E D L K D T G N S D L T L S L G S Y A S D L G A K T L E
310 320 330 340
Av-β G T W K H E V P K L N I P M G L D W T D E F L M K V S E I S G Q P I P
Kp-β E M W N Q P A T E V A I P L G L A A T D E L L M T V S Q L S G K P I A
An-β T Q W K Q E T Q V L R - P F G V K G T D E F L T A V S E L T G K A I P
Bj-β E H G Q D V L S F - N Y P V G L S A T D D F I V A L S R I S G K E I P
Cp-β K K C K V P F K T L R T P I G V S A T D E F I M A L S E A T G K E V P
350 360 370
Av-β A S L T K E R G R L V D M M T D S H T W L H G K R F A L W G D P D F V
Kp-β D A L T L E R G R L V D M M L D S H T W L H G K K F G L Y G D P D F V
An-β E E L E I E R G R L V D A I T D S Y A W I H G K K F A I Y G D P D L I
Bj-β E Q L A R E R G R L V D A I A D S S A H V H G K K F A I Y G D P D L C
Cp-β A S I E E E R G Q L I D L M I D A Q Q Y L Q G K K V A L L G D P D E I
380 390 400 410
Av-β M G L V K F L L E L G C E P V H I L C H N G N K R W K K A V D A I L A
Kp-β M G L T R F L L E L G C E P T V I L S H N A N K R W Q K A M N K M L D
An-β I S I T S F L L E M G A E P V H I L C N N G D D T F K K E M E A I L A
Bj-β Y G L A A F L L E L G A E P T H V L S T N G N K A W Q E K M Q A L L A
Cp-β I A L S K F I I E L G A I P K Y V V T G T P G M K F Q K E I D A M L A
420 430 440
Av-β A S P Y G K N A T V Y I G K D L W H L R S L V F T D K P D F M I G N S
Kp-β A S P Y G R D S E V F I N C D L W H F R S L M F T R Q P D F M I G N S
An-β A S P F G K E A K V W I Q K D L W H F R S L L F T E P V D F F I G N S
Bj-β S S P F G Q G C Q V Y P G R D L W H M R S L L F T E P V D F L I G N T
Cp-β E A G - I E G S K V K V E G D F F D V H Q W I K N E G V D L L I S N T
450 460 470 480
Av-β Y G K F I Q R D T L H K G K E F E V P L I R I G F P I F D R H H L H R
Kp-β Y G K F I Q R D T L A K G K A F E V P L I R L G F P L F D R H H L H R
An-β Y G K Y L W R D T S I - - - - - - - P M V R I G Y P L F D R H H L H R
Bj-β Y G K Y L E R D T A T - - - - - - - P L I R I G F P I F D R H H H H R
Cp-β Y G K F I A R E E N I - - - - - - - P F V R F G F P I M D R Y G H Y Y
490 500 510
Av-β S T T L G Y E G A M Q I L T T L V N S I L E R L D E E T R G M Q A T D
Kp-β Q T T W G Y E G A M N I V T T L V N A V L E K L D S D T S Q L G K T D
An-β Y S T L G Y Q G G L N I L N W V V N T L L D E M D R S T N I T G K T D
Bj-β F P I W G Y Q G G L N V L V K I L D K I F D E I D N K T N I L G K T D
Cp-β N P K V G Y K G A I R L V E E I T N V I L D K I E R E C - - - - - T E
520
Av-β Y N H D L V R
Kp-β Y S F D L V R
An-β I S F D L I R
Bj-β Y S F D I I R
Cp-β E D F E V V R

B

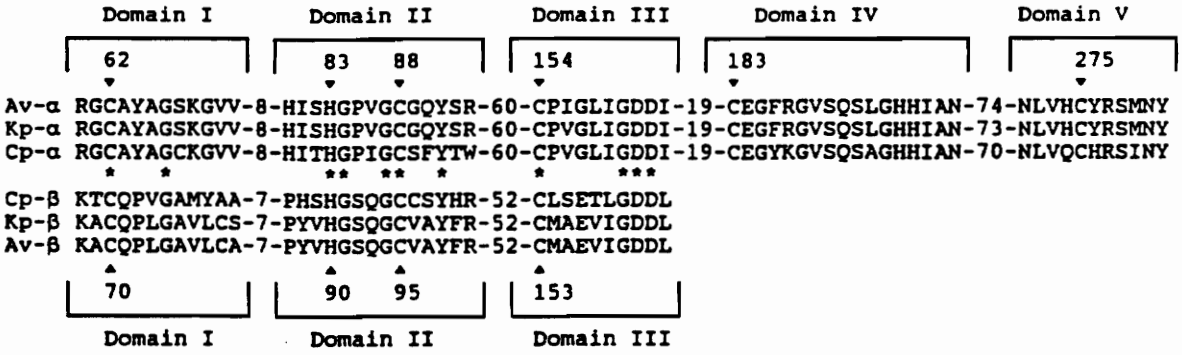

Figure 3. Alignment of interspecifically conserved Cys residues from the MoFe protein α- and β-subunits from *A. vinelandii*, *K. pneumoniae* and *C. pasteurianum*. Numbers refer to the *A. vinelandii* sequence. Residues which are conserved in both subunits are indicated by asterisks. Domain I, II and III are targeted as potential P-cluster environments and Domain IV and V are targeted as FeMo-cofactor environments (from Dean and Jacobson, 1992).

Shah and Brill, 1977; Smith and Lang, 1974). This working model (Fig. 3) has been described previously (Dean & Jacobson, 1992; Dean, et al., 1990a, b; Scott et al., 1992).

Important aspects concerning the possibility that the α-Cys-275 residue provides a thiol ligand to the FeMo-cofactor were reported previously (Dean et al., 1990a; Kent et al., 1989; Kent et al., 1990; Smith et al., 1988). Significant differences were observed in residues that immediately flank the α-Cys-275 residue when the *A. vinelandii* and *C. pasteurianum* primary sequences within the α-Cys-275 domain were compared. The *A. vinelandii* sequence within this region, His-Cys-Tyr, is replaced by the sequence, Gln-Cys-His, in *C. pasteurianum.* Substitution of this portion of the *C. pasteurianum* sequence for the corresponding *A. vinelandii* sequence resulted in a significant change in the EPR spectrum of the MoFe protein from the mutant strain. This spectral change might arise from different constraints placed on the FeMo-cofactor and suggest that the Cys-275 residue is a thiol ligand. Other evidence was provided by experiments on the α-Ala-275 mutant strain of *K. pneumoniae*. An increase in the amount of FeMo-cofactor in crude extracts of the mutant strain was observed by an FeMo-cofactor reconstitution experiment and EPR spectroscopy. These results indicated that the FeMo-cofactor is loosely bound to the altered MoFe protein because of the absence of the potential thiol ligand (α-Cys-275).

The region surrounding the α-Cys-183 residue contains conserved amino acid residues that may function as N-donor ligands. The study on the potential role for this region in FeMo-cofactor binding involved the comparison of amino acid sequences of the NifE product with those of MoFe protein α-subunit, and the NifN product with the β-subunit (Brigle et al., 1987b). The FeMo-cofactor biosynthetic gene products, NifE and NifN, form a tetrameric complex similar to the MoFe protein. According to the previous studies

(Brigle et al., 1987b; Paustian et al., 1989), the FeMo-cofactor binding environment within the MoFe protein and the NifEN complex must be different because: 1) the FeMo-cofactor is synthesized on the NifEN complex rather than on the MoFe protein; 2) the FeMo-cofactor is not catalytic within NifEN and must escape from NifEN after its synthesis; and 3) the FeMo-cofactor is inserted into the MoFe protein permanently and results in its activity. There seems to be more structural rather than functional homology between the NifEN complex and MoFe protein considering that the NifEN complex provides a scaffold for the synthesis of FeMo-cofactor but does not have catalytic activity. However, there must be also a significant structural dissimilarity between the two complexes because FeMo-cofactor is naturally released from the NifEN complex but not from the MoFe protein. Therefore, the residues that are found within the MoFe protein FeMo-cofactor binding regions but not at the corresponding regions within the NifEN complex might have some functional and/or structural significance for MoFe protein's catalytic properties. Primary sequence comparison of the FeMo-cofactor environments within the MoFe protein α-subunit and NifE product show the conservation in amino acid sequence and the folding pattern (Fig. 4). For example, three glycine residues are conserved within the FeMo-cofactor binding regions of both proteins. There are certain residues that are found within the α-subunit FeMo-cofactor binding region but not found at the corresponding region within the NifE protein (e.g., the Cys-183, Gln-191, His-195, and His-196 residues). Substituting these residues within the MoFe protein sequence by the corresponding residues from the NifE product can alter the functional properties of the FeMo-cofactor binding environment without severely changing the global protein structure. The altered biochemical effects resulting from such substitutions are described below.

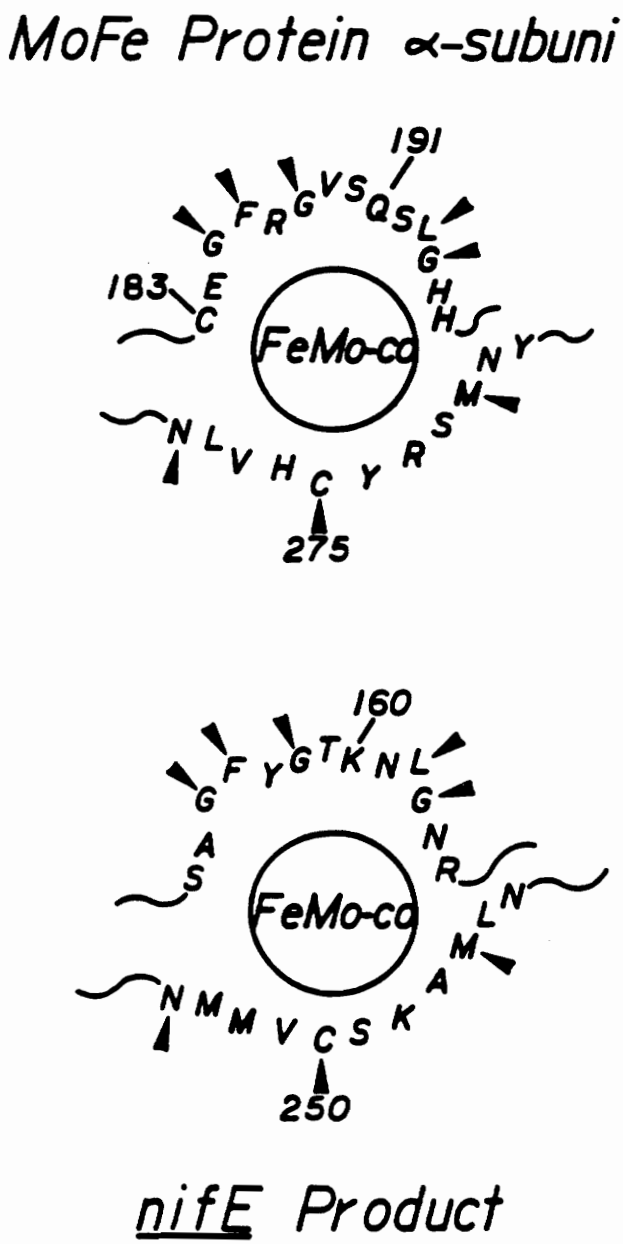

Figure 4. Schematic representation of residues conserved within FeMo-cofactor binding environment of the MoFe protein α-subunit and the corresponding region of the *nifE* product. Arrowheads indicate residues conserved within both the MoFe protein α-subunit and the *nifE* product (from Dean and Jacobson, 1992).

Effects of some amino acid substitutions within the FeMo-cofactor environment

Altered MoFe proteins with single amino acid substitutions within the targeted FeMo-cofactor binding regions have been characterized in order to understand the role of the FeMo-cofactor polypeptide environment (reviewed by Newton and Dean, 1993). Two mutant strains having substitutions either at the α-Gln-191 or α-His-195 residue with corresponding residues from the NifE product, were described previously (Scott et al., 1990; Scott et al., 1992). These mutant strains DJ255 (α-191^{lys}) and DJ178 (α-195^{asn}) are unable to grow diazotropically. EPR spectra from whole cells of both mutant strains are changed in both the g-value and the line shape when compared with the wild type EPR signal. These indicate that the region including the α-Gln-191 and α-His-195 residue is important in FeMo-cofactor binding, and that the FeMo-cofactor-binding environment is perturbed by substituting these residues.

Crude extracts from DJ255 can not reduce N_2 but can reduce acetylene (C_2H_2) to ethylene (C_2H_4) at a lower rate (≈10% of wild type). The altered nitrogenase in crude extracts, in an atmosphere of 10% C_2H_2, is also capable of reducing C_2H_2 to ethane (C_2H_6), a four-electron product which is not produced by the wild type nitrogenase. The reduction of C_2H_2 to C_2H_6 is also a property of the V-dependent nitrogenase and is used for the identification of this alternative nitrogenase (Dilworth et al., 1987). However, the possibility that C_2H_6 production by the α-191^{lys} MoFe protein from DJ255 resulted from the catalysis of V-dependent nitrogenase, was eliminated by spectroscopic, electrophoretic and catalytic evidence (Scott et al., 1990). Further experiments indicated that C_2H_6 formation from C_2H_2 catalyzed by the α-191^{lys} MoFe protein occurred by a different

mechanism than that of the vanadium-dependent system (Scott et al., 1992). Proton reduction catalyzed by the α-191^{lys} MoFe protein is inhibited by the presence of carbon monoxide (CO), with 10% CO inhibiting the proton reduction by ≈65% under Ar, N_2 or 10% C_2H_2. It is also important to note that total electron flux through the altered MoFe protein decreases under CO, which is the result of the decrease in overall product formation. CO-sensitive proton reduction and decrease in total electron flux under CO are not properties of the wild type nitrogenase but are exhibited by the *nifV*(-) nitrogenase (McLean, 1983). The NifV- nitrogenase, whose FeMo-cofactor structure is modified by containing citrate rather than homocitrate as its organic constituent, when compared to the wild type, reduces C_2H_2 and protons comparably but reduces nitrogen at a much lower rate compared to the wild type. The similar catalytic properties exhibited by the altered nitrogenases from DJ255 (α-191^{lys}) and NifV- mutant raised the possibility that changes in the FeMo-cofactor polypeptide environment might also have caused some alterations in its molecular structure or composition. However, biochemical reconstitution experiments using FeMo-cofactors extracted from the wild type and α-191^{lys} MoFe proteins showed that the catalytic and spectroscopic properties exhibited by the altered MoFe protein arose from alterations in the polypeptide environment not from the FeMo-cofactor itself (Scott et al.,1992). Recent X-ray crystallography data revealed that the α-Gln-191 residue interacts with a carboxyl group of homocitrate, which is then coordinated to the Mo atom of the FeMo-cofactor through the hydroxyl and carboxyl oxygens (Kim and Rees, 1992b). Thus, it appears that the similar effects observed in NifV- and α-191^{lys} MoFe proteins result from the different constraints induced upon the FeMo-cofactor via homocitrate.

The α-195^{asn} MoFe protein from DJ178 can reduce protons and C_2H_2 at moderate rates

but can not reduce N_2. The C_2H_2 reduction catalyzed by this altered MoFe protein also produce C_2H_6 in even larger quantities (35% of total electron flux) than that of the α-191^{lys} MoFe protein. Another interesting feature of the α-195^{asn} MoFe protein comes from spectroscopic studies. Electron spin echo envelope modulation (ESEEM) spectroscopy is used to analyze the N-coordination of the FeMo-cofactor within the MoFe protein. The whole-cell ESEEM spectra of variuos mutant strains of *A. vinelandii* (including the α-Asn-195 mutant), which have single amino acid substitutions in many conserved histidine residues, show that only α-195^{asn} MoFe protein does not exhibit the ESEEM signal characteristic of N-coordination. These data indicated that the α-His-195 residue is required for the N-coordination of the FeMo-cofactor within the MoFe protein. The recently reported X-ray crystallography results, however, show that α-His-442 residue is the only direct N-ligand to FeMo-cofactor. The α-His-195 residue, although not a direct ligand to the FeMo-cofactor, appears to be the N-donor of the hydrogen bonding to one of the central bridging sulfides of the FeMo-cofactor.

Structural models of the MoFe protein and its metal centers

Mössbauer spectroscopy combined with analytical and cluster extrusion experiments introduced the initial P-cluster model (Lowe et al., 1985; Kurtz et al., 1979). In this model, one [4Fe-4S]-type cluster is distributed in each subunit of the MoFe protein, constituting 4 P-clusters per MoFe protein tetramer. This hypothesis was challenged when EPR studies of thionine-oxidized MoFe protein and Mössbauer studies using ^{57}Fe-enriched MoFe protein, indicated that P-clusters might be present within the MoFe protein in the form of two 8 Fe centers (Hagen et al., 1987; McLean et al., 1987). X-ray anomalous

scattering data conclusively supported the idea that the P-clusters are organized into two pairs of slightly inequivalent clusters (Bolin et al., 1990).

An endogenous organic component of the FeMo-cofactor was recognized by the combined genetic and biochemical studies on NifV- strains of *K. pneumoniae* (Hawkes et al., 1984; McLean and Dixon, 1981; McLean et al., 1983). FeMo-cofactor isolated from the purified NifV- MoFe protein was inserted into the cofactorless MoFe protein synthesized by NifB- strains. The resulting reconstituted holo MoFe protein exhibited a NifV- phenotype indicating that the structural change of the NifV- FeMo-cofactor was responsible for its phenotype. In 1989, Hoover et al. synthesized the FeMo-cofactor *in vitro* in the presence of ^{3}H-labeled homocitrate and discovered that the label was incorporated into the synthesized FeMo-cofactor. Analytical and spectroscopic experiments from the FeMo-cofactor showed that homocitrate was the organic moiety of the cofactor existing at a stoichiometric ratio of 1 Mo:1 homocitrate. It was also discovered that citrate replaced homocitrate in the NifV- MoFe protein.

The proposed metal compositions of the individual metalloclusters were consistent with the overall metal composition of the MoFe protein, considering that two copies each of the FeMo-co and P-clusters are present within the MoFe protein. A recent structural model of the MoFe protein from *A. vinelandii* and *C. pasteurianum* provides information concerning the structure and organization of the metalloclusters (Kim and Rees, 1992a; Kim and Rees, 1992b; Chan et al., 1993; Bolin et al., 1993; Kim et al., 1993). Each P-cluster contains two [4Fe-4S] clusters linked by two protein cysteinyl ligands (α-Cys-88, β-Cys-95) (Fig. 5). The four remaining Fe atoms on the edge of the cluster are coordinated by four cysteine residues (α-Cys-62, α-Cys-154, β-Cys-70 and β-Cys-153) from the α- and β-subunits.

A

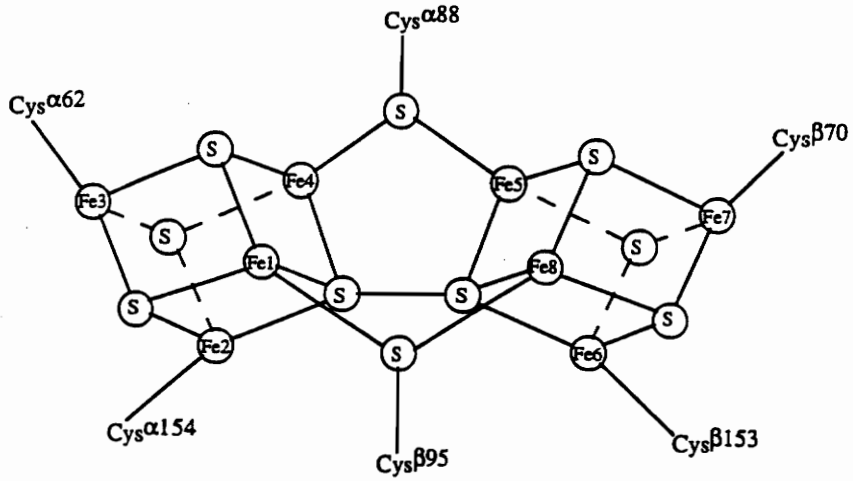

B

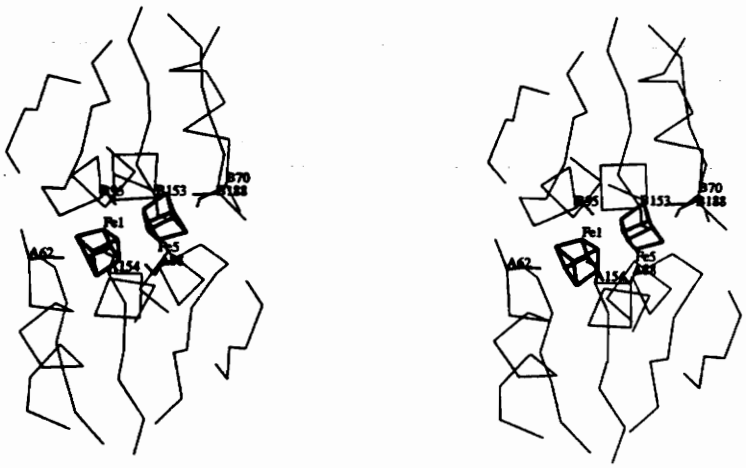

Figure 5. (A) Schematic representation of the P-cluster model. (B) Stereoview of the P-cluster and surrounding amino acid residues (from Kim and Rees, 1992b).

The β-Ser-188 residue was suggested to also coordinate one Fe atom (Fe6) along with the β-Cys-153 residue. The higher resolution analysis showed that the two [4Fe-4S] clusters are further joined by a disulfide bond between S atoms in each cluster. The FeMo-cofactor contains [4Fe-3S] and [1Mo-3Fe-3S] clusters linked by three non-protein ligands (Fig. 6). Two of the bridging ligands are sulfur while the identity of the third ligand is not clear, although it also appears to be sulfur. Molybdenum is coordinated by 2-hydroxyl and 2-carboxyl groups of homocitrate, the organic constituent of the cofactor. Protein ligation to the FeMo-cofactor is contributed by the α-Cys-275 residue to Fe1 and the α-His-442 residue to molybdenum. Two other residues, α-His-195 and α-Gln-191, are also involved in the binding of the FeMo-cofactor to the polypeptide matrix, although the residues are not directly ligated. The α-His-195 residue appears to be the N-donor of the hydrogen bonding to one of the central bridging sulfides of the FeMo-cofactor, whereas the side chain of the α-Gln-191 residue interacts with one of the carboxyl groups of the homocitrate through a hydrogen bond.

The structure of the MoFe protein has also been determined from X-ray crystallographic studies (Kim and Rees, 1992a, 1994; Kim et al., 1993) and is briefly described below. The α- and β-subunits of the MoFe protein consist of three domains (I, II, III of α-subunit and I′, II′, III′ of β-subunit), each of which is composed of several α-helices and β-sheets (Fig. 7). The overall protein folding patterns of the α- and β-subunits are similar to each other. The FeMo-cofactor resides in a cleft between the three domains in the α-subunit. The α- and β-subunits are engaged with each other by a two-fold rotation axis which passes through the P-cluster pair located in the center of the dimer. The P-cluster pair bridges Domain I of the α-subunit and Domain I′ of the β-subunit via cysteinyl mercaptide

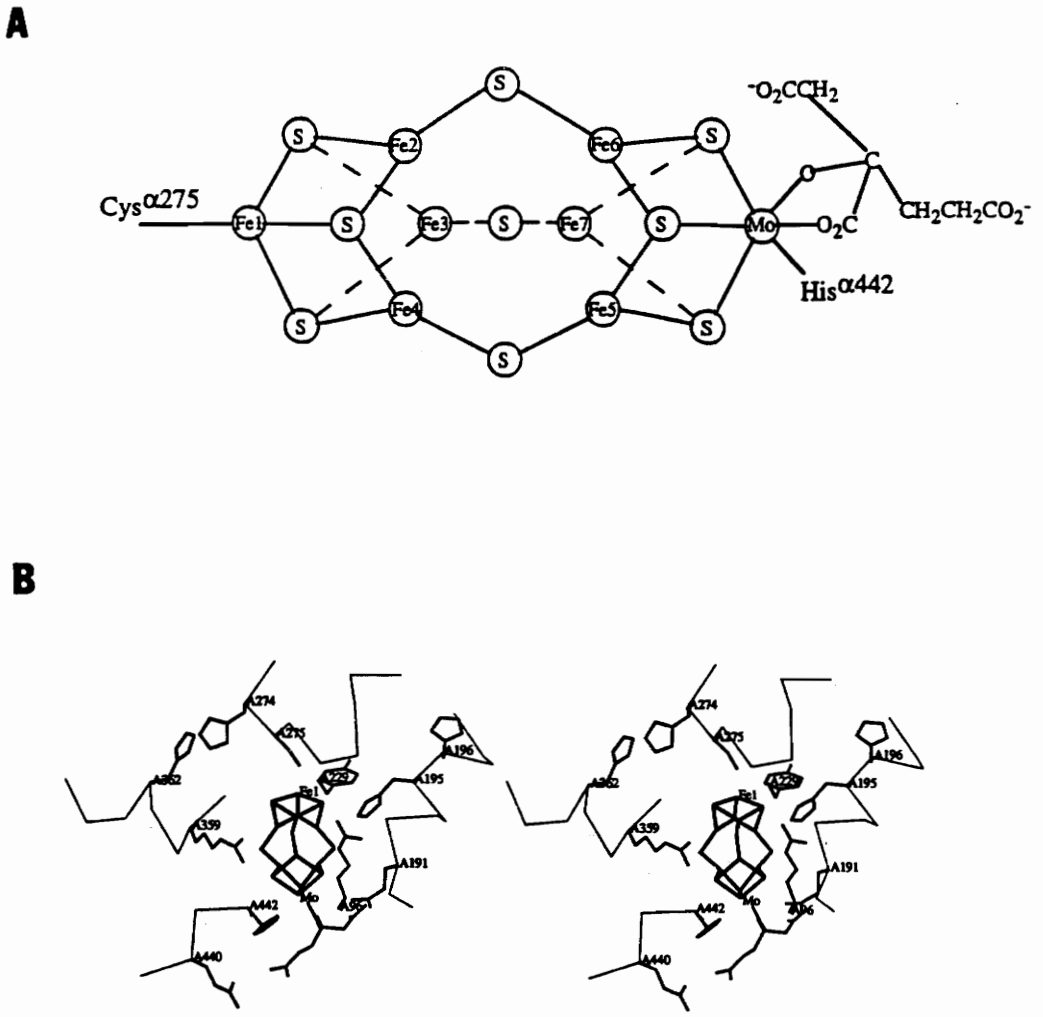

Figure 6. (A) Schematic representation of the FeMo-cofactor model. (B) Stereoview of the FeMo-cofactor and surrounding amino acid residues (from Kim and Rees, 1992b).

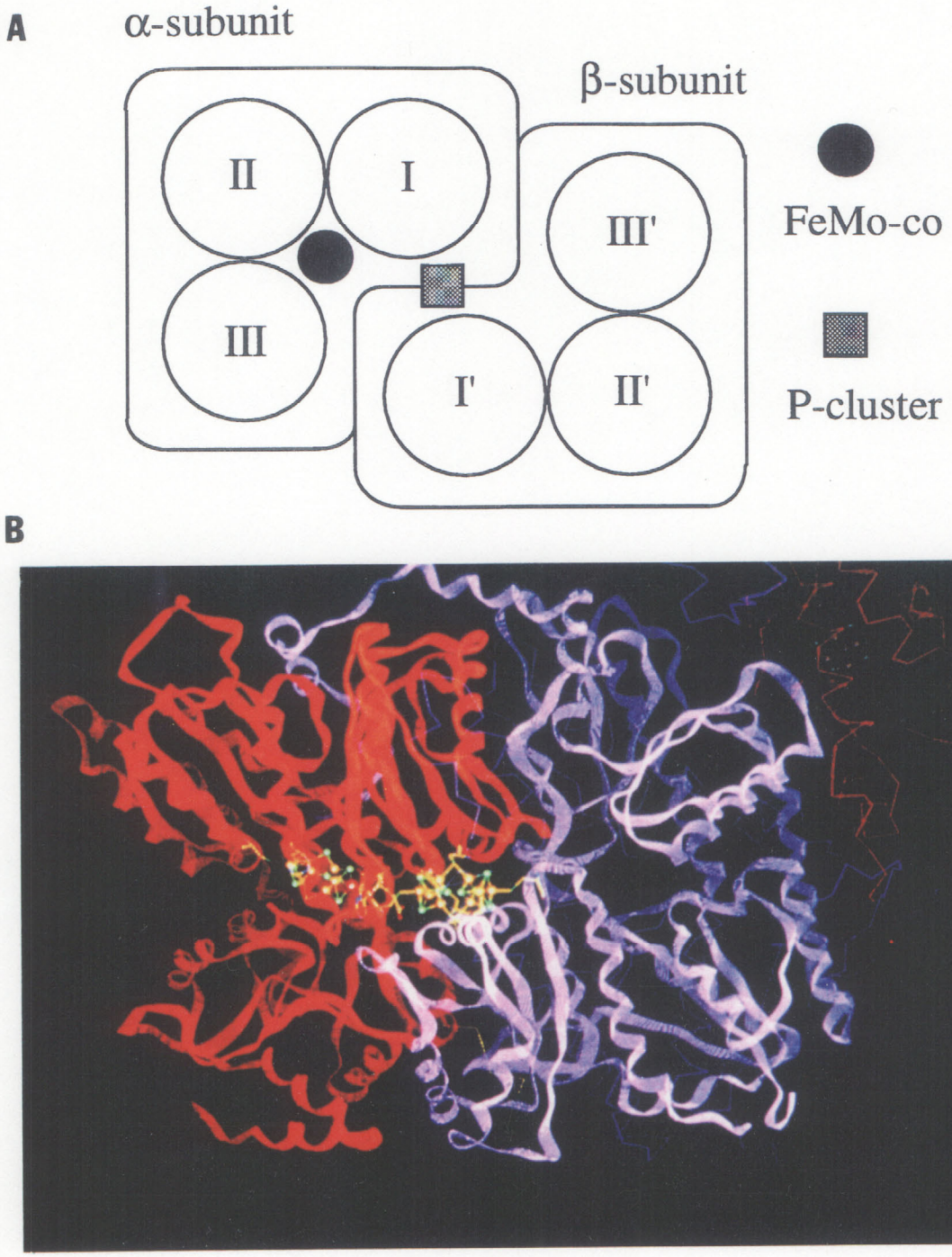

Figure 7. (A) Schematic diagram of the MoFe protein αβ subunit pair. (B) Ribbons diagram of the polypeptide fold of the MoFe protein αβ subunit pair. The α-subunit is in red and the β-subunit is in purple. The P-cluster is located in the center of each diagram. The FeMo-cofactor is located within the α-subunit. The ribbons diagram was provided by Dr. Bolin of Purdue University.

ligations. Intersubunit contacts occur between α-subunit Domain I and β-subunit Domains II′ and III′. Likewise, β-subunit Domain I′ contacts with α-subunit Domains II and III. The $\alpha_2\beta_2$ tetramer is formed from the two pairs of αβ dimers that are related by a two-fold rotation (Fig. 8). There are extensive α-helical packing interactions between Domains II′ and III′ of the two β-subunits at the tetramer interface with some additional interactions involving Domain III of each α-subunit. Electrostatic, hydrophobic and hydrogen bonding interactions are also important for the quaternary structure of the MoFe protein. The divalent cation binding site may exist at the tetramer interface where either Ca^{2+} or Mg^{2+} has an octahedral coordination to some amino acid residues and water molecules. These sites seem to be important for the stabilization of the subunit associations.

The FeMo-cofactor is buried at least 10 Å below the protein surface and is fully surrounded by its polypeptide environment which is primarily provided by hydrophilic residues (Fig. 6). As described above, the α-Cys-275 and α-His-442 residues serve as direct ligands to the FeMo-cofactor, whereas the α-Gln-191 and α-His-195 residues interact with the FeMo-cofactor indirectly through homocitrate and a central bridging sulfide, respectively. In addition to these residues, other highly conserved residues are also found in the vicinity of the FeMo-cofactor: 1) α-Ser-278 is hydrogen-bonded to the S_γ of α-Cys-275; 2) α-Gly-356 and α-Gly-357 may serve as the stabilizing factors; 3) α-Arg-96 and α-Arg-359 can interact with the cluster sulfurs in the FeMo-cofactor via hydrogen bonding; and 4) α-Glu-380, α-Gln-440, and α-Glu-427 interact with homocitrate through water molecules. There are also some aromatic and hydrophobic residues surrounding the FeMo-cofactor, α-Tyr-229, α-Ile-231, α-Val-70, α-Phe-381, α-Leu-358, and α-Ile 355.

The P-cluster pair is also at least 10Å under the protein surface and surrounded mainly

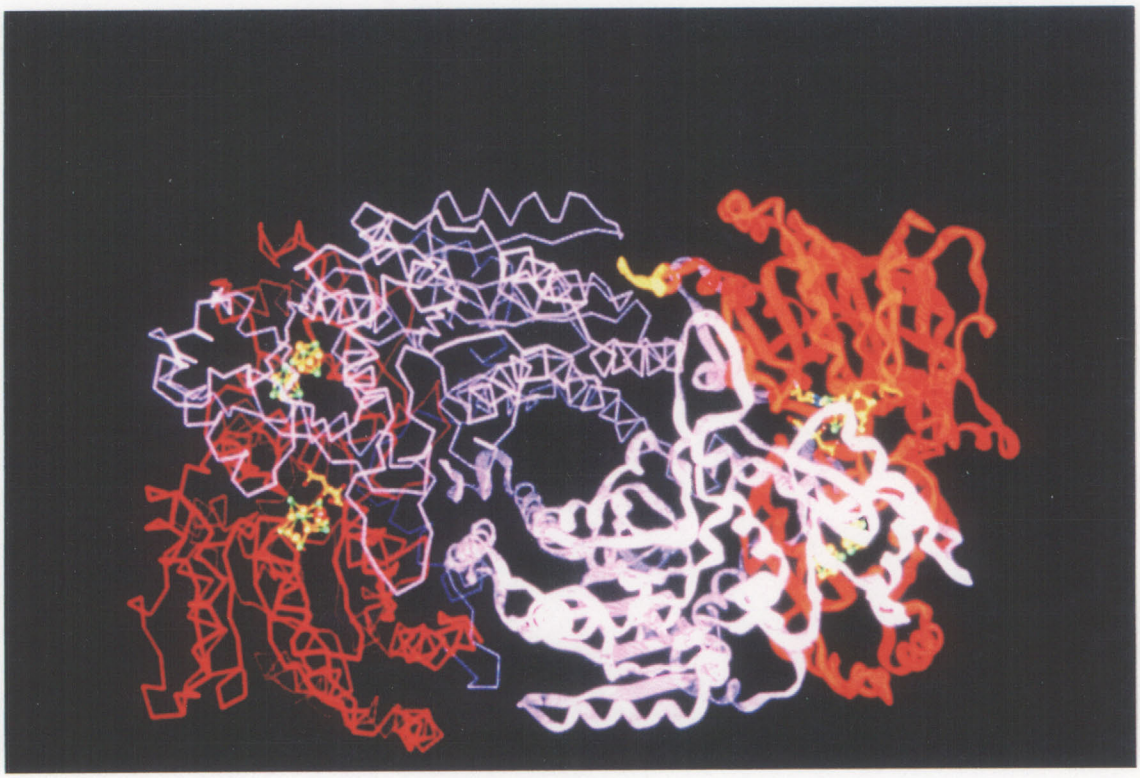

Figure 8. Diagram of the polypeptide fold of the MoFe protein $\alpha_2\beta_2$ tetramer. One $\alpha\beta$ subunit pair is shown in wire model and the other pair is shown in ribbons (provided by Dr. Bolin of Purdue University).

by highly conserved hydrophobic residues (Fig. 5). The six cysteinyl ligands along with the β-Ser-188, β-Gln-93, and β-Thr-152 residues are highly conserved while other hydrophilic residues, such as α-Glu-153, α-Glu-184, α-Ser-92, α-Ser-152, and β-Ser-92 are generally not conserved among MoFe protein sequences. Three Gly residues (α-Gly-87, α-Gly-185, and β-Gly-94) are strictly conserved and may be structurally important.

Primary sequence comparisons, site-directed mutagenesis, and biochemical characterizations of the resulting mutants provided a basis for predicting some features of the polypeptide environments surrounding the FeMo-cofactors and P-clusters. These predictions turned out to be remarkably accurate as the structural models of the MoFe protein were established. The examples of the accurate predictions are: 1) The working model (Fig. 3) assigned the metallocluster environments in the MoFe protein primary sequence as follows: six strictly conserved Cys residues (three Cys residues in each subunit) as P-cluster ligands; two other Cys regions as FeMo-cofactor ligands (α-Cys-275 as a direct ligand and α-His-195 near α-Cys-183 as an indirect N-donor ligand). 2) The α-Gln-191 residue interacts with a carboxyl group of the homocitrate. 3) Secondary structure predictions based on the primary sequence indicated that the P-cluster might be located near the subunit interface and actually arranged into two subclusters bridged between the α- and β-subunits. X-ray crystallography, however, revealed some features that were not anticipated from the sequence comparisons and amino acid substitution studies, such as : contributions of certain β-subunit residues to the FeMo-cofactor environment; direct coordination of the α-His-442 residue; and some residues of potential importance (α-Arg-96, α-Arg-359, and α-Phe-381). Table II lists highly conserved amino acid residues constituting the FeMo-cofactor environment within the MoFe protein and their potential

Table II. Conserved amino acid residues in the FeMo-cofactor polypeptide environment. The numbering refers to *Azotobacter vinelandii* sequence.

Residue	Structural information	Potential Function
α-191-Gln	ligated to homocitrate through hydroxyl and carboxyl group	
α-195-His	NH→S hydrogen bond to bridging sulfur of FeMo-co	
α-275-Cys	direct ligand to FeMo-co	keep FeMo-co attached to polypeptide
α-442-His	direct ligand to FeMo-co	keep FeMo-co attached to polypeptide
α-278-Ser	hydrogen bond to Sγ of 275-Cys	
α-96-Arg	potential to form hydrogen bond to bridging or cluster sulfur of FeMo-co	stabilize FeMo-co/intermediate proton transfer
α-359-Arg	potential to form hydrogen bond to bridging or cluster sulfur of FeMo-co	stabilize FeMo-co/intermediate proton transfer
α-356-Gly	NH→S hydrogen bonded to bridging sulfur of FeMo-co	stabilize FeMo-co/intermediate
α-357-Gly	NH→S hydrogen bonded to bridging sulfur of FeMo-co	stabilize FeMo-co/intermediate
α-380-Glu	interact with homocitrate through water	proton transfer
α-440-Gln	interact with homocitrate through water	proton transfer
α-427-Glu	interact with homocitrate through water	proton transfer
α-381-Phe		
α-70-Val		

functions predicted from the structural analysis. The structural information described above now can provide a basis to interpret the spectroscopic and catalytic effects resulting from the amino acid substitutions placed within the metallocluster environments. This information can also be used for directing further site-directed mutagenesis strategy to determine the function of these amino acid residues.

Substrates and inhibitors of nitrogenase

Nitrogenase can reduce not only N_2, the physiological substrate, but also a variety of low molecular weight compounds. The alternative substrates for nitrogenase include nitrous oxide (N_2O), azide (N_3^-), cyanide (CN^-), hydrazine (N_2H_4), nitrite (NO_2^-), cyanamide ($N{\equiv}CNH_2$), cyclopropene (C_3H_4), diazirin (CH_2N_2), proton (H^+), acetylene (C_2H_2), and analogues of some of these compounds (reviewed by Yates, 1992). The reactions catalyzed by nitrogenase using the various substrates are shown in Table III. These substrates inhibit each other since they all compete for electrons from the same pool of the reduced nitrogenase. The inhibition patterns observed from the kinetic experiments can not often be explained by the conventional enzymatic models because different substrates bind to different forms (oxidation states) of the enzyme (Chatt, 1980; Liang and Burris, 1988; Thorneley and Lowe, 1985). The discordant inhibition patterns observed between N_2 and C_2H_2 is an example. C_2H_2 is a non-competitive inhibitor of N_2 reduction suggesting that C_2H_2 and N_2 bind to different forms of the enzyme. However, a competitive pattern by N_2 against C_2H_2 supports the concept of a single form and indicate that an excessive concentration of C_2H_2 can completely overcome the inhibitory effect of N_2. Rivera-Ortiz et.al (1975) proposed a model where C_2H_2 and N_2 bind to different

Table III. Nitrogenase reactions (adapted from Yates, 1992).

Reaction	Reference
$N_2 + 6H^+ + 6e^- \rightarrow 2NH_3$	Burris, 1976
$HCN + 6H^+ + 6e^- \rightarrow CH_4 + NH_3$	Kelly et al., 1967
$HCN + 4H^+ + 4e^- \rightarrow CH_3NH_2$	Kelly et al., 1967
$CH_3NC + 6H^+ + 6e^- \rightarrow CH_4 + CH_3NH_2$	Kelly et al., 1967
$CH_3NC + 4H^+ + 4e^- \rightarrow CH_3NHCH_3$	Kelly et al., 1967
$HN_3 + 6H^+ + 6e^- \rightarrow N_2H_4 + NH_3$	Dilworth and Thorneley, 1981
$N_3^- + 3H^+ + 2e^- \rightarrow N_2 + NH_3$	Schollhorn and Burris, 1967a
$N_2O + 2H^+ + 2e^- \rightarrow N_2 + H_2O$	Hardy and Knight, 1966
$C_2H_2 + 2H^+ + 2e^- \rightarrow C_2H_4$	Dilworth, 1966; Schollhorn and Burris, 1967b
$3\overline{CH=CHCH_2} + 6H^+ + 2e^- \rightarrow \overline{CH_2CH_2CH_2} + 2CH_3CH=CH_2$	McKenna et al., 1980
$2H^+ + 2e^- \rightarrow H_2$	Hoch et al., 1957
$\overline{CH_2–N=N} + 6H^+ 6e^- \rightarrow CH_3NH_2 + NH_3$	Orme-Johnson et al., 1981
$\overline{CH_2–N=N} + 8H^+ + 8e^- \rightarrow CH_4 + 2NH_3$	Orme-Johnson et al., 1981
$NO_2^- + 7H^+ + 6e^- \rightarrow NH_3 + 2H_2O$	Vaughn and Burgess, 1989
$N{\equiv}CNH_2 + 6H^+ + 6e^- \rightarrow CH_3NH_2 + NH_3$	Miller and Eady, 1988
$N{\equiv}CNH_2 + 8H^+ + 8e^- \rightarrow CH_4 + 2NH_3$	Miller and Eady, 1988
$C_2H_4 + 2H^+ + 2e^- \rightarrow C_2H_6$	Ashby et al, 1987
$N_2H_4 + 2H^+ + 2e^- \rightarrow 2NH_3$	Burgess et al., 1981

forms. In this model, N_2 binds at an active site only when the enzyme is at least six-electron reduced whereas C_2H_2 binds to its own site when the enzyme contains two electrons. Therefore, C_2H_2, at its saturated level, will completely overcome the N_2 inhibition by depleting the N_2-binding form (six-electron reduced) of the enzyme. New experimental observations by Thorneley et.al (1978) led to some modifications of this model. Liang and Burris (1988) suggested that C_2H_2 binds to two different redox forms of the enzyme, one form has a higher binding affinity for C_2H_2 and completely exclude the binding of N_2 while the other form has a lower affinity for C_2H_2 and also accommodate N_2. This idea is supported by the observation of two Km's for C_2H_2 (Davis et al., 1979).

N_2O was first reported as an alternative substrate for nitrogenase in 1954 (Mozen and Burris). N_2O is first reduced by two electrons by nitrogenase to N_2 plus H_2O and N_2 is further reduced to NH_3. Kinetic experiments were performed with purified nitrogenase component proteins to show the interactions between N_2O and some other products including N_2, C_2H_2, and H_2 at the active site (Jenson and Burris, 1986; Liang and Burris, 1988; Liang and Burris, 1989). In studying the effect of N_2 on N_2O reduction, $^{15}N_2O$ was used as a substrate to differentiate N_2O-derived N_2 from the inhibitor N_2. N_2O inhibit C_2H_2 reduction competitively but C_2H_2 is a non-competitive inhibitor of N_2O reduction. The nonreciprocal response, which was also observed between N_2 and C_2H_2, was explained by the model involving two different forms of the enzyme that bind only C_2H_2 or both C_2H_2 and N_2O. N_2 and N_2O are competitive with each other. As implicated by the comparable responses between N_2 and N_2O and by the relationship of N_2 or N_2O toward C_2H_2, N_2O appears to bind to the same enzyme form as N_2 does. However, difference remains in that N_2O completely suppress H_2 evolution while N_2 can not completely block

H_2 evolution at a saturated concentrations and N_2O reduction is insensitive to H_2 inhibition.

Mechanism of nitrogenase action

A number of mechanisms of nitrogenase action have been proposed, but by far the most comprehensive is that of Thorneley and Lowe (Thorneley and Lowe, 1985). Since N_2 reduction to $2NH_3 + H_2$ is an eight electron process, their model consists of eight sequential one electron reductions of the MoFe protein with concomitant substrate binding and product release reactions occurring at various levels of reduction. The MoFe protein ultimately returns to its initial highest oxidation state, E_0.

The Fe protein cycle is a redox cycle during which one electron is transferred from the Fe protein to the MoFe protein in a series of reactions that involve the hydrolysis of MgATP. It can be represented by the partial reactions shown in Figure 9. Stopped-flow spectroscopy was used to analyze the partial reactions of this protein cycle. The Fe protein cycle consists of four essential reactions: 1) protein complex formation; 2) electron transfer coupled with the hydrolysis of MgATP; 3) protein complex dissociation; and finally 4) the re-reduction of oxidized Fe protein by $SO_2^{\cdot-}$. These reactions are discussed in detail below. The individual rate constants were determined from the time course of the absorbance changes at 430nm, the wavelength that gives the maximum absorption for oxidized Fe protein.

1. Reduced Fe protein and MoFe protein complex formation (k_+1)

Before electron transfer from the Fe protein to the MoFe protein can occur, the protein

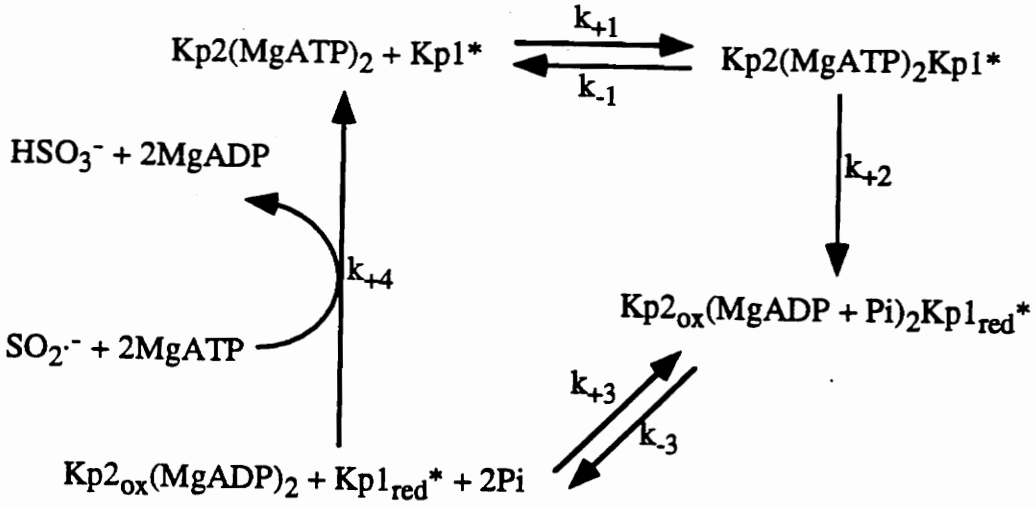

Figure 9. Redox cycle for the Fe protein. Kp1 refers to *Klebsiella pneumoniae* MoFe protein. Kp2 refers to *Klebsiella pneumoniae* Fe protein. Each Kp1* represents one of two independently functioning halves of the tetrameric MoFe protein and contains one Kp2 binding site (adapted from Thorneley and Lowe, 1983).

complex must be formed. Kinetic studies (Hageman and Burris, 1978; Lowe and Thorneley, 1984a, b; Thorneley et al., 1975; Thorneley and Lowe, 1984a, b) have provided the best evidence for formation of a functional complex. A lower limit of $k_{+1} = 5 \times 10^7$ M^{-1} s^{-1} has been estimated (Lowe and Thorneley, 1984b) by monitoring the MgATP induced electron transfer from Fe to MoFe protein as a function of the component protein concentrations at 23°C using stopped-flow spectrophotometry. Such a fast protein association reaction must be occurring at close to the diffusion limit. A high value of k_{+1} is thought to increase the efficiency of nitrogenase for N_2 reduction relative to H_2 evolution (Thorneley and Lowe, 1985).

2. Electron transfer from Fe protein to MoFe protein coupled to MgATP hydrolysis (k_2)

This reaction has been studied with nitrogenase isolated from *K. pneumoniae* (Smith et al., 1973, Thorneley, 1975), *A. vinelandii* (Orme-Johnson et al.,1972; Hageman et al.,1980) and *C. pasteuranium* (Zumft et al., 1974) using EPR and Mössbauer spectroscopy using ^{57}Fe enriched MoFe-proteins (Smith & Lang, 1974; Zimmerman et al., 1978). These data defined the direction of electron transfer and demonstrated that one electron was transferred from the Fe-protein to the FeMo cofactor of the MoFe-protein. This electron may pass transiently to the 'P' centers before internal electron transfer to the FeMo-cofactor where substrates are bound and subsequently reduced. The coupling of MgATP hydrolysis to the electron transfer between the complexed proteins has been demonstrated by rapid quench studies followed by analysis of Pi formed on ATP hydrolysis (Eady et al., 1978; Hageman et al., 1980). The electron transfer from

$Fe(MgATP)_2$ to MoFe protein at 10°C monitored by stopped-flow spectrophotometry together with analysis of Pi released by the rapid quench technique has shown that MgATP hydrolysis occurs concomitantly with electron transfer (Eady et al., 1978). The coupling of electron transfer, between Av1 and Av2, to MgATP hydrolysis has also been observed (Hageman et al., 1980). From the amplitudes of the time courses it was concluded that two molecules of MgATP were hydrolyzed per electron transferred between the two proteins. Mensink et al.(1992), using a pH indicator to measure proton production, observed ATP-dependent proton production at a rate slower than ATP-induced electron transfer, but slightly faster than dissociation of the complex of oxidized Fe-protein and reduced MoFe protein. This suggests a model where binding of MgATP allows electron transfer from Fe protein to MoFe protein, and ATP hydrolysis is obligatory for dissociation of the complex after electron transfer. However, this does not agree with the proposal put forward by Thorneley et al. (1989), based on stopped-flow microcalorimetry data, that at 6°C nitrogenase liberates protons at a faster rate than electron transfer.

Monitoring of the absorbance change of the Fe protein by stopped-flow spectrophotometry at 430 nm has allowed the accurate measurement of the rate constant for electron transfer between the component proteins and also the determination of the dependence on MgATP and MgADP concentrations. Thus k_2 has been measured at 200 s^{-1} at 23°C (Thorneley, 1975) and 24 s^{-1} at 10°C (both at pH 7.4) (Eady et al., 1978).

3. The dissociation of oxidized Fe protein from reduced MoFe protein (k_{-3})

The kinetics of the reduction by dithionite of oxidized Fe protein in the presence of MgADP at 23°C and pH 7.4 has been investigated with stopped-flow spectrophotometry

and EPR spectroscopy (Thorneley and Lowe, 1983). The inhibition of this reduction reaction by MoFe protein has enabled the determination of the rate of dissociation of $Fe_{ox}(MgADP)_2$ from MoFe protein (k_{-3}). The value of k_{-3} of 6.4 ± 0.8 s^{-1} allowed Thorneley and Lowe (1983) to conclude that the rate limiting step in the catalytic cycle of nitrogenase was the dissociation of oxidized Fe protein from the MoFe protein. This follows from the equivalence of the calculated value of the specific activity of MoFe protein using $k_{-3} = 6.4 \pm 0.8$ s^{-1} as the rate-limiting step to that measured with a steady-state assay for H_2 evolution at 23°C.

Pre-steady-state kinetics of H_2 formation show that two slow steps (k_{-3}) have to occur before a product can be detected. Therefore if Fe protein is a one electron donor, to explain the calculated steady-state rate of H_2 evolution, Fe protein must interact with each αβ MoFe protein-dimer independently (Thorneley and Lowe, 1983). This also implies that the two FeMo-cofactors function independently consistent with them being 70 Å apart in the Bolin (Bolin et al., 1990) and Rees structures (Kim and Rees, 1992a).

4. Reduction of oxidized Fe protein by $SO_2^{\cdot-}$ (k_4)

Thorneley and Lowe studied the reduction of oxidized *K. pneumoniae* (Thorneley and Lowe, 1983) and *A. chroococcum* (Thorneley et al., 1976) Fe protein by $SO_2^{\cdot-}$. The reduction of $Kp2_{ox}(MgADP)_2$ by $SO_2^{\cdot-}$ can be described by a single exponential decay with a first-order rate constant $k_{obs} = 10.3$ s^{-1} with 10 mM $Na_2S_2O_4$. A linear dependence of k_{obs} on $[S_2O_4^{2-}]^{1/2}$ confirms that $SO_2^{\cdot-}$, from the pre-dissociation of $S_2O_4^{2-} \leftrightarrow 2SO_2^{\cdot-}$, is the active reductant, and a value of $k_4 = 3 \times 10^6$ M^{-1} s^{-1} was obtained at 23°C. Thorneley and Lowe (1983) assigned the limiting value of $k_{obs} = 25$ s^{-1} at $[S_2O_4^{2-}] > 50$

mM, to either a rate limiting conformation change or release of MgADP prior to rapid reduction by $SO_2^{\cdot-}$. Uncomplexed Fe_{ox} is reduced approximately 30 times faster than $Fe_{ox}(MgADP)_2$ at 23°C ($k > 10^8$ M^{-1} s^{-1}) (Thorneley et al., 1976). $Fe_{ox}(MgADP)_2$ is reduced prior to the replacement of bound MgADP by MgATP at the end of the cycle.

One electron is transferred from the Fe protein to the MoFe protein during each Fe protein cycle. The reduction of N_2 to NH_3 and the concomitant evolution of H_2 requires eight electrons. This eight step, one-electron at a time, mechanism is known as the MoFe protein cycle and is shown in Figure 10. The species E_n represents Kp1 (an $\alpha\beta$ moiety of tetrameric MoFe protein) and n refers to the number of times Kp1 completes the Fe protein cycle. It also indicates the number of rate-limiting protein dissociation steps (k_{-3}) that MoFe protein has undergone as well as the number of electron equivalents by which it has been reduced relative to the resting state, E_0. The initial state E_0 is that of free protein isolated in the presence of dithionite. The three arrows linking E_n to E_{n+1} are the first three reactions of the Fe protein cycle. The kinetics of the Fe protein cycle are independent of the level of oxidation of the MoFe protein (Fisher et al.1991).

Computer simulations of the time course for H_2 formation under an atmosphere of either Ar or N_2 indicated that species E_2, E_3, and E_4 can all evolve H_2. The first species of the MoFe-protein cycle that can release H_2 is E_2, and in doing so it reverts back to E_0. The concentration of E_2 determines the rate of H_2 evolution, so a slow rate of dissociation (k_{-3} = 6.4 ± 0.8 s^{-1}) minimises the build up of E_2. Secondly the rate of conversion to E_3, the N_2 binding species, is maximised by reduced Fe-protein reacting at close to the diffusion controlled rate ($k_1 = 5 \times 10^7$ $M^{-1}s^{-1}$). Only free MoFe protein at all levels of reduction can bind substrates or inhibitors and release products (Thorneley and Lowe, 1985). The Fe

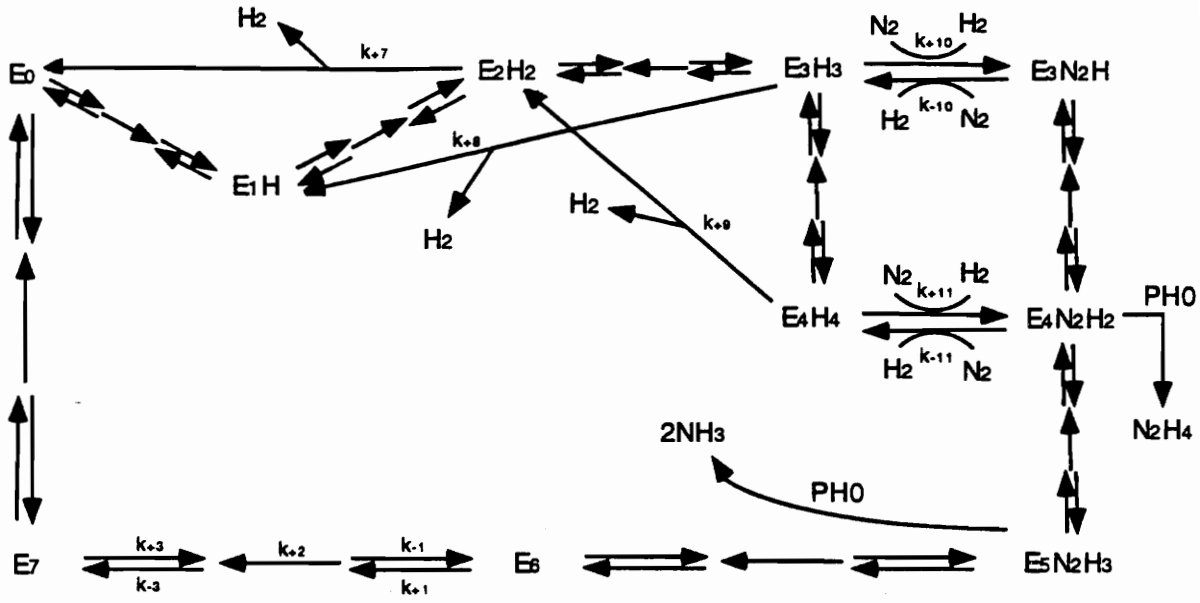

Figure 10. MoFe protein cycle. E_n represents Kp1 (an $\alpha\beta$ moiety of tetrameric MoFe protein) and n refers to the number of times Kp1 completes the Fe protein cycle. The three arrows linking E_n to E_{n+1} are the first three reactions of the Fe protein cycle (from Lowe and Thorneley, 1984a).

protein bound to the MoFe protein prevents H_2 evolution by restricting access of protons to the reduction site on the MoFe protein. Therefore, the role of Fe protein is not only to pass electrons to the MoFe protein and the bound substrate but also to cause MoFe protein to act as nitrogenase not as hydrogenase. This also explains the effect of Fe:MoFe protein ratio upon the distribution of total electron flow toward H_2 evolution or N_2 reduction. Under conditions of low flux through the MoFe protein (Fe:MoFe=1:100), essentially all the electrons are used for H_2 evolution whereas about 75% of electron flow is redirected toward N_2 reduction at high flux. N_2 reduction is not observed at low electron flux because of the domination of the first-order H_2 evolution reaction from species E_2H_2 over the second order reaction of E_2H_2 with reduced Fe protein. The latter reaction occurs at high electron flux to form the MoFe-Fe protein complex which leads to the MoFe protein becoming further reduced to the N_2-binding states, E_3 and E_4 (as will be discussed below). The 2:1 stoichiometry of NH_3 production to H_2 evolution was observed at high electron flux and saturated N_2. Chatt (1980) proposed that N_2 binds to nitrogenase by displacement of H_2 from a metal hydride, probably Mo, however, in the recent FeMo-cofactor structure proposed by Kim and Rees (1992a) the open central cavity of FeMo-cofactor was proposed to provide a site for N_2 binding (Chan et al., 1993). Lowe and Thorneley (1984a) proposed that N_2 binds reversibly at the three and four electron-reduced levels of the MoFe-protein in (E_3 and E_4) by displacing H_2. This would account for the competitive H_2 inhibition of N_2 reduction and the limiting stoichiometry of one H_2 evolved for each N_2 reduced.

The reduction of N_2 to NH_3 and the formation of hydrazine (N_2H_4) on acid-quenching of the enzyme were analyzed to provide a kinetic model for N_2 reduction. N_2H_4 is formed

from the enzyme-bound dinitrogen-hydride intermediate by non-enzymatic hydrolysis when the enzyme is quenched with acid or alkali. Analysis of the pre-steady state time course for N_2H_4 formation under N_2 and computer simulations using the kinetic models (Figure 9 and 10) indicated that N_2H_4 is released from $E_4N_2H_2$. The identity of the intermediate bound to E_4 was proposed to be a hydrazido (2-) group (E_4=N-NH_2) (Thorneley et al., 1978). It was proposed that two electrons would be used in the evolution of H_2 when N_2 is bound and two more electrons would reduce the bound N_2 to the hydrazido(2-) level. The two additional electrons required for conversion to hydrazine, a four electron reduction product of N_2, would be obtained by oxidation of the metal centers in the protein on quenching with acid or alkali. Thorneley and Lowe (1984a) have shown that the kinetic data can only be explained by stoichiometric reduction of one N_2 molecule at each Mo and the displacement of one H_2 when N_2 binds. The assumption that N_2 is coordinated to Mo of the MoFe protein was based on the observation that Mo and W react with the various nitrogenous species (Thorneley et al., 1978). Two moles of NH_3 are liberated on acid quenching after only five or six slow steps at species E_5 or E_6. This is equivalent to a three or four electron reduction of MoFe protein (one $\alpha\beta$ moiety), since two electrons are necessary to produce H_2 on N_2 binding. Thorneley and Lowe (1984a) suggested that these electrons are used to cleave the nitrogen-nitrogen triple bond to yield NH_3 and an enzyme bound nitrido (≡N) or imido (=NH) intermediate. This intermediate would hydrolyze under acid conditions employed in the rapid quench technique to give the second NH_3 and an oxidized protein. It was further concluded (Lowe et al., 1985) that at least one NH_3 is formed after only three or at most four electron reductions of the bound N_2. This supports the theory of Chatt (1980) that the triple bond of N_2 is weakened by

progressive protonation of the β-nitrogen atom. Thus E_5 is likely to be a hydrazido(2-) derivative (Mo=N-NH_3, assuming N_2 binds to Mo) and E_6 a nitrido species (Mo≡N). The pre-steady-state data and simulations on the time course for NH_3 formation were analyzed after quenching the enzyme with acid and therefore the conclusions made from the acid-quench data may not necessarily be true for NH_3 formation under physiological conditions. However, identification of the oxidized states of the MoFe protein would provide the strong evidence for the above proposal.

The kinetic model introduced above also provides a basis for interpreting some experimental observations on H_2 evolution rate. Dependence of H_2 evolution rate on total component protein concentration and Fe:MoFe protein ratio will be discussed here. A disproportionate decrease in substrate reduction activity can be observed when the concentration of nitrogenase component proteins is decreased below 0.5 μM, while a constant Fe:MoFe protein ratio is maintained. This is known as the "dilution effect" and arises from a change in the rate-limiting step in the Fe-protein cycle. Lowe and Thorneley (1984b) used computer simulations to show that the rate of association of reduced Fe protein with the MoFe protein become rate-limiting at low protein concentrations. Under normal assay conditions, dissociation of the oxidized Fe protein-MoFe protein complex is rate-limiting and the maximal rate of H_2 evolution is achieved. The kinetic model also explains another observation that the H_2 evolution specific activity of the MoFe protein is inhibited by high protein concentrations. This is due to the significant increase in the back reaction of the dissociation step involving association of oxidized Fe protein with the MoFe protein. In addition to the high protein concentrations, a decrease in dithionite concentration or Fe:MoFe protein ratio could give rise to a decrease in specific activity of

the MoFe protein by promoting the back reaction. In order to minimize the unessential H_2 evolution that occurs in the absence of N_2 or alternative substrates nature has selected for a high concentration of nitrogenase proteins in vivo (approximated to be 100μM, Eady et.al.,1978). Thorneley and Lowe (1983) have proposed that in order to minimize this reaction nitrogenase has also evolved as a slow enzyme.

The dependence of H_2 or C_2H_4 formation at a constant MoFe protein concentration, on increasing Fe protein concentration constitutes the titration curve that gives the specific activity of the MoFe protein. A simplistic explanation for the curve is that Fe protein acts as a substrate to MoFe protein, and that product inhibition by $Fe_{ox}(MgADP)_2$ can occur. Lower specific activity of MoFe protein is observed when the MoFe protein concentration is much greater than the Fe protein concentration or dithionite concentration is limiting. This occurs because the concentration of reduced Fe protein is insufficient to associate all available MoFe protein to give the maximum activity. The specific activity of the Fe protein is also inhibited by a high MoFe:Fe ratio. This is due to the back reaction involving the oxidized Fe protein binding to the MoFe protein i.e. MoFe protein competes with $SO_2^{\cdot-}$ for free $Fe_{ox}(MgADP)_2$. Maximum Fe protein activity is observed at the MoFe protein concentration when the steady state concentrations of free $Fe(MgATP)_2$, free $Fe_{ox}(MgATP)_2$ and free $Fe_{ox}(MgADP)_2$ are minimal and all the Fe protein is present in the complexed form. Under these conditions substrate reduction is limited by complex dissociation.

HD formation

Protons are required for all nitrogenase catalyzed substrate reductions and in the absence

of exogenously added reducible substrates all electrons are channeled to H_2 formation. The rate of H_2 evolution varies depending on experimental conditions and the different types and concentrations of the substrates being used. There are no nitrogenase substrates which give a greater maximal rate of reduction than that obtained when all electrons are directed toward the reduction of protons, therefore the maximum rate of the enzyme is often defined as the rate of H_2 evolution under Ar. At present the exact chemical mechanism for H_2 evolution is unknown, but it is likely that a metal hydride or dihydride is involved which can produce H_2 either by reaction with protons or by reductive elimination. The mechanism proposed by the Sussex group describes the reaction steps required for H_2 evolution which require MoFe protein to be reduced by a certain number of electron equivalents (Lowe and Thorneley, 1984a). Another H_2 evolution pathway which occurs by H_2 displacement upon binding of N_2 was also included in the model. N_2-dependent HD formation was first observed by Hoch et al. (1960) when significant amounts of HD were formed from D_2 by soybean nodules in the presence of N_2. Earlier evidence supported the speculation that HD formation occurs by the reversible exchange of D_2 with an enzyme-bound intermediate. However, the electron balance studies indicated that one electron was required for each HD formed assuming total electron flow through nitrogenase remained constant (Newton et al., 1977; Guth and Burris, 1983). Further studies ruled out the reversible exchange mechanism for HD production by demonstrating that the rate of incorporation of tritium from T_2 into the aqueous phase was negligible (Burgess et al., 1981).

H_2 is not only a product but also a specific inhibitor of N_2 reduction. Reduction of other nitrogenase substrates including protons, nitrous oxide, azide, acetylene, cyanide,

methyl isocyanide, and hydrazine are not inhibited by H_2 (Burgess et al., 1981; Burns and Bulen, 1965; Hoch et al., 1960; Hwang et al., 1973). HD formation from D_2 is stimulated by N_2 but not by the alternative substrates. In addition, HD formation occurs at the expense of ammonia (NH_3) formation in the presence of D_2 and N_2. For example, in one experiment, 50% less NH_3 was formed under 50% H_2 / 40% N_2 / 10% Ar when compared to 40% N_2 / 60% Ar (Burgess et al., 1981). The percentage of electrons that would have gone to NH_3 formation was redirected toward N_2-dependent HD formation. These observations by the Kettering group have led to the suggestion that H_2 inhibition of NH_3 production and HD formation under D_2 / N_2 are different manifestations of the same molecular process involving an enzyme-bound diazene-level intermediate (E-N_2 H_2) (Burgess et al., 1981; Wherland et al., 1981). In this model (Figure 11), D_2 reacts with an enzyme-bound intermediate of N_2 fixation resulting in the release of the N_2 molecule, the production of two molecules of HD, and the net consumption of two electrons. Thus D_2 inhibits N_2 reduction by diverting electrons from NH_3 formation to N_2-dependent HD formation with one electron being utilized per HD in this process. The diazene-level intermediate in the reduction of N_2 to NH_3 implies a hydrazine-level species (E-N_2H_4) as the next reduction intermediate. In fact, Thorneley et al. (1978) reported the first detection of an enzyme-bound dinitrogen intermediate, which produced N_2H_4 on acid and alkali quenching of the enzyme reaction. The Kettering group demonstrated that N_2H_4 does not enhance HD formation in the presence of D_2 and that N_2H_4 reduction to NH_3 is not inhibited by N_2. Therefore, under the assumption that the added N_2H_4 forms an enzyme complex which is comparable to the hydrazine-enzyme intermediate in the N_2 reduction pathway, they concluded that H_2 inhibition and HD formation reactions occur at the diazene

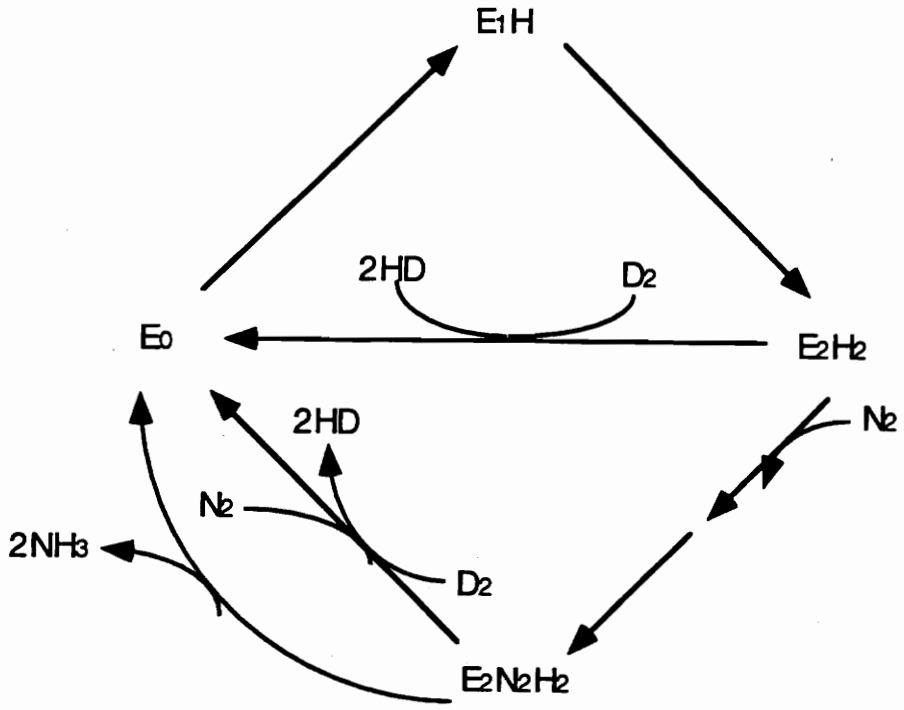

Figure 11. Proposed mechanism for HD formation by nitrogenase (Kettering model). The letter E represents one half of the tetrameric MoFe protein and contains one substrate binding site. The subscript n refers to the number of electrons by which the MoFe protein has been reduced relative to E_0, the dithionite reduced state (adapted from Wherland et al., 1981).

level.

A great deal of controversy still exists with respect to the N_2 dependence of HD formation. A little, but significant amount of HD formation is always observed in reactions free of N_2. One interpretation was that there was either contaminating N_2 in the gas mixture or N_2 leakage from the atmosphere during the assay manipulations which acted as a catalyst for HD formation. An alternative proposal was the N_2-independent mechanism for HD formation. The Kettering group supported the existence of the N_2-independent HD formation according to their observation that the percentage of total electron flow used to form HD in the absence of N_2 was much lower than the percentage of total electron flow to HD formation under N_2, <10% and 25% respectively (Wherland et al., 1981). The N_2-independent HD formation is also supported by the difference in apparent Km (N_2) observed for HD and NH_3 formation. (discussed below)

An alternative model for HD formation by nitrogenase was proposed by Guth and Burris (1983, Figure 12). In this model, D_2 and N_2 compete for the same form of the enzyme. N_2 can also bind to the D_2-bound form. Thus, N_2 is reduced to NH_3 if D_2 is absent, but in the presence of D_2, HD is formed with the concomitant release of the N_2 molecule. The major difference between this model and that of the Kettering model is that D_2 binds to nitrogenase before N_2 and cannot react with an enzyme-bound intermediate. The N_2-independent HD formation was excluded in this model because they demonstrated that HD formation was almost completely eliminated (less than 1-2% of total electron flux) in the absence of N_2 (Guth and Burris, 1983). Their experiments were performed in an all-glass system to avoid any N_2 contamination. This model is supported by their experimental observations that D_2 was competitive with N_2 and the HD/NH_3 production

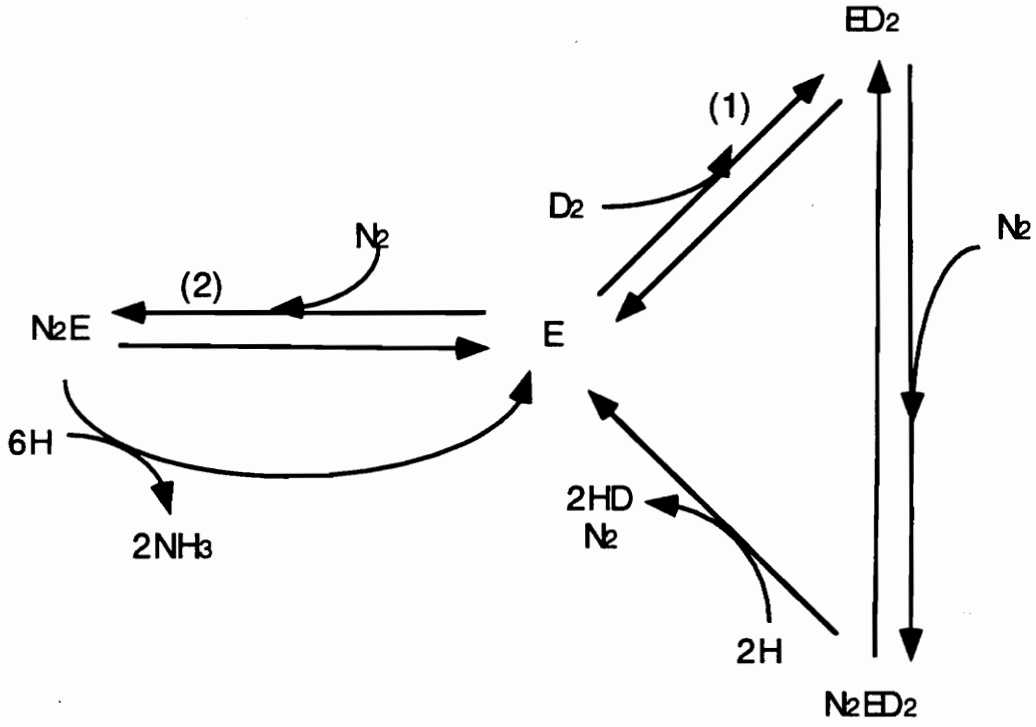

Figure 12. Proposed mechanism for HD formation by nitrogenase (Guth and Burris model) (adapted from Guth and Burris, 1983).

ratio was decreased to 0 at very high pN_2. According to this model, high pN_2 can successfully compete for all free enzyme (E) and completely block the binding of D_2 on the enzyme and HD formation.

It was reported that the apparent Km (N_2) for NH_3 is higher than the apparent Km (N_2) for HD formation (Bulen, 1976; Burgess et al., 1981; Burris and Orme-Johnson, 1976; Li and Burris, 1983; Turner and Bergersen, 1969). According to the Kettering model, the non-identical Km (N_2) is due to the HD formation in the absence of N_2. In Guth and Burris model, Km's (N_2) for the formation of HD and NH_3 are different because N_2 enhances HD formation on binding to E-D_2 and simultaneously inhibits HD formation by competing for E with D_2. The major drawback of this model is that it does not explain the stoichiometric ratio of one H_2 evolved per two NH_3 formed under saturating N_2. The third model was suggested by Cleland (Guth and Burris, 1983, Figure 13). In this model, H_2 is released upon binding of N_2 molecule which accounts for the stoichiometry of one H_2 evolved per N_2 fixed. The reversible exchange reaction (E-N_2 + D_2 $\leftrightarrow$ E-D_2 + N_2) is shifted toward the formation of the E-D_2 species in the presence of D_2 and HD is formed at the expense of N_2 fixation. This mechanism implies that N_2-dependent H_2 evolution, H_2 inhibition of N_2 fixation, and HD formation are caused by the same mechanism. Despite the successful features of this model, the unavoidable stoichiometric ratio of one H_2 production per two HD formed does not meet most of the experimental observations (Guth and Burris, 1983; Burgess et al., 1981; Newton et al., 1977). However, Jensen and Burris (1985) showed that the $2HD/H_2$ ratio extrapolated to one at saturating pN_2 and infinite pD_2. These results support the Cleland mechanism for HD formation.

All three mechanisms support the initial proposal by the Kettering group that H_2

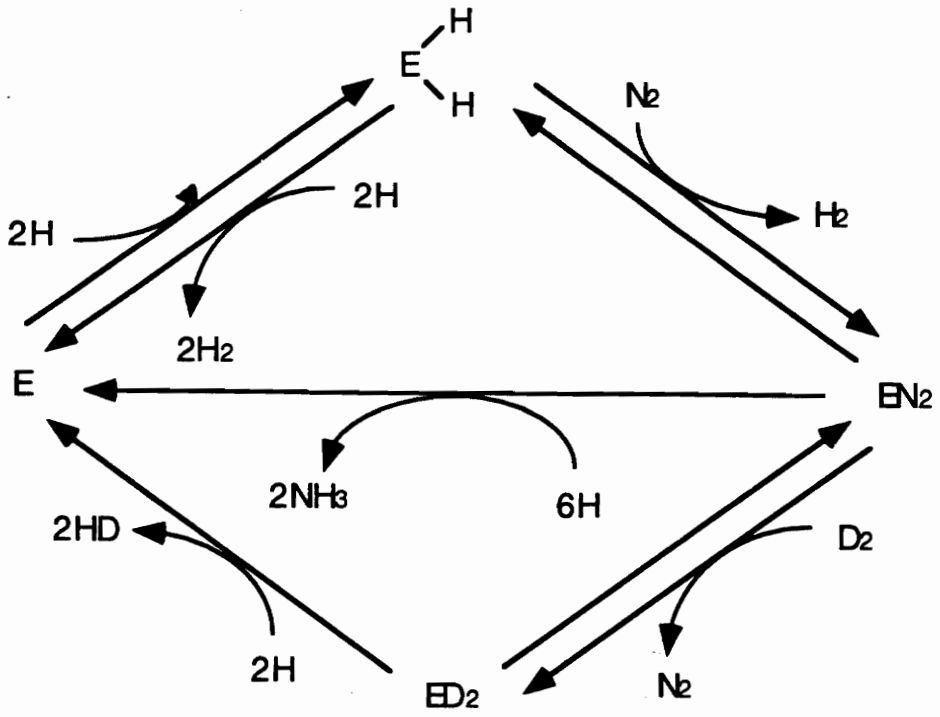

Figure 13. Proposed mechanism for HD formation by nitrogenase (Cleland model) (adapted from Guth and Burris, 1983).

inhibition of NH_3 formation and N_2-dependent HD formation are different manifestations of the same molecular process. There are some discrepancies between these models and each model conflicts with some experimental observations. The continued study on HD formation will be crutial for the understanding of the mechanism for nitrogenase catalysis.

Role of P-clusters in reducing dinitrogen

Lowe et al. (1993) extended their study on the pre-steady state reactions catalyzed by *Klebsiella pneumoniae* nitrogenase by investigating the absorbance changes occurring after primary electron transfer in an attempt to examine the redox changes occurring on the metal clusters of the MoFe protein. They analyzed the absorbance changes over the first 500 ms as the MoFe protein becomes reduced from E_0 through to E_4 and correlated these changes with the computed concentrations (using the Lowe-Thorneley model) of the various species as they change with time, substrate, and component protein ratio. The nature of the redox changes taking place in the metal clusters of the MoFe protein during substrate reduction was probed by complementary EPR experiments. The analysis undertaken in their investigation showed that the metal clusters of the MoFe protein undergo complex redox changes as electrons are transfered from the Fe protein. For example, the absorbance changes associated with the electron transfer between the Fe protein and the MoFe protein were observed as E_1 becomes reduced to E_2 (decrease in absorbance) and as E_3 is reduced to E_4 (increase in absorbance). Their analysis suggested that the absorbance changes could be due to the reduction ($E_1 \rightarrow E_2$) and oxidation ($E_3 \rightarrow E_4$) of a metal cluster within the MoFe protein. Further analysis on the affects of different gases (Ar, N_2, C_2H_2, and CO) on the EPR signals observed during nitrogenase turnover led them to propose that the centers

undergoing redox changes are likely to be the P-clusters. It is hypothesized that attaining the E_4 level triggers a transfer of electron density from the P-clusters onto FeMo-cofactor and that this transfer of electron density generates an enhanced reducing power for substrate reduction.

Experimental Procedures

Schlenk Line installation, operation, and maintenance

The Schlenk Line is an anaerobic manifold system which provides an anaerobic atmosphere in flasks, vessels and reaction vials containing oxygen-sensitive biological compounds. It is used in our laboratory regularly for the purpose of preparing *A. vinelandii* crude extracts, purifying nitrogenase component proteins and other *nif* gene products, and assaying nitrogenase activity. This chapter includes information on the installation, operation and maintenance of the Schlenk Line.

1. Installation

Sturdiness of the metal frame and convenient spacing of the glassware on the frame are two important factors to consider in mounting the manifold system. Schematic diagram and pictures of our system are shown in Figure 14. Sources of the parts are described in Table IV. The metal frame is made of stainless steel rods connected with each other both vertically and horizontally by aluminum clamps. The glassware is mounted on the metal frame which is tightly fixed on the wall or the bench. The setup has to be made in such a way that the stopcocks and lines are readily accessible for handling, and the bubbler and mercury gauge are easily observed. The function of each component in Figure 14 is described below.

(1) Manifold - The manifold has two lines connecting the inert gas (Ar) and vacuum source. The two-way stopcock provides an alternative connection of inert gas and vacuum lines to the system. A gas reservoir is attached to the manifold so that when a large volume

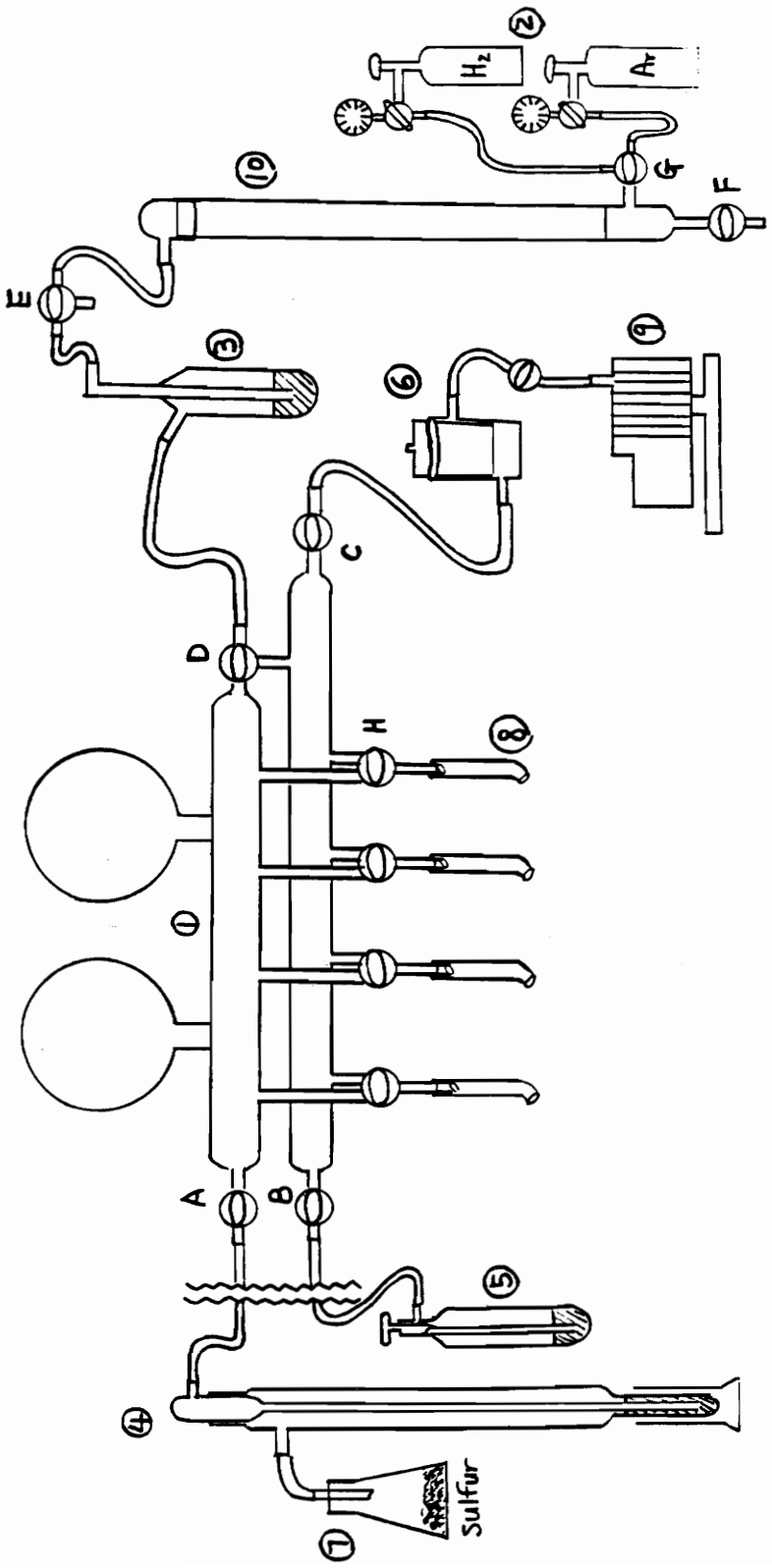

Figure 14. Schematic diagram of the Schlenk Line.

Table IV. Schlenk Line parts and sources

Item	Source	Catalog No.
Inert gas tank (Ar, H_2)	Airco	
Gas pressure regulator	Kontes	216150
Bubbler	Ace Glass	8761
Catalyst column	Ace Glass	7818-34
Screen Support	Ace Glass	7818-35
Adapter ST45/50	Ace Glass	7818-36
Catalyst R3-11	BASF via Ace Glass	7818-60
Manifold	Kontes	216050
Mercury manometer	Ace Glass	8733
Macro VirTis trap	Scientific Products	D-7300
Vacuum pump	Precision Scientific	Model DD 90
Electric heater	Staco Energy Products	Type 3PN1010
Apiezon grease	Thomas Scientific	Type H, N
Norprene tubing	Baxter	76571-10
Schlenk flasks and adapters	Kontes-airless ware section	6278-6392

of gas is drawn into the system it prevents the rapid gas flow through the catalyst column, and allows the gas to be completely O_2-free by the catalyst.

(2) Inert gas tank - Argon is used as an inert gas to provide an anaerobic environment in the manifold system. Trace amounts of oxygen in the inert argon gas are removed by the BASF catalyst column.

(3) Bubbler - A bubbler is used to monitor the inert gas flow into the system. There should be no bubbling occurring when the system is closed. If there is bubbling activity with all the stopcocks closed, the system must have a leakage problem.

(4) Gas pressure regulator - A gas pressure regulator designed as a mercury-filled tower is used to observe excessive positive pressure in the system.

(5) Mercury manometer - This graduated manometer monitors the negative pressure generated by the vacuum pump.

(6) Macro VirTis Trap - This Trap is filled with dry ice and is used to prevent moisture contamination of the vacuum pump oil.

(7) Mercury overflow trap - The mercury overflow trap acts as a safety system to trap mercury overflow caused by excessive positive pressure accidentally applied to the system.

(8) Tubing - Black Norprene tubing is used as the connection between manifold glassware and valves. This tubing is also used to attach glassware to the individual lines for handy manipulations.

(9) Vacuum pump - A vacuum system that is powerful and quiet is crucial and a pump capacity of 90 L/min (3.2 CFM) is required.

(10) BASF catalyst column - The BASF catalyst (R3-11) used in the column is composed of approximately 30% copper in a highly dispersed form, and stabilized on a

carrier. The catalyst, in its reduced state, catalytically removes oxygen from the inert gas by the following reaction:

$$Cu + 1/2\ O_2 \rightarrow CuO$$

The reaction rate is highly dependent on temperature, thus, the catalyst column is maintained at 120°C for maximum efficiency.

(11) Procedure for activation and regeneration of BASF catalyst column

BASF catalyst R3-11 is supplied in its oxidized state and has to be activated (reduced) before use. Activation occurs in the presence of hydrogen or carbon monoxide by the following reactions.

$$CuO + H_2 \rightarrow Cu + H_2O \ ; \Delta H = -20.7\ Kcal$$

$$CuO + CO \rightarrow Cu + CO_2 \ ; \Delta H = -30.5\ Kcal$$

After the system has been setup as in Figure 14, the adaptor is disconnected from the column and the BASF catalyst is loaded into the column. A thermometer is placed inside the column so that the 120°C mark is visible. The adapter is put back on top of the column and the bubbler is filled with approximately 1 inch of mineral oil. All the joints and connections are checked for leaks using the grease (Apiezon H) which is resistant to high temperature. With A, B, C, F valves closed and D, E, G, H valves open, argon flow is allowed at a slow rate (a few bubbles per second) and the catalyst column is heated gradually up to ≈120°C by using a heater (140 V output, Staco Energy Product Company). When the temperature is stabilized at ≈120°C, hydrogen gas is applied to the column at about 50% of the argon flow. The temperature is carefully monitored throughout the process such as not to exceed much greater than ≈150°C. If the temperature is increased higher than ≈150°C, the rate of hydrogen flow should be decreased, and vice versa. It

requires several hours to a whole day to completely reduce the catalyst R3-11 in the column depending upon the flow settings. Water generated by the reaction above is collected by opening the valve F as needed. A color change of the catalyst from faint-green to coal black will be observed as the reduction proceeds to completion. The temperature should be maintained below ≈150°C otherwise catalytic efficiency of the column will be decreased. After the catalyst turns coal-black, pure hydrogen can be passed through the catalyst column for 1 hr to ensure complete reduction of the catalyst. Argon is then passed through the column for 1 hr to remove hydrogen from the system. Then valves A, B, C, D, E, and G are opened and F and H are closed, and the column is cooled down by readjusting the power setting on the heater. The column is maintained at 120°C for more efficient operation.

2. Operation

The Schlenk Line is a two-way manifold system with one line connected to an inert gas tank and the other connected to a vacuum source. The manifold consists of four lines, each of which can be connected to either gas line or vacuum line independently via individual stopcocks. Therefore, four stopcocks control the corresponding lines independently with each other so that one line can be used for blowing argon while the other lines are being used for pulling a vacuum or for disconnecting from the system. Additional service lines can be created by connecting one manifold next to another as required. General procedure for the Schlenk Line operation is described below.

Gas line preparation - Positive argon atmosphere is produced by gently opening the regulator on the argon gas tank. Careful attention must be paid to this procedure because

too much pressure will disturb the mercury in the gas pressure regulator. Gas pressure should be constantly maintained at a rate low enough not to disturb the mercury regulator but high enough to provide sufficient pressure in the sample vessels and/or flasks.

Vacuum line preparation - The stainless steel dry ice trap is filled with crushed dry ice. The vacuum pump is turned on with all the Schlenk Line stopcocks in a horizontal position. Negative pressure generated by pulling the vacuum can be observed as a falling of the mercury level on the manometer . When a vacuum is applied to a vessel, the mercury level will be elevated and then go back down due to gravity, as the negative pressure is stabilized inside the vacuum line. The following points could be checked if the mercury level does not go down: 1) All stopcocks must be in the horizontal position (closed); 2) the three-way valve between the ice trap and the vacuum pump should be properly aligned; 3) the ice trap should be tightly fitted to the trap container; and 4) there should be no leaks along the vacuum line.

Each stopcock is painted red on one end and is clear on the other end. When a stopcock is turned so that the red end is pointing down, the line is blowing argon; when the red end is pointing up, the line is pulling a vacuum. It is important to carefully monitor the gas pressure in the system by observing either the mercury manometer when pulling a vacuum, or the bubbler and gas pressure regulator when blowing argon.

When a line is being used for the first time or being changed from blowing argon to pulling a vacuum or vice versa, the stopcocks should be manipulated slowly to prevent air from being accidentally introduced from outside the system. It is especially important when pulling a vacuum on a liquid because hurried operation may introduce the liquid up into the manifold.

When alternating cycles of blowing argon and pulling a vacuum are repeated to prepare an anaerobic atmosphere in a vessel or a flask, it is important to allow enough time between each manipulation. For example, it is necessary to allow the mercury to go up and come back down to the original level in the manometer before switching to the argon line for exhaustive evacuation when pulling a vacuum.

The proper use of the Schlenk Line is described using an anaerobic buffer preparation as an example ; A 2 L flask containing Tris-HCl buffer is connected to the line by tightly joining the side arm of the buffer flask to the Norprene tubing. A stir bar is placed in the flask and the top of the flask is sealed with a rubber stopper. A vacuum is drawn in the flask by opening the stopcock corresponding to the employed line. The vacuum is maintained and the flask is stirred to completely evacuate air not only in the headspace but also from the buffer solution. The length of the degassing period depends on the volume of the solution in the flask; normally 1 hr is sufficient for 1.5 liters. It is important to have enough headspace in the flask and to position the Norprene tubing higher than the liquid in the flask to prevent any liquid from getting into the tubing. After the flask is completely degassed, argon is introduced in place of the vacuum. Sodium dithionite (0.174 g/L) is added while the flow of argon is briefly interrupted. The flask is then subjected to the vacuum once again and stirred to dissolve the dithionite. The buffer solution is now ready for anaerobic experiments.

3. Maintenance

Maintenance of the stopcocks is important because they are the primary source of air leaks. The stopcocks are connected to the manifold via standard taper joints. Stiffness of

the stopcock operation may be due to insufficient grease applied to the joint; this grease (Apiezon N) should be applied as a thin film onto the ground glass surface of the joint. After the parts are joined and tightened by springs, the stopcocks should be turned in both directions a couple of times to spread the grease evenly around the joint area. Too much grease should be avoided because it will block the openings to the vacuum or blow lines.

Mercury vapor is absorbed through the respiratory tract and skin and can cause severe mercury poisoning symptomized by headache, nervous disorders and loss of memory. Preventive measures to avoid mercury poisoning are to keep a clean and well ventilated laboratory and to have a proper mercury-trap device as shown in Figure 14. In case of a mercury spill, elemental sulfur, iodine-treated charcoal or zinc dust may be spreaded onto the spill area to coat the surface of mercury and thereby reducing its evaporation. Small mercury droplets can be cleaned effectively by picking up with a Pasteur pipette.

There is an obvious leakage problem in the gas line when a serious bubbling activity occurs with all the stopcocks closed. When the mercury level in the manometer does not go back down, on the other hand, it can be concluded that the vacuum line is leaking. Proper greasing of the stopcocks and all other joints might solve and prevent most of the leakage problems. However, if there is a leakage problem not related to the stopcocks or joints, systematic isolation of each section of the Schlenk Line by closing the valves might help localize the source of the leakage. The vacuum pump oil should be changed every 3 months for maximum pump efficiency.

Azotobacter vinelandii growth conditions and nitrogenase derepression

A. vinelandii cell cultures were performed on a small scale (500 ml) and whole-cell

EPR spectra were obtained and crude extract enzyme activities were determined. Large scale cultures (20 L) were performed for purification of the nitrogenase component proteins from wild type and mutant strains.

Small scale culture - Burk medium (500 ml) supplemented with 20 mM ammonium acetate (BN medium) was inoculated with wild type or mutant strains of *A. vinelandii* cells from a culture plate. The cells were grown at 30°C in an incubator shaker (New Brunswick Scientific) maintained at 350 rpm. To repress the alternative nitrogenases and insure the derepression of the Mo-based system, 0.01 mM $NaMoO_4$ (J. T. Baker) was included in the medium. After an initial cell growth up to mid to late log phase (≈180 units on Klett-Summerson Turbidimeter, No. 54 filter), the cells were centrifuged at 5000 rpm for 10 min (Sorvall, SS-34 rotor). The cell pellet was resuspended in N-free Burk medium (500 ml), and derepressed for 4 hours for the synthesis of nitrogenase. The cells were then harvested by centrifuging at 5000 rpm for 10 min and the pellet stored at -80°C until needed for whole-cell EPR spectra or crude extract preparation.

Large scale culture - The inoculum was prepared by growing wild type cells in 500 ml BN media to log phase as described above. The inoculum was added to 20 liters of N-free Burk media in a 30-L fermentor (New Brunswick Scientific) fitted with a microprocessor which controlled aeration, temperature and vessel pressure. Culture conditions were 30°C at 350 rpm with the aeration rate and vessel pressure maintained at 12 L/min and 5 psi, respectively. Cells were harvested at a turbidometer reading of ≈180, by concentrating the cell culture down to 1.5 L (Pellicon cell concentrator, Millipore) and then cetrifuging at 5000 rpm for 10 min (Sorvall, GSA rotor). The cell pellet was stored at -80°C until needed for purification of the nitrogenase component proteins. DJ540 (α-195^{gln}), which exhibits

the Nif(-) phenotype, was initially grown in 500 ml of BN media and then used as the inoculum for 20 liters of BN media. At a turbidometer reading of 180, the cells were concentrated to 1.5 L and then re-inoculated into 20 L fresh N-free Burk media. Cells were then derepressed for 4 hours and harvested as described above.

Gel electrophoresis

Sodium dodecyl sulfate-polyacrylamide gel electrophoresis (SDS-PAGE) was used to evaluate effective derepression of nitrogenase in whole cells and also to monitor the progress of component protein purification. Gels were prepared according to the Laemmli procedure (1970) using 12% polyacrylamide (1.35% cross-linker) for the running gel and 4% for the stacking gel. Samples were treated with SDS-sample buffer containing 0.06 M Tris-HCl, pH 6.8, 10% glycerol, 2% SDS (w/v), 0.05% β-mercaptoethanol, and 0.002% bromophenol blue (w/v) and boiled for 3 minutes. Electrophoresis was performed at 20 mA/gel in a Hoefer Mighty Small apparatus (Hoefer, San Francisco, CA). The gels were stained with 0.1% Coomassie Blue (R-250, Sigma) and destained with 40% methanol / 10% acetic acid / 60% water solution.

Crude extract preparation

A frozen cell pellet, harvested from a 500-ml liquid culture, was resuspended in 3 volumes anaerobic 50 mM Tris-HCl buffer, pH 8.0 containing 1 mM sodium dithionite ($Na_2S_2O_4$). The cell suspension was transferred to a cooled, 30-ml rossette cell (Branson) using a syringe flushed with the anaerobic buffer; the cells were lysed on ice under positive argon atmosphere with a cell disruptor (Branson, micro tip) for 5 min with a 50%

duty cycle at a power level of 4. The ruptured cell suspension was transferred to a centrifuge tube (Sorvall, SS 34 rotor) containing DNase and RNase (Sigma), both at a final concentration of 10 mg/L. The resulting suspension was incubated for 15–20 min at room temperature, and then centrifuged at 35,000 rpm for 30 minutes (Beckman, TY35 rotor). The supernate was removed, mixed completely under anaerobic conditions using a 10-ml syringe and pelleted into liquid nitrogen until assayed for crude extract activity.

Purification of MoFe protein

Wild type and DJ540 (α-195^{gln}) MoFe proteins were purified in parallel using the following procedure to provide for comparative biochemical characterizations. The specific activity of hydrogen evolution and the migration pattern on an SDS-PAGE gel were monitored at each stage of the protocol to evaluate the stability of the protein and to determine the further scheme of purification. Buffers were degassed completely before the addition of $Na_2S_2O_4$ to a final concentration of 1 mM, and all columns were equilibrated with anaerobic 25 mM Tris-HCl buffer, pH 7.4.

Thawed cells were resuspended in 3 volumes of 50 mM Tris-HCl buffer, pH 8.0 and disrupted in a 150-ml rossette cell under argon for 5 min with a 50% duty cycle at a power output of 8. The ruptured cell suspension was treated with nucleases as above, heated in a water bath for 5 min at 56°C (wild type) or 50°C (DJ540), cooled and centrifuged at 35,000 rpm for 30 minutes (Beckman, TY35 rotor). The dark brown supernatant was then loaded at 8 ml/min on a 5 X 15 cm Q–sepharose column (Pharmacia) using a peristaltic pump (Pharmacia). The nitrogenase component proteins in the column eluate were monitored by absorbance of the Fe-S cluster at 405 nm. Neutral or positively-charged

molecules including basic proteins were eluted by washing the column with two column volumes of the above buffer until the absorbance value equaled the baseline absorbance. The nitrogenase component proteins were eluted using a linear NaCl gradient (0.1 to 0.7 M with a total volume of 1.4 L) controlled by FPLC apparatus (Pharmacia). Under these conditions both the wild type and the altered MoFe protein elute at approximately 0.37 M NaCl, and thus are separate from the Fe protein which elutes at approximately 0.6 M NaCl. The partially purified fraction of the MoFe protein collected from the Q–sepharose column was brought to 0.5 M ammonium sulfate ($(NH_4)_2SO_4$) by the addition of an equal volume of anoxic 1M $(NH_4)_2SO_4$ and loaded on a 3 X 15 cm phenyl sepharose column (Pharmacia), equilibrated with degassed 25 mM Tris-HCl buffer, pH 7.4 containing 1 mM $Na_2S_2O_4$ and 0.5 M $(NH_4)_2SO_4$. A linear, decreasing $(NH_4)_2SO_4$ gradient (0.5 M to 0 M) was applied to elute the MoFe protein. The gradient was paused when MoFe protein eluted at 0.1 M $(NH_4)_2SO_4$. The collected MoFe fraction from this step was then placed in a ultrafiltration cell concentrator (Amicon) fitted with XM30 membrane, and was first concentrated under 20 psi argon pressure. Then, the residual $(NH_4)_2SO_4$ was removed by repeated dilution and concentration of the fraction using degassed 25 mM Tris-HCl, pH 7.4, 0.25 M NaCl, 1 mM $Na_2S_2O_4$ buffer as the diluent. The purified, dialyzed, and concentrated MoFe protein was then stored in liquid nitrogen. The Fe protein fraction obtained from the Q-sepharose column was also concentrated by ultrafiltration as described above. This step was especially efficient in removing the small molecular weight flavodoxin (MW $\approx$ 20,000) from the Fe protein fraction. This Fe protein was of sufficient purity at this stage.

Purification of Fe protein

Two Pharmacia Q-Sepharose columns (3 x 15 cm and 1.5 x 12 cm) were prepared by equilibrating with anoxic 25 mM Tris-HCl buffer, pH 7.4 containing 1 mM $Na_2S_2O_4$. Crude extracts were prepared from approximately 50 g cells of wild type (Av2-100^{Arg}), DJ275 (Av2-100^{Leu}), DJ285 (Av2-100^{Tyr}), or DJ359 (Av2-100^{Phe}) strains by the procedure described above that includes the heat treatment (56°C, 5 min). The resulting extract was then loaded at 10 ml/min on the Q-Sepharose column (3 x 15 cm) using a peristaltic pump. Using a Pharmacia FPLC instrument, the column was washed with two column volumes of the Tris equilibration buffer, and a linear NaCl gradient (0.1 M to 1 M, total volume of 2 L) was applied to elute the nitrogenase component proteins. The MoFe and Fe proteins were separately eluted at NaCl concentrations of approximately 0.35 M and 0.5 M, respectively. The collected high salt solution of the Fe protein was brought to ≈ 0.1 M NaCl by diluting with 5 volumes of the anoxic 25 mM Tris-HCl buffer, pH 7.4 and then loaded at 5 ml/min on the second Q-Sepharose column (1.5 x 12 cm). After washing the column with one column volume of the Tris buffer, 0.6 M NaCl was applied to the column in a reversed direction to elute the Fe protein. The resulting concentrated Fe protein fraction was pelleted into liquid nitrogen until needed. The MoFe protein fraction obtained from the first Q-Sepharose column (3 x 15 cm) was also concentrated on the second Q-Sepharose column as described for the Fe protein, and was of sufficient purity to complement the Fe protein assay.

Nitrogenase assays

MoFe protein and Fe protein specific activities were measured in crude extracts in the

presence of an optimal amount of the separately added, purified, complementary component protein. Acetylene reduction and proton reduction activities were assayed in 9.25-ml reaction vials fitted with butyl rubber serum stoppers and aluminum seals. Each 1-ml reaction contained 25 mM TES, pH 7.4, 2.5 mM ATP, 5 mM $MgCl_2$, 30 mM creatine phosphate, 0.125 mg creatine phosphokinase, and 20 mM $Na_2S_2O_4$. The reaction vials which contained the ATP regeneration system and distilled water were degassed and flushed with the appropriate gases on an automated manifold system with 4 cycles of 100-sec evacuation and 20-sec gassing. A gas mixture of 10% C_2H_2 / 90% Ar or 100% Ar was used for C_2H_2 reduction or proton reduction assays, respectively. Dithionite and an optimal amount of Fe protein were added to each reaction vial using gas tight syringes (Hamilton), and the vials were incubated at 30°C for 5 minutes. The nitrogenase reaction was started by adding 50 µl of crude extract and terminated after incubation at 30°C for 8 min, by the addition of 0.25 ml 2.5 M H_2SO_4.

The headspace gas was analyzed for products of nitrogenase catalysis by injecting 0.2 ml gas into a gas chromatograph using a 0.5-ml open-lock syringe. The amounts of C_2H_4 and C_2H_6 produced were determined by gas chromatography using a Poropak N column and a FID detector (Shimatsu). Hydrogen evolution was measured using a molecular sieve 5A column and a TCD detector. Calibrations were performed using standard gases of 1 ppm C_2H_4, 1 ppm C_2H_6, or 1% H_2 (Scottys). Activities of purified MoFe proteins were measured under conditions of high electron flux using 0.075 mg MoFe protein and 0.925 mg Fe protein per each reaction. These concentrations represent a molar ratio of approximately 40 Fe protein : 1 MoFe protein. Assays were performed as described above except that the reactions were started by addition of purified MoFe protein.

Preparation of gas mixtures for the kinetic experiments

Pre-purified Ar, N_2 and 10% C_2H_2 (in Ar) were obtained from Airco, and CO was purchased from Matheson gas products. Argon was passed through the BASF catalyst column to remove residual O_2, whereas the other gases were used directly. Each gas was analyzed by gas chromatography to insure the absence of O_2 and other contaminants (for example, C_2H_4 in 10% C_2H_2 gas tank) that affect the enzyme assays. Gas tight syringes (Hamilton) with hypodermic needles (gauge 22) were used to transfer the gases. Application of a very small amount of gas (CO) involved serial dilution in Ar before being mixed with other gases. Serum vials (60 ml and 9 ml, Wheaton) sealed with butyl rubber stoppers and aluminum seals, were used to hold gases before they were mixed into reaction vials. The small serum vials (9 ml) were used as the reaction vials. The headspace volume in each reaction vial was approximately 8 ml after subtracting the reaction liquid (1 ml) from the original volume. The total pressure in the assay vials was maintained at 1 atmosphere.

Figure 15 and Table V describe the preparation of gas mixtures of desired concentrations in each assay vial. Procedures are explained in detail by using Vial #6 as an example. The serum vials (four 60-ml Ar, eight 60-ml N_2, and sixteen 9.5-ml 10% C_2H_2 vials) are degassed and filled with the appropriate gases using the automated evacuate-fill machine at 4 duty cycles of 100-sec evacuation and 20-sec fill. Assay vials containing distilled water and the ATP generating system are degassed and filled with Ar using the suck-blow machine. A hypodermic needle is inserted through the butyl rubber stopper of each vial and quickly removed to release the gas pressure inside. A 10-ml gas tight syringe with a hypodermic needle is flushed with argon several times in a vial placed on a

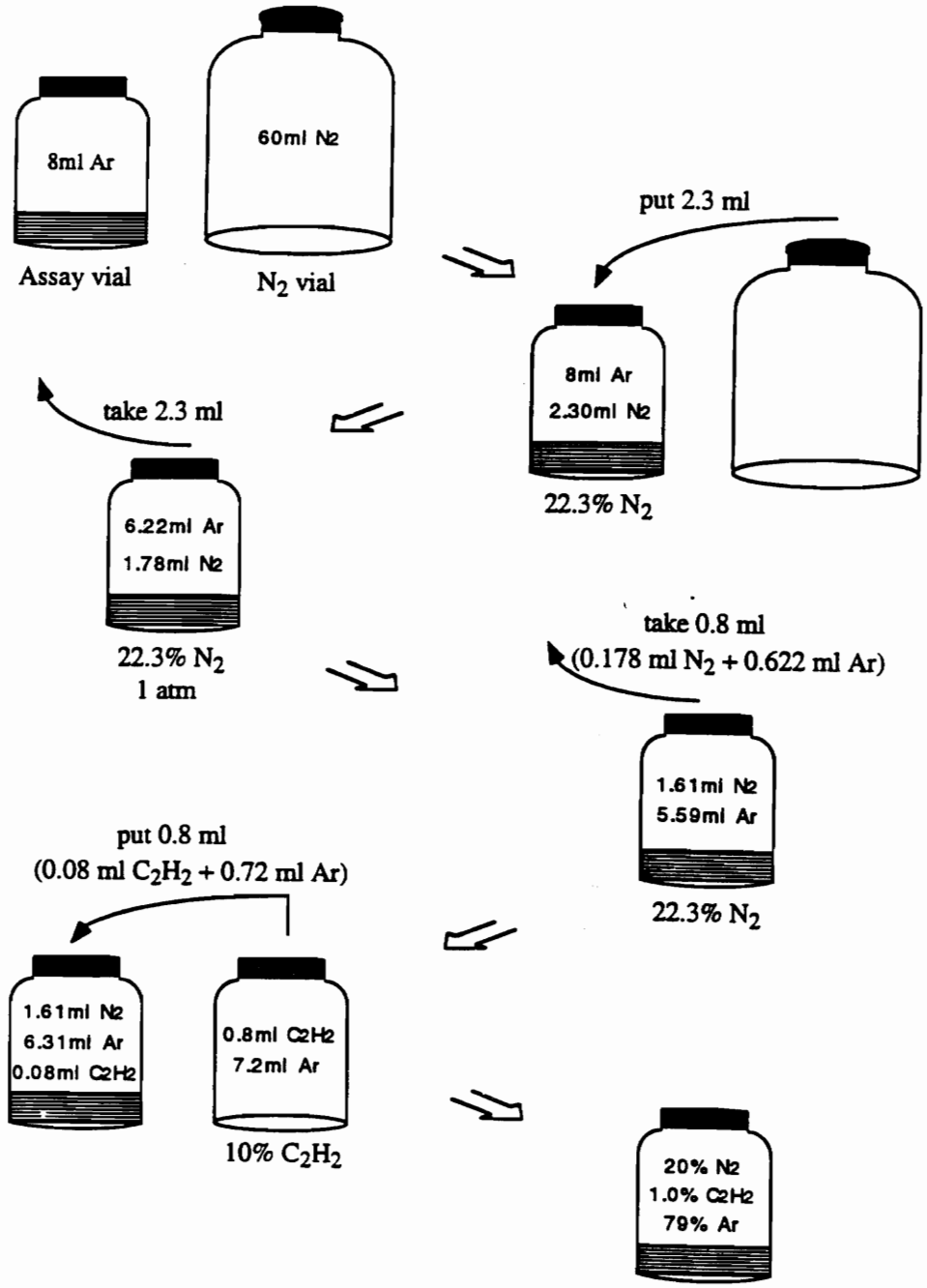

Figure 15. Preparation of gas mixtures of desired concentrations in the Vial #6 of Table V.

Table V. Preparation of gas mixtures in the assay vials. Gas concentrations are shown in percentage. The headspace of the assay vials is 8 milliliters. The symbols used are: (■) ml C_2H_2 to add to vial; (●) % N_2 before addition of C_2H_2; (□) ml N_2 to add to vial; and (○) ml Ar to add to vial.

C_2H_2	N_2			
	0%	20%	40%	60%
0.5% ■ 0.4ml	Vial #1 ● 0% □ 0 ml	#2 ● 21.0% □ 2.13 ml	#3 ● 42.1% □ 5.82 ml	#4 ● 63.1% ○ 4.68 ml
1.0% ■ 0.8ml	#5 ● 0% □ 0 ml	#6 ● 22.3% □ 2.30 ml	#7 ● 44.5% □ 6.41 ml	#8 ● 66.6% ○ 4.01 ml
1.5% ■ 1.2ml	#9 ● 0% □ 0 ml	#10 ● 23.5% □ 2.46 ml	#11 ● 47% □ 7.09 ml	#12 ● 70.6% ○ 3.33 ml
2.0% ■ 1.6ml	#13 ● 0% □ 0 ml	#14 ● 25% □ 2.67 ml	#15 ● 50% □ 8.00 ml	#16 ● 75% ○ 2.67 ml

manifold. Nitrogen (2.3 ml) is drawn from a N_2 vial using this syringe. The volume of N_2 drawn from the 60-ml N_2 vial should not exceed 10 ml to avoid creating great negative pressure inside the vial; this way no air will be pulled into the syringe when the needle is removed. Nitrogen (2.3 ml) contained in the syringe is then injected into Vial #6 and mixed thoroughly with Ar in the vial by pumping the syringe 2 to 3 times. Positive pressure inside the reaction vial, generated by introducing the extra 2.3 ml of N_2, is immaterial as the system is gas-tight. The same volume (2.3 ml) of the homogeneous N_2-Ar mixture is then removed to maintain the inside pressure at 1 atmosphere. The assay Vial #6 now contains 22.3% N_2 and 77.7% argon. A 1-ml syringe fitted with a needle is flushed with argon as described above and inserted into Vial #6 to remove 0.8 ml gas mixture; the syringe is flushed again with argon. An equal amount (0.8 ml) of 10% C_2H_2 is taken from one of the 10% C_2H_2 vials and injected into Vial #6. The gases are mixed as above and the needle is withdrawn. The Vial #6 now contains a 20% N_2, 1.0% C_2H_2, and 79% Ar mixture. Two different techniques were used in the procedure; one which generates positive pressure inside the assay vial and the other which creates negative pressure. When dealing with a volume larger than the headspace volume of the reaction vial, the latter (the technique that creats negative pressure) is avoided because the excessive negative pressure may introduce air into the vial. Assay Vials #4, #8, #12, and #16 were degassed and filled with N_2 instead of Ar, and the appropriate amount of Ar is injected to make the desired N_2 concentration. Generation of too much positive pressure in the assay vials was therefore avoided. Calculations of the volume of each gas to add to a vial are shown below using Vial #6 as an example.

1. If A is the amount of 10% C_2H_2 to be added to make 1% C_2H_2 in vial, then;

(A / 8) x 100 x 0.1 = 1%, therefore, A = 0.8 ml

2. Calculate the percent N_2 in the vial (the amount of N_2 denoted by B) before addition of C_2H_2. When 0.8 ml 10% C_2H_2 is added to the vial, the final N_2 concentration will be 20 percent.

   B - (0.8 x B) / 8 = 8 x 0.2, therefore, B = 1.78 ml (1.78 / 8) x 100 = 22.3%

3. Calculate what volume of 100% N_2 (denoted by C) to add to make a final N_2 concentration of 22.3% in the vial.

   [C / (C + 8)] x 100 = 22.3, therefore, C = 2.30 ml

Treatment of kinetic data

Kinetic data were analyzed by a computer program called EZ-FIT (described by Frank W. Perrella, DuPont, Glenolden, Pa). Experimental data points obtained from several measurements were used to obtain double-reciprocal plots (1/velocity versus 1/substrate). The inhibition patterns observed from these double-reciprocal plots were used to choose the appropriate rate equations for the program. Data showing competitive inhibition pattern were fitted to the equation $v = VA/[K(1 + I/Ki) + A]$ in which A = substrate concentration, I = inhibitor concentration, v = initial velocity, V = maximum velocity, and Ki = inhibition constant. Data showing non-competitive inhibition were fitted to the equation $v = VA/[K(1 + I/Ki) + A(1 + I/Ki)]$.

Ammonia (NH_3) assay

Nitrogen reduction assays were performed under 100% N_2 in 35 mM HEPES buffer, pH 7.4, because TES buffer used in all the assays for gas analysis, interfered with NH_3

analysis. In these assays, the nitrogenase reaction was terminated by 0.4 M EDTA, pH 8.0, and the liquid mixture was applied to Dowex 1 X 2 ion exchange column (Cl- form, 200-400 mesh, Bio-Rad) to remove inhibitory components of the assay. Each reaction mixture was then assayed for NH_3 by the indophenol method (Chaney and Marbach, 1962). The flow through (0.5 ml) from the column was added to a mixture of 0.3 ml Na phenate (5% (w/v) phenol plus 2.5% (w/v) NaOH), 0.45 ml nitroprusside (0.02%, w/v), and 0.45 ml Na hypochlorite (100%), and incubated for 40 min at room temperature. Ammonia was measured by the indophenol absorbance at 630 nm using $(NH_4)_2SO_4$ as the standard (0 - 0.2 μmole/ml). Creatine which is produced during ATP regeneration from creatine phosphate interfered with the assay when it was present in large quantities in the reaction (Dilworth et al., 1992). The inhibitory effect of creatine, however, was not significant in our 8-min assays based on the calibration curves developed to correct for the creatine interference.

Assay for ATP hydrolysis (creatine assay)

The liquid sample collected from the Dowex ion exchange column was assayed for creatine as previously described by Ennor (1957). Samples (0.5 ml) were treated with 1 ml 0.05 M *p*-chloromercuribenzoate followed by 2 ml 1% α-naphthol and 1 ml 0.05% diacetyl. The volume was adjusted to 10 ml by the addition of distilled water and the reaction was incubated for 20 min at room temperature. Sample absorbance at 520 nm was determined using a spectrophotometer. The concentration range of the creatine standard used was 0 - 2.0 μmole per milliliters.

Hydroxylamine (NH_2OH) assay

Modified Blom's method (Novak and Wilson, 1948) was used to determine the potential NH_2OH production by the altered MoFe protein. Preparation of the reagents is described in detail in the Novak and Wilson paper. The EDTA-stopped reaction mixture (1 ml) was treated with 1 ml sulfanilic acid reagent and 0.5 ml iodine-acetate and mixed for 2 min by hand. Excess iodine was decolorized with thiosulfate. The resulting diazo compound was reacted with 1 ml α-naphthylamine reagent and the amount of NH_2OH was quantitated by measuring the sample absorbance at 500 nm (standard NH_2OH range ≈ 0 - 9 μg/ml).

Hydrazine (N_2H_4) assay

Enzyme-bound hydrazine (N_2H_4) was assayed by quenching the nitrogenase reaction with acid during the nitrogenase turnover as described previously (Thorneley et al., 1978). Assays were performed for 5 min under N_2 and quenched with 2 ml 95% ethanol containing 1 M HCl and 0.07 M *para*-dimethylaminobenzaldehyde. The reaction mixture was centrifuged for 10 min to remove protein and N_2H_4 was measured as *para*-dimethylaminobenzaldehyde hydrazone at 458 nm using hydrazine sulfate (0 - 0.75 μM) as a standard.

Protein assay

Protein concentration of the crude extracts and purified proteins was determined by the Biuret method using bovine serum albumin (0 - 1mg/ml) as a standard.

Chapter I. Studies on the role of the MoFe protein α–subunit histidine–195 residue in FeMo–cofactor binding and nitrogenase catalysis

This chapter represents a submitted publication (Kim, C-H., Newton, W. E., & Dean, D. R. 1994) solely based on the author's work. I thank Claudia Vigil for help in mutant strain constructions, Dick Dunham (University of Michigan) for performing EPR spectroscopy and Jeff Bolin and Steve Muchmore (Purdue University) for helpful discussions and computer modelling.

Introduction

Biological nitrogen fixation is catalyzed by nitrogenase, an enzyme composed of two metal–containing component proteins called the Fe protein and the MoFe protein. During catalysis, electrons are delivered one at a time from the Fe protein to the MoFe protein in a process involving component–protein association and dissociation and hydrolysis of at least two MgATP for each electron transfer. Among the important questions attached to nitrogen fixation research are understanding: (i) the structures of the metal centers that participate in electron transfer and/or substrate binding; (ii) the organization of the metalloclusters within the polypeptides and the contribution of those corresponding polypeptide environments to substrate binding and electron transfer; and (iii) the integration of MgATP binding and hydrolysis with intermolecular electron transfer. Considerable insight concerning these issues has been gained by recent reports on the three dimensional structures of both nitrogenase component proteins (Georgiadis *et al.*, 1992; Kim and Rees 1992a; Kim and Rees 1992b; Kim *et al.* 1993; Bolin *et al.*, 1993) and this insight has been

summarized in recent review articles (Kim and Rees, 1994; Dean *et al.* 1993).

There is compelling evidence that one of the metalloclusters contained within the MoFe protein, called FeMo–cofactor (Shah and Brill, 1977), provides the substrate–binding and –reduction site (Shah and Brill, 1977; Rawlings *et al.*, 1978; Hawkes *et al.*, 1984; Scott *et al.*, 1990). FeMo–cofactor is currently modeled as having a metal–sulfide core constructed from sulfide bridged $MoFe_3S_3$ and Fe_4S_3 subcluster fragments (Kim and Rees, 1992a; Chan *et al.*, 1993; also see Figure 16). In addition to its metal–sulfide core, FeMo–cofactor also contains an organic constituent, homocitrate (Hoover *et al.*, 1989), which is covalently attached to the Mo atom through its 2–hydroxyl and 2–carboxyl groups.

Prior to the availability of direct structural information, Dean and Newton proposed a model (Dean and Jacobson, 1992; Dean *et al.*, 1990a, b; Scott *et al.*, 1992), based primarily on deduced amino–acid sequence comparisons and amino–acid substitution studies, where certain of the amino acid residues contained within the MoFe–protein α–subunit from *A. vinelandii* were targeted as being located within the FeMo–cofactor–binding domain. These residues were suggested to have structural roles in positioning FeMo–cofactor within the polypeptide pocket and to have potential catalytic functions in fine tuning FeMo–cofactor's electronic features. Relevant to the present work, an altered MoFe protein which has an asparagine substitution for the interspecifically conserved α–histidine–195 residue, was shown to exhibit significantly changed catalytic and spectroscopic properties (Scott *et al.*, 1990; Scott *et al.* 1992). The subsequent structural models confirmed that this α–histidine residue is closely associated with FeMo–cofactor but it is apparently not bonded covalently to the FeMo–cofactor. In the

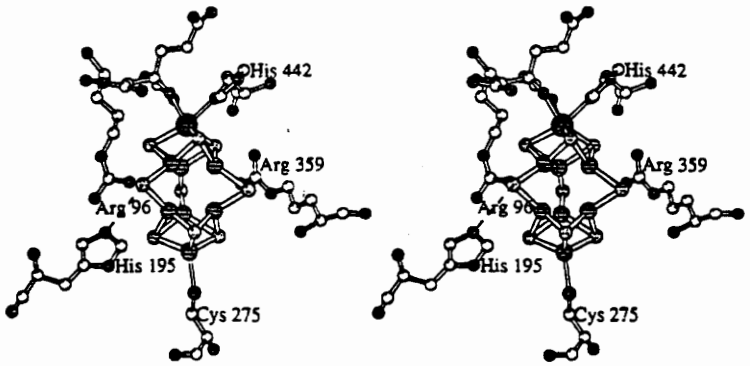

Figure 16. Stereoscopic view of FeMo–cofactor and selected polar residues in its environment. FeMo–cofactor is ligated to two protein residues, α-442^{his}, and α-275^{cys}. Also interacting closely with FeMo–cofactor are α-96^{arg},α-195^{his}, and α-359^{arg}. A molecule of homocitrate provides two bonds to the Mo atom of FeMo–cofactor, and is shown in the upper portion of the figure. An NH→S hydrogen bond of α-195^{his} to FeMo–cofactor is represented by a dashed line. The largest and darkest of the spheres in FeMo–cofactor is the Mo atom. The spheres of intermediate size and shade are Fe atoms, while the smallest and lightest spheres represent S atoms. In the homocitrate and protein components, C atoms are unshaded, whereas the O and N atoms are the same, darker shade. The figure was generated by Dr. Jeff Bolin and Steve Muchmore at Purdue University with the program MOLSCRIPT (Kraulis, 1991).

present study, several new mutant strains, which produce altered MoFe proteins that have other amino acids substituted for the α–histidine–195 residue, were constructed. The effect of these amino–acid substitutions on the catalytic and spectroscopic features of the altered MoFe proteins produced by the corresponding mutant strains are described and discussed in the context of the available structural models of FeMo–cofactor and its polypeptide environment.

It was also previously concluded, based on information gained from a spectroscopic technique called electron spin echo envelope modulation, that the observed N–coordination of FeMo–cofactor requires the α–histidine–195 residue (Thomann *et al.* 1991). Structural studies have revealed that the α–histidine–442 residue rather than the α–histidine–195 residue, is covalently coordinated to FeMo–cofactor.

Methods and materials

Mutant strain construction. Site–directed mutagenesis, gene replacement, and the isolation of mutant strains were performed as described or cited previously (Brigle *et al.*, 1987; Jacobson *et al.*, 1989). The isolation of strain DJ528 was described previously (Scott *et al.*, 1990). A mixed set of oligonucleotides having the sequence, 5'TCCCAGTCCCTGGGCXXXCACATCGCCAACGAC3', was used for mutagenesis of the *nifD* gene during construction of other mutant strains. XXX indicates degenerate positions within the mixed oligonucleotide set and corresponds to the 195^{his} codon within the *nifD* gene sequence (Brigle *et al.*, 1985). For clarity in presentation, strains are indicated by both a numerical designation and the amino acid that occupies the MoFe protein α–subunit–195 position. For example, DJ527 (α–195^{his}) designates the parental strain

used in the construction of mutants strains. It produces wild–type MoFe protein having a histidine residue at the α–subunit–195 position. This strain also contains a deletion and an insertion mutation within the *hoxKG* gene cluster (Menon *et al.*, 1990) such that uptake hydrogenase activity is eliminated. Mutants were constructed using a parental strain having *hoxKG* deleted so that nitrogenase–catalyzed hydrogen–evolution activities could be accurately measured in crude extracts without interference from uptake hydrogenase activity. The plasmid necessary for construction of DJ527, pALMZ'1, was kindly provided by Rob Robson (University of Georgia).

Preparation of crude extracts and nitrogenase purification. Techniques for culturing *A. vinelandii*, media preparation, nitrogenase derepression, preparation of crude extracts, anaerobic purification of nitrogenase, and maintaining anoxic conditions were performed as previously described or cited by Scott *et al.* (1992). Isolation of nitrogenase component proteins from crude extracts prepared from DJ527 (α–195^{his}, the isogenic parental strain) and DJ540 (α–195^{gln}) was performed as follows. Heat–treated crude extracts (heat treatment was either at 56 °C for 5 min for the wild–type crude extract or 50 °C for 5 min for the mutant crude extract) was prepared in a degassed 25 mM Tris-HCl buffer, pH 7.4, made anoxic by the addition of 1 mM $Na_2S_2O_4$ and loaded on a 5 X 15 cm Pharmacia Q Sepharose column using a peristaltic pump. Flow rates for all column chromatography procedures were maintained at approximately 8 ml/min. After washing the loaded protein sample with two column volumes of the above buffer, the nitrogenase component proteins were eluted using a linear NaCl gradient (0.1 to 0.7 M) controlled by Pharmacia FPLC pumps. Under these conditions, both the wild–type and the altered MoFe proteins eluted at

approximately 0.37 M NaCl and Fe protein eluted at approximately 0.6 M NaCl. The partially purified MoFe protein was then brought to 0.5 M $(NH_4)_2SO_4$ by the addition of an appropriate amount of a degassed $(NH_4)_2SO_4$ stock solution (1.0 M in 25 mM Tris-HCl buffer, pH 7.4) made anaerobic by the addition of 1.0 mM $Na_2S_2O_4$ and loaded on a 3 X 15 cm Pharmacia Phenyl Sepharose column pre–equilibrated with degassed 25 mM Tris-HCl buffer (pH 7.4) containing 1 mM $Na_2S_2O_4$ and 0.5 M $(NH_4)_2SO_4$. A linear, decreasing $(NH_4)_2SO_4$ gradient (0.5 M to 0 M) eluted the MoFe protein at about 0.1 M $(NH_4)_2SO_4$. The MoFe protein was then concentrated in an Amicon microfiltration concentrator fitted with an XM30 membrane using approximately 20 psi Ar pressure. The residual $(NH_4)_2SO_4$ was removed by repeated dilution and concentration of the sample using degassed 25 mM Tris-HCl, pH 7.4, 0.25 M NaCl and 1 mM $Na_2S_2O_4$ buffer as the diluent. The Fe–protein fraction obtained from the Q–Sepharose column was also concentrated as described for the MoFe protein and was of sufficient purity at this stage for the described studies. Purity of protein samples was determined by gel electrophoresis using the procedure of Laemmli (1970) as modified by Scott *et al.* (1992).

Electron paramagnetic resonance spectroscopy. Derepressed whole cells of wild type and the various mutant strains were treated individually in 50 mM Tris, pH 8.0, with 5 mM $Na_2S_2O_4$ and 0.1 mM methyl viologen under argon for 5 min. The suspension was then transferred under anoxic conditions to a degassed, capped EPR tube. After centrifugation at 600 g for 5 min, the supernatant was removed and the contents of the EPR tube frozen in liquid nitrogen. The EPR spectra of whole–cell preparations were recorded at 9.22 GHz and 5 mW on a Varian Associates E–line Spectrometer with a 100–kHz field modulation of

10 G at 12 K maintained by liquid helium boil–off. The EPR spectra of purified wild type and α–195^{gln} MoFe proteins were recorded under identical spectral conditions, except the microwave power was 20 mW and the 100–kHz field modulation was 25 G.

Assays and preparation of gases for kinetic experiments. MoFe–protein and Fe–protein specific activities were respectively measured in crude extracts in the presence of an added optimal amount of the separately purified, complementary component protein. Acetylene– and proton–reduction activities were assayed in 9.25–ml reaction vials fitted with butyl rubber stoppers and aluminum seals. Each 1.0–ml reaction contained 25 mM TES, pH 7.4, 2.5 mM ATP, 5.0 mM $MgCl_2$, 30 mM creatine phosphate, 0.125 mg creatine phosphokinase, and 20 mM $Na_2S_2O_4$. A gas mixture of either 10% C_2H_2 / 90% Ar or 100% Ar were used for determination of acetylene reduction and proton reduction, respectively. For crude extract assays, the reaction was started by the addition of 50 µl of crude extract and terminated after incubation at 30 °C for 8 min by injecting 0.25 ml of 2.5 M H_2SO_4. Ethylene and ethane production was quantified by gas chromatography using a Poropak N column and a flame ionization detector (Shimatsu, Tokyo, Japan). H_2 evolution was also quantified by gas chromatography using a 5A molecular sieve column (Supelco, Bellefonte, PA) and a thermal conductivity detector. Calibrations were performed using standard gases of 1 ppm C_2H_4, 1 ppm C_2H_6 or 1% H_2 (Scott Specialty Gasses, Plumsteadville, PA). Activities of purified MoFe proteins were measured under conditions of high electron flux using 0.075 mg MoFe protein and 0.925 mg Fe protein per reaction. These concentrations represent a molar ratio of approximately 40 Fe protein : 1 MoFe protein. Assays were performed as described above except that the reactions were

started by addition of purified MoFe protein. For the determination of kinetic parameters, gas mixtures of the desired concentrations were prepared individually in each assay vial using gas stocks in 60–ml serum vials. Gas–tight syringes (Hamilton, Reno, NV) with 22–gauge hypodermic needles were used to mix and transfer the gases. The very small amounts of CO required for some experiments involved prior serial dilution in Ar before mixing with the other gases. Total pressure in all assay vials was 1 atm. After the gas mixtures were prepared, assays were performed as described above. Nitrogen–reduction assays were performed in 35 mM HEPES buffer, pH 7.4, because the TES buffer used in other assays interferes with the NH_3 analysis. In these assays, N_2 reduction was terminated by the addition of 0.25 ml of 0.4 M EDTA, pH 8.0. Each reaction mixture was then individually applied to a Bio–Rad Dowex 1 x 2 cm ion–exchange column (Cl^- form, Dilworth *et al.*, 1992) before being assayed for NH_3 by the indophenol method (Chaney and Marbach, 1962). Hydrolysis of MgATP during nitrogenase turnover was also measured from the liquid sample collected from the Dowex column by the creatine assay as previously described (Dilworth *et al.*, 1992; Ennor, 1957). Assays for hydroxylamine and hydrazine formation were performed as described by Novak and Wilson. (1948) and Thorneley *et al.* (1978), respectively. In experiments designed to determine whether or not N_2 is a reversible inhibitor of proton reduction, MoFe protein was first assayed under Ar or N_2 atmosphere at 30°C for 5 min. The reaction vial was then degassed and flushed with Ar and re–incubated at 30°C for 8 min. and then terminated by the addition of 0.25 ml of 2.5 M H_2SO_4.

Results

Diazotrophic growth characteristic and nitrogenase catalytic activities in crude extracts.

Site–directed mutagenesis and gene–replacement procedures were used to construct six different *A. vinelandii* mutant strains, each of which produces an altered MoFe protein having an individual amino–acid substitution located at the α–subunit 195 position occupied by a histidine residue in the wild–type strain. Each of these individual substitutions (asn, tyr, gln, leu, thr, and gly) results in a strictly Nif- phenotype in the corresponding mutant strain (Table VI). Crude extracts prepared from nitrogenase–derepressed wild–type and mutant strains were assayed for nitrogenase component–protein activities and the results of these assays are compared in Table VI. All strains constructed in the present study were prepared in a *hoxGK* background (see Experimental Procedures) so that proton–reduction activities could be accurately measured in crude extracts. It should be noted that, because crude extracts are prepared from nitrogenase–derepressed cells, it is difficult to accurately compare activities of the MoFe protein in different preparations without an estimate of the relative levels of nitrogenase derepression. In the present experiments, estimation of the relative levels of nitrogenase accumulation in crude extracts from different strains was accomplished by either comparison of one–dimensional gel electrophoresis profiles (data not shown) or by measuring the corresponding levels of Fe–protein activity (Table VI). Because the relative levels of accumulation of the nitrogenase components were shown to be roughly equal by these measurements, quantitative differences in MoFe–protein specific activities present in different mutant–strain crude extracts can be attributed to specific alterations in their respective MoFe proteins. Although none of the mutant strains is able to fix N_2 at a level

Table VI: Nif phenotypes of α–195^{his} mutant strains and MoFe protein and Fe protein activities in crude extracts from those strains.

Strain[a]	Substitution at α-195	Codon	Nif Phenotype	MoFe Specific Activity[b]			Fe Specific Activity[b]
				C_2H_4	C_2H_6	H_2	H_2
DJ527	WT (His)	CAC	+	45.3	0.0	64.0	35.8
DJ528	Asn	AAC	–	3.7	1.0	13.0	36.4
DJ538	Tyr	UAU	–	5.5	0.0	20.7	23.3
DJ540	Gln	CAA	–	30.7	0.0	48.8	36.0
DJ542	Leu	UUA	–	11.7	0.2	22.0	49.7
DJ544	Thr	ACA	–	2.8	0.0	18.2	27.1
DJ546	Gly	GGG	–	2.6	0.0	16.1	33.1

[a] All strains are deleted for the uptake hydrogenase structural genes. [b] Crude extract specific activity is expressed as nmoles of C_2H_4, C_2H_6, or H_2 produced per min x mg total extract protein. C_2H_4 and C_2H_6 were produced under a 10% C_2H_2 / 90% Ar atmosphere and H_2 was produced under a 100% Ar atmosphere in the presence of saturating levels of purified complementary protein. WT indicates the parental wild type strain.

sufficient to support diazotrophic growth, crude extracts prepared from the mutant strains exhibited various levels of acetylene– and proton–reduction activities. These properties are particularly striking in the case of DJ540 (α–195^{gln}) where acetylene and proton reduction activities were, respectively, 67% and 76% of the corresponding wild–type activities.

It was previously shown that MoFe protein from DJ528 (α–195^{asn}) catalyzes the reduction of acetylene by both two and four electrons to yield ethylene and ethane (Scott *et al.*, 1992), an activity not exhibited by wild type. Mutant–strain crude extracts were, therefore, examined for their ability to produce both ethylene and ethane (Table VI). Extracts from DJ528 (α–195^{asn}) and DJ542 (α–195^{leu}) are able to reduce acetylene to both ethylene and ethane, but extracts from wild type and the other mutant strains can only reduce acetylene by two electrons to yield ethylene. The possibility that ethane formation catalyzed by extracts from DJ528 and DJ542 results from the activity of a V–dependent nitrogenase was eliminated by spectroscopic, electrophoretic, and catalytic considerations as described previously (Dean *et al.*, 1990a, Scott *et al.*, 1990).

Effect of CO and N_2 on MoFe protein catalyzed proton reduction.

Previous studies have shown that certain amino–acid substitutions located within FeMo–cofactor–binding domains result in proton reduction that is sensitive to CO (Scott *et al.*, 1992). For example, substitution of the α–191glutamine residue by lysine results in MoFe protein–catalyzed proton–reduction activity that is about 50% inhibited by CO (Scott *et al.*, 1992), whereas, wild–type MoFe protein–catalyzed proton reduction is insensitive to CO (Hardy *et al.*, 1965; Bulen *et al.*, 1965). Results summarized in Table VII show that the DJ544 MoFe protein (α–195^{thr}) also exhibits CO–sensitive proton–reduction activity

Table VII: CO and N_2 inhibition of H_2 evolution catalyzed by crude extracts prepared from wild type and α–195^{his} mutant strains.

	Specific Activity[a] of H_2 evolution under		
Substitution at α-195	100% Ar	10% CO / 90% Ar	100% N_2
WT (His)	66.0	61.0	19.4
Asn	12.8	15.0	12.2
Gln	53.7	48.6	18.8
Leu	27.8	25.8	32.1
Thr	23.5	10.7	18.2

[a] Specific activity is expressed as nmoles of H_2 produced per min x mg crude extract protein assayed in the presence of optimal levels of purified Fe protein.

but proton reduction catalyzed by the altered MoFe protein from the other mutant strains examined is insensitive to CO.

The observation that various amino–acid substitutions placed at the α–195 position result in MoFe proteins which exhibit detectable acetylene– and proton–reduction activities, but are apparently unable to reduce N_2 (see later results), raises the question of whether or not these altered MoFe proteins have the ability to bind N_2. To investigate this possibility, we asked if N_2 is able to inhibit proton reduction catalyzed by the mutant–strain crude extracts. These experiments reveal that N_2 causes marked inhibition of proton reduction catalyzed by either wild–type MoFe protein (α–195^{his}) or DJ540 MoFe protein (α–195^{gln}). In contrast, N_2 does not significantly inhibit proton reduction catalyzed by altered MoFe protein from the other mutant strains (Table VII).

Whole–cell EPR spectra.

The electron paramagnetic resonance (EPR) spectra of whole cells of the mutant strains all exhibit line shapes that are similar to wild type (data not shown). However, the spectra of strains, DJ542 (α–195^{leu}), DJ528 (α–195^{asn}), and DJ546 (α–195^{gly}), exhibit greatly diminished EPR intensity (10%, 8%, and 3%, respectively, of wild type). The apparent g values of these samples are also slightly shifted with respect to those of wild type. In contrast, the whole–cell EPR spectrum of DJ540 (α–195^{gln}) has an intensity comparable to wild type but is more rhombic with apparent g values of 4.36 and 3.64. Compared with the other strains studied, there is only a mild modification in the whole–cell EPR signal of DJ540 (α–195^{gln}) indicating only a slight perturbation in the FeMo–cofactor environment caused by the substitution. The changed EPR signals from the various altered nitrogenases

are correlated with changes in their corresponding catalytic properties; a correlation that supports the idea that FeMo–cofactor is located at or is part of the substrate–reduction site. However, although a rough correlation exists between EPR signal intensity and H_2–evolution activity, no obvious correlation exists between the EPR changes and either the ability to produce ethane from acetylene or the sensitivity of proton reduction to CO (see Tables VI and VII).

Purification and EPR analysis of α–195^{gln} MoFe protein from DJ540.

Crude extract activity measurements show that the α–195^{gln} MoFe protein is able to reduce efficiently both protons and acetylene. In contrast, although the α–195^{gln} MoFe protein is apparently able to bind N_2, it is unable to reduce this substrate to yield NH_3. Thus, the α–195^{gln} MoFe protein was purified in order to further characterize its catalytic properties and to determine whether or not it is able to reduce N_2 to a product other than NH_3. MoFe protein produced by both the wild type (α–195^{his}) and DJ540 (α–195^{gln}) was purified in parallel from crude extracts using a three–step procedure involving a heat step, anion–exchange chromatography, and hydrophobic–interaction chromatography. One–dimensional SDS polyacrylamide gel electrophoretic analyses of the wild type and α–195^{gln} MoFe proteins purified in this way reveal only two bands which correspond to the α– and β–subunits of the MoFe protein (Figure 17).

For unambiguous interpretation of the experiments described in the following sections, it was important to establish that any differences in the catalytic properties of the α–195^{gln} MoFe protein, when compared to the wild–type MoFe protein, can be ascribed to genuine changes in catalytic properties rather than to changes arising from an artifact of the

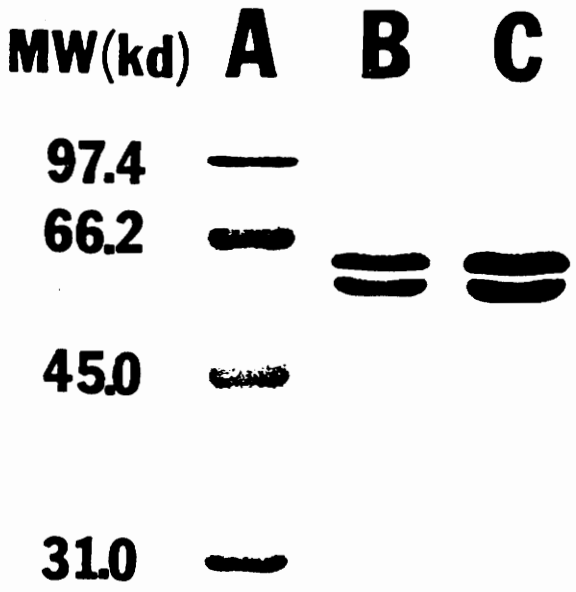

Figure 17. SDS-PAGE of purified wild-type and α-Gln-195 MoFe proteins. Lane A, Molecular weight standard markers. The standards are: phosphorylase b (97400), bovine serum albumin (66200), ovalbumin (45000), carbonic anhydrase (31000). Lane B, wild-type MoFe protein. Lane C, α-195^{Gln} MoFe protein.

purification procedure. This concern was addressed in several ways. First, the line shape and g values of the EPR spectra from the purified MoFe proteins were compared to their respective whole–cell EPR spectra. Neither the line shape nor the enhanced rhombic character around $g \approx 4$ of the EPR spectrum of α–195^{gln} MoFe protein changes during purification, indicating that the altered MoFe protein was not compromised structurally, compositionally or functionally during the purification process. Second, a quantitative comparison of the EPR spectra of the purified wild–type and α–195^{gln} MoFe proteins shows that, although the respective EPR line shape and g values are slightly changed when the two proteins are compared, their intensities are about the same (Figure 18). Thus, although the FeMo–cofactor polypeptide environment of the α–195^{gln} MoFe protein is somewhat different than that of the wild–type MoFe protein, a feature also revealed by whole–cell EPR spectra, the α–195^{gln} MoFe protein apparently has a full complement of FeMo–cofactor. Third, several of the catalytic properties of the α–195^{gln} MoFe protein were monitored during different stages of purification. For example, the relative levels of acetylene reduction and proton reduction activities, the insensitivity of proton reduction to CO, and the sensitivity of proton reduction to N_2, did not change during purification.

The α–195^{gln} MoFe protein does not reduce N_2.

Like the wild–type MoFe protein, α–195^{gln} MoFe protein exhibits N_2 inhibition of proton reduction. In the wild type, such inhibition of proton reduction caused by N_2 can be explained by diversion of electrons to N_2 reduction resulting in NH_3 formation. However, DJ540, which produces the altered α–195^{gln} MoFe protein, is incapable of diazotrophic growth so it is impossible that N_2 inhibition of proton reduction catalyzed by

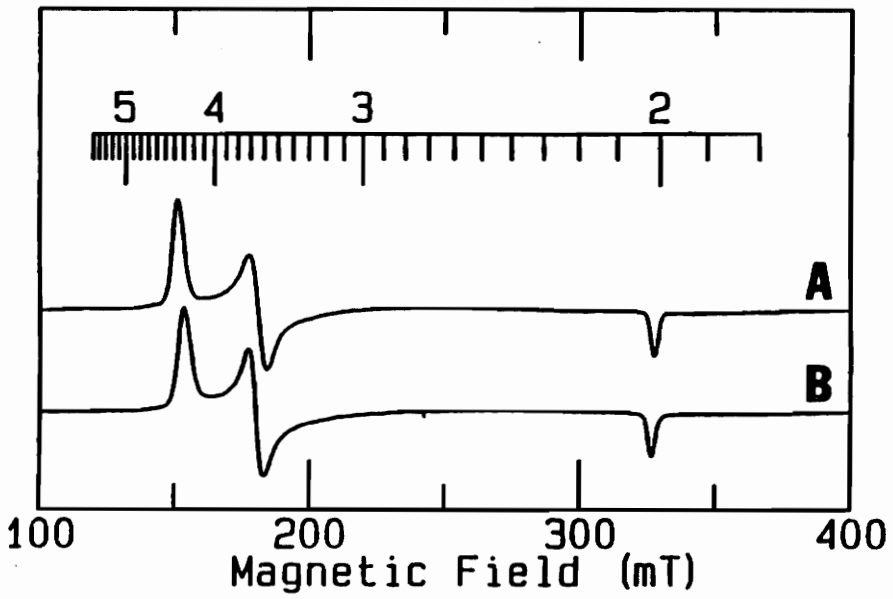

Figure 18. EPR spectra of purified α-195^{Gln} MoFe protein (A) and purified wild-type MoFe protein (B).

the altered MoFe protein is a consequence of NH_3 formation. This conclusion was independently confirmed by our inability to detect NH_3 production from N_2 catalyzed by the purified α–195^{gln} MoFe protein. The possibility that the α–195^{gln} MoFe protein is able to catalyze reduction of N_2 to yield some other nitrogenous product was also examined. Because there is evidence that hydrazine is formed as a bound intermediate during the course of N_2 reduction catalyzed by nitrogenase, we tested for its formation by using the acid quenched reaction assay previously described by Thorneley *et al.* (1978). Hydroxylamine was also sought as a potential product, although it is neither a natural product of wild–type nitrogenase catalysis nor an intermediate formed during NH_3 formation. Hydrazine was detected during nitrogenase turnover from acid–quenched samples of wild type MoFe protein at a level comparable to that previously reported (Thorneley *et al.*, 1978; Dilworth and Eady, 1991), but the α–195^{gln} MoFe protein was found incapable of catalyzing the production of any detectable hydrazine. As expected, neither the wild–type nor the α–195^{gln} MoFe protein was able to catalyze formation of hydroxylamine.

Whether or not N_2 is a reversible inhibitor of both acetylene reduction and proton reduction catalyzed by the α–195^{gln} MoFe protein was determined in an experiment where proton reduction activity is first assayed under an N_2 atmosphere. Subsequently, the reaction vessel was flushed with Ar and proton reduction assayed a second time but under an Ar atmosphere. Near full recovery of proton reduction was achieved after replacing N_2 with Ar demonstrating that N_2 binding to the altered MoFe protein is reversible. The reversible nature of N_2 binding to both the wild type and α–195^{gln} MoFe proteins also became evident in the kinetic analyses described below.

N_2 inhibition of electron flux to proton reduction in the α–195^{gln} MoFe protein by uncoupling MgATP hydrolysis from substrate reduction.

Although neither hydrazine nor hydroxylamine was produced by the α–195^{gln} MoFe protein, the possibility that it reduces N_2 to some other unknown product remained a plausible explanation for N_2 inhibition of proton reduction. This possibility was eliminated by the results of proton–reduction assays performed under either an Ar or N_2 atmosphere and under conditions of limiting reductant, in this case $Na_2S_2O_4$ (Figure 19). The rationale for this experiment is that, upon exhausting the source of reductant, it should be possible to trace all the available electrons to specific product formation. Panel A of Figure 19 shows that, under N_2, the wild–type MoFe protein distributes approximately 67% of the available electron flux to NH_3 production and 33% of electron flux to proton reduction. This conclusion is apparent by comparing the total amount of H_2 produced under an Ar atmosphere versus H_2 produced under an N_2 atmosphere. The distribution of electron flux to H_2 formation and NH_3 formation, when wild type MoFe protein was assayed under N_2, was separately confirmed in an experiment where all the products were quantified. In addition, the allocation of electrons to specific products, when wild–type MoFe protein is assayed under an N_2 atmosphere, has been well established by other investigators (see, for example, Burris, 1991; Lowe and Thorneley, 1984). In contrast, Panel B of Figure 19 shows that, in the case of the α–195^{gln} MoFe protein, N_2 does not divert electron flux to form a different product, but instead slows the overall rate of proton reduction. Namely, all of the available reducing equivalents are ultimately accounted for by H_2 formation whether catalysis occurs under either an Ar or a N_2 atmosphere.

In a different series of experiments, proton reduction catalyzed by the wild type and

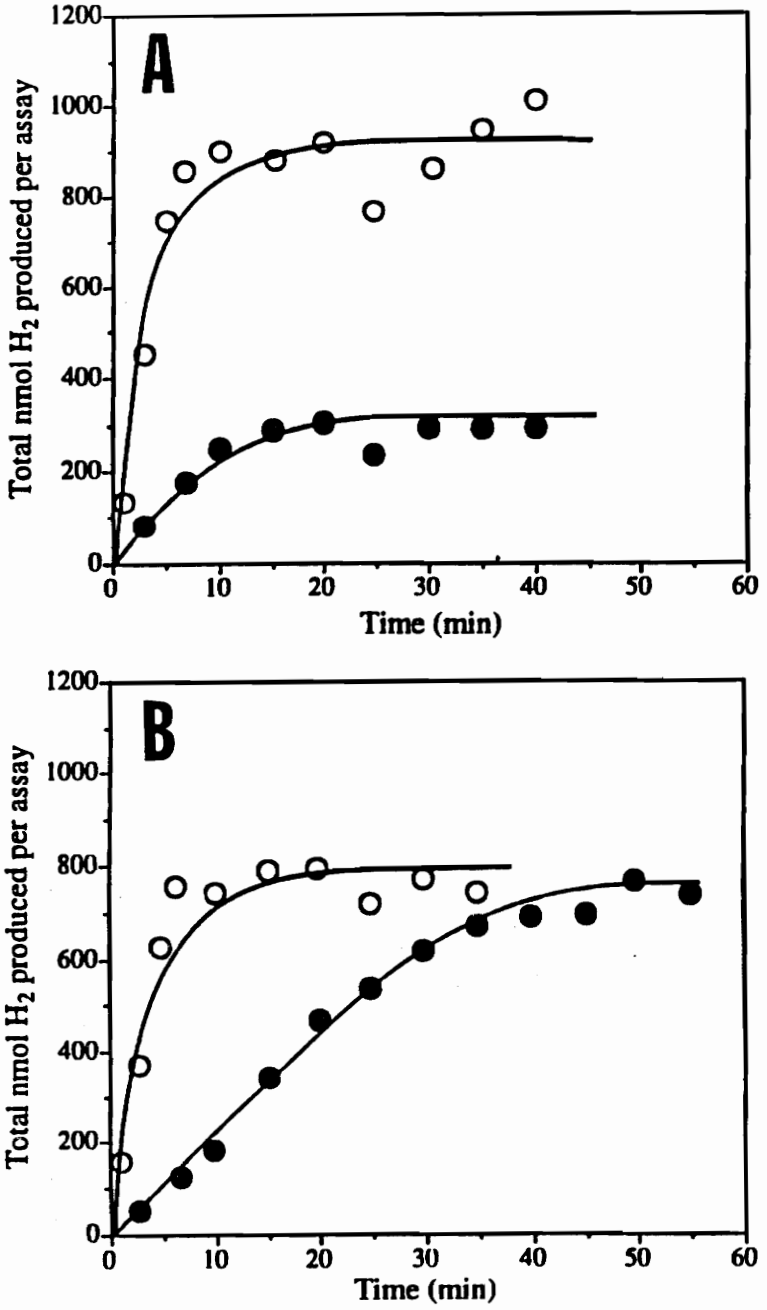

Figure 19. Time course of H_2 evolution catalyzed by purified wild-type MoFe protein (A) and purified α-195^{Gln} MoFe protein (B) under limiting concentrations of $Na_2S_2O_4$ under either 100% Ar (open circles) or 100% N_2 (closed circles) atmospheres. The assay conditions were as described in Experimental Procedures except that the initial $Na_2S_2O_4$ concentration was 1 μmole per 1 ml total reaction mixture.

α–195^{gln} MoFe proteins was measured under conditions of limiting MgATP under either an Ar or N_2 atmosphere (Figure 20). As discussed above for the condition of limiting reductant, a decrease in the amount of H_2 produced by wild–type MoFe protein catalysis under a N_2 atmosphere compared to an Ar atmosphere can also be accounted for by diversion of electron flux to NH_3 formation. Again, this assumption was separately confirmed in other experiments where NH_3 production was also monitored. In contrast to the condition of limiting reductant, where the α–195^{gln} MoFe protein ultimately catalyzes the same amount of H_2 production under either an Ar or a N_2 atmosphere, MgATP limitation resulted in a lowered level of H_2 production when catalysis occurred under a N_2 atmosphere than when under an Ar atmosphere (Figure 20, panel B). Thus, in the case of the α–195^{gln} MoFe protein, N_2 uncouples MgATP hydrolysis from electron transfer. This feature of the α–195^{gln} MoFe protein was found to be true whether or not MgATP was limiting. These results are summarized in Table VIII where it is shown that wild–type MoFe protein hydrolyzes about 5.0 MgATP for each electron pair delivered to substrate reduction (i.e., about 5 MgATP/2e–) when assayed under either an Ar or a N_2 atmosphere. In contrast, the α–195^{gln} MoFe protein hydrolyzes approximately 5.4 MgATP/2e– when assayed under Ar, but hydrolyzes about 23 MgATP/2e– when assayed under N_2.

Determination of kinetic parameters.

N_2 is not a substrate for the α–195^{gln} MoFe protein, yet, it is an inhibitor of both proton and acetylene reduction. This feature allowed determination of the binding affinity of both N_2 and acetylene for the substrate–reduction site, and also allowed determination of the pattern of N_2 inhibition of acetylene reduction by the altered MoFe protein. These

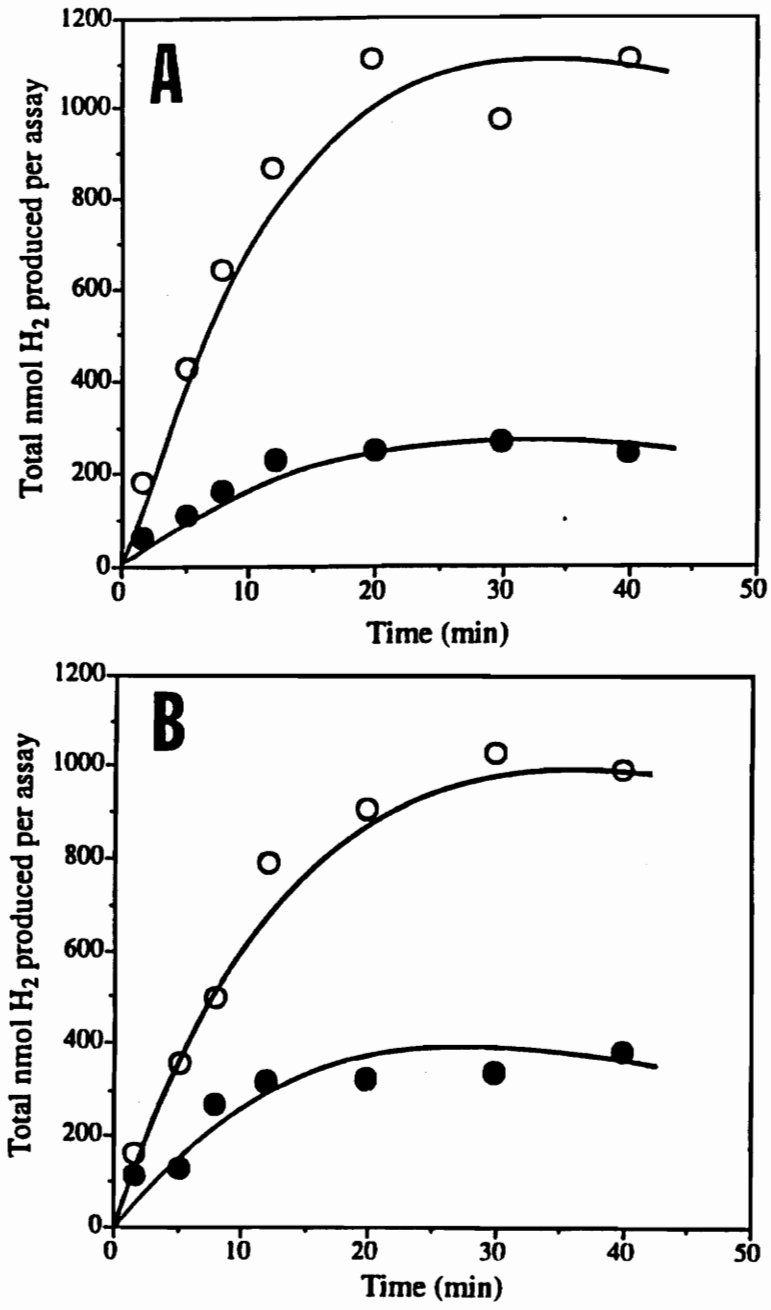

Figure 20. Time course of H_2 evolution catalyzed by purified wild-type MoFe protein (A) or purified α–195^{gln} MoFe protein (B) under limiting concentrations of MgATP under either 100% Ar (open circles) or 100% N_2 (closed circles) atmospheres. The assay conditions are as described in Experimental Procedures except that the initial MgATP concentration was 5 μmoles per 1 ml total reaction mixture with no ATP-regenerating system present.

Table VIII: Kinetic parameters[a] and ATP/2e$^-$ ratio of wild type and α–195^{Gln} MoFe protein.

MoFe protein	Km (C_2H_2)[b]	Ki (N_2)[c]	Ki (CO)[d]	ATP/2e$^-$ under	
				100% Ar	100% N_2
Wild type	0.005	0.219	0.00033	4.8	5.5
α-Gln-195	0.006	0.357	0.00004	5.4	23.0

[a] Km and Ki values were obtained from the Lineweaver-Burk plots using a computer program (EZ-FIT) and are expressed in atmospheres. [b] Km (C_2H_2) and [c] Ki (N_2) values were obtained from figure 21. [d] Ki (CO) values represent average values obtained from Figure 22 and Figure 23.

parameters were determined by measuring acetylene–reduction rates as a function of acetylene concentration in the presence of various fixed concentrations of N_2. A series of Lineweaver–Burk plots generated from these measurements is shown in Figure 21. These results show that N_2 is a competitive inhibitor of acetylene reduction catalyzed by either the wild–type or the α–195^{gln} MoFe protein, exhibiting K_i values of 0.219 atm and 0.357 atm, respectively. Km values for acetylene binding are 0.005 atm for wild–type MoFe protein and 0.006 atm for the α–195^{gln} MoFe protein. In these experiments, H_2 produced during catalysis did not interfere with N_2 inhibition of acetylene reduction because the acetylene concentrations (>1%) were sufficiently high to suppress H_2 evolution to minimal levels. The possibility that H_2 produced by catalysis might interfere with N_2 inhibition of acetylene reduction was considered because H_2 is known to inhibit N_2 reduction (Wilson and Umbreit, 1937).

Because the patterns of CO inhibition of both acetylene reduction and N_2 binding might be altered by the α–195^{gln} substitution, the appropriate comparisons with wild–type MoFe protein were run. Acetylene reduction rates were measured as a function of substrate concentration with various fixed concentrations of CO (Figure 22). In Figure 23, CO inhibition of N_2 binding was determined by monitoring proton reduction when assayed in the presence of both N_2 and CO. These latter experiments provide an indirect way to examine CO binding to the altered MoFe protein by asking whether or not CO is able to reverse the inhibition by N_2 on proton reduction. The results show that, for both the wild–type and α–195^{gln} MoFe protein, CO is a non–competitive inhibitor of both acetylene reduction and N_2 binding. These data also permitted calculation of the corresponding K_i's for CO and an estimation of the Km's for acetylene binding independent from that obtained

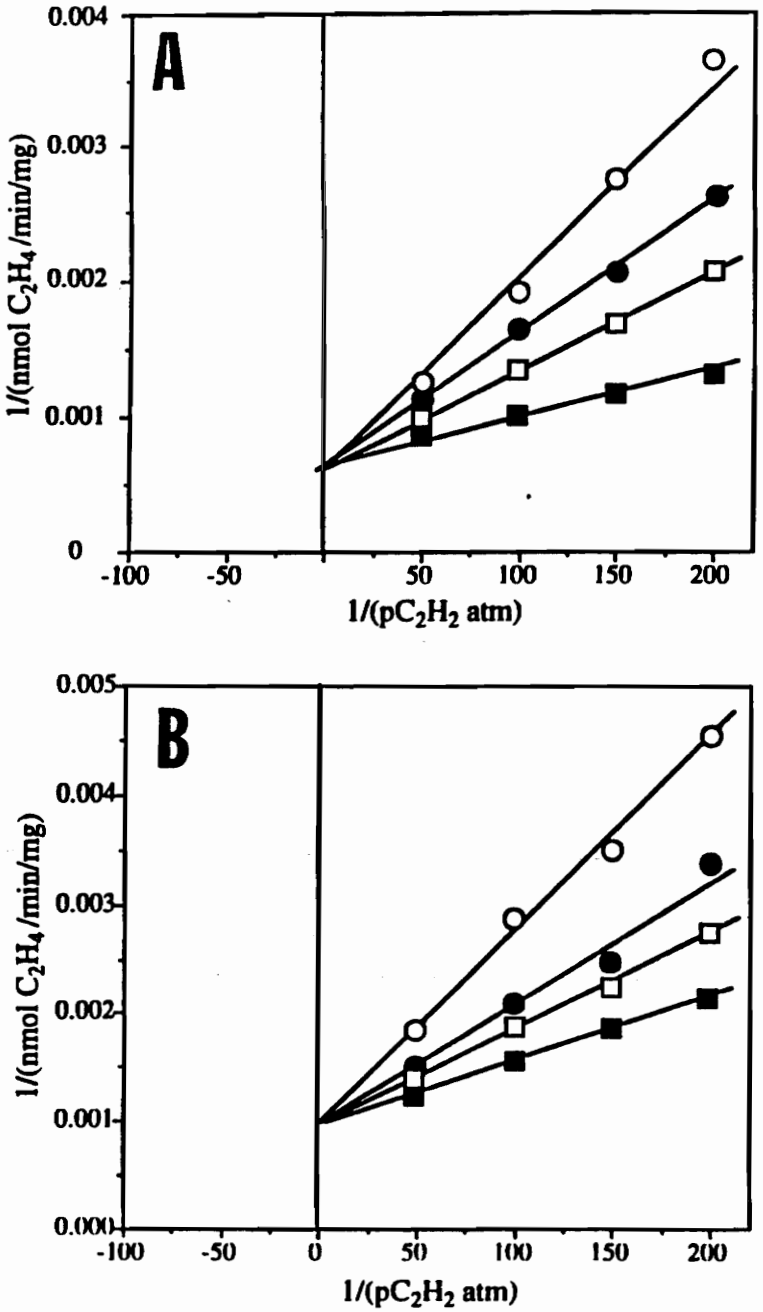

Figure 21. N_2 inhibition of acetylene reduction catalyzed by purified wild-type MoFe protein (A) or purified α–195^{gln} MoFe protein (B). The graph represents a series of Lineweaver-Burk plots where the reciprocal of the acetylene-reduction specific activity is plotted against the reciprocal of the acetylene concentration. Each plot was determined in the presence of a fixed level of N_2: $pN_2 = 0$ atm (filled squares), 0.2 atm (open squares), 0.4 atm (filled circles), and 0.6 atm (open circles).

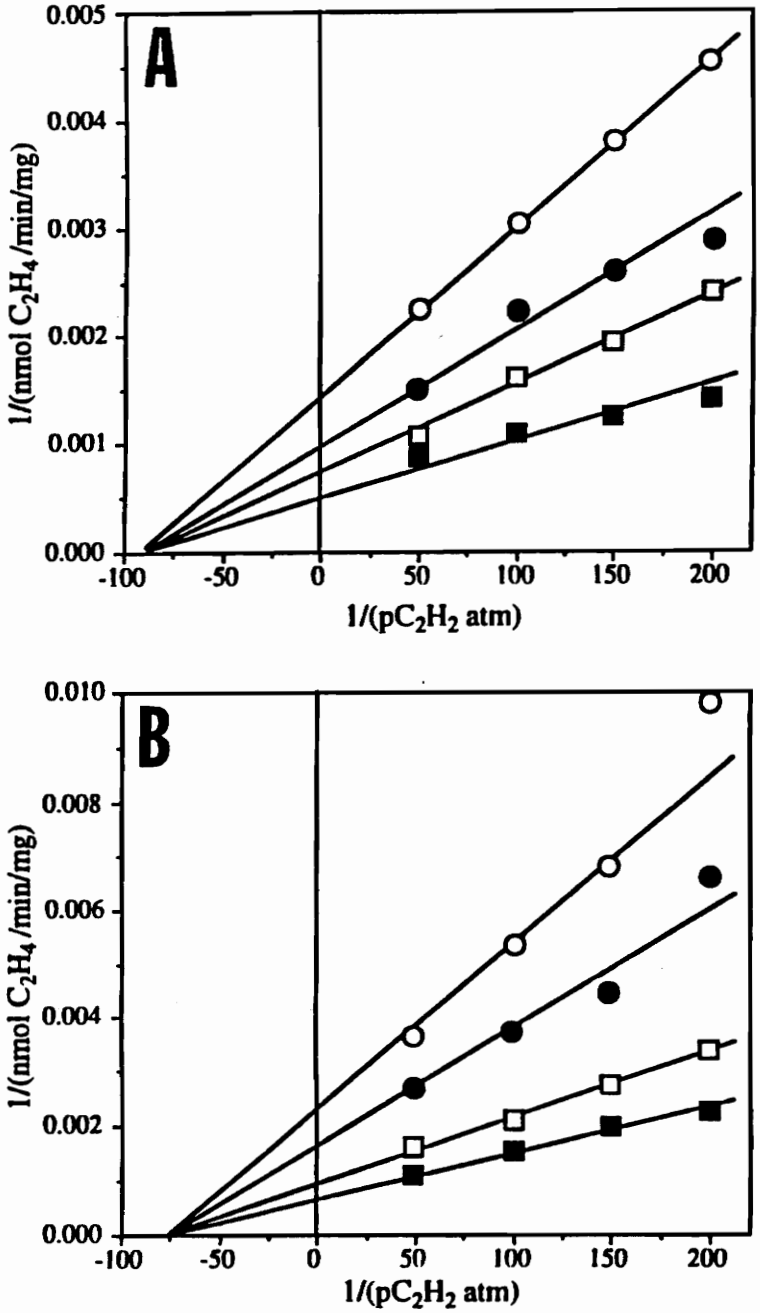

Figure 22. CO inhibition of acetylene reduction catalyzed by purified wild-type MoFe protein (A) or purified α–195^{Gln} MoFe protein (B). The graph represents a series of Lineweaver-Burk plots where the reciprocal of the C_2H_2-reduction specific activity is plotted against the reciprocal of the C_2H_2 concentration. For panel A, each plot was determined in the presence of the following fixed level of CO: pCO = 0 atm (filled squares), 0.00015 atm (open squares), 0.00025 atm (filled circles), and 0.0005 atm (open circles). For panel B, each plot was determined in the presence of the following fixed level of CO: pCO = 0 atm (filled squares), 0.000025 atm (open squares), 0.000063 atm (filled circles), and 0.0001 atm (open circles).

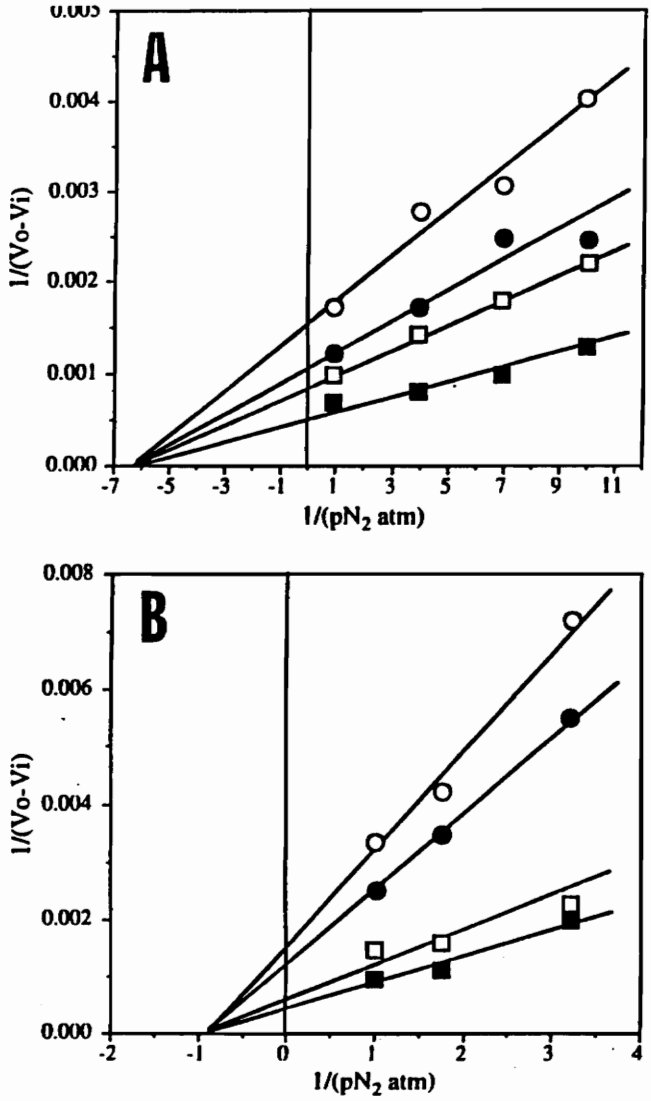

Figure 23. CO inhibition of N_2 binding to purified wild-type MoFe protein (A) or purified α–195^{gln} MoFe protein (B). The specific activity for H_2 evolution (nmol H_2 produced per min x mg of MoFe protein) decreases upon binding of N_2 and this suppression is inhibited by CO. Therefore, CO inhibition of N_2 binding was determined in the absence of N_2 reduction by measuring H_2 evolution. H_2 evolution was measured with increasing pN_2 at fixed levels of pCO. When the difference between H_2-evolution specific activities under no pN_2 and a given pN_2 (Vo-Vi) was plotted against pN_2 at fixed levels of pCO, a series of curves similar in shape to the Michaelis-Menten curves were obtained. H_2 evolution of 2000 nmoles produced per min x mg MoFe protein, which was measured under no pN_2 and no pCO, was used as Vo. Resulting double-reciprocal plots are shown above. For panel A, each plot was determined in the presence of the following fixed level of CO: pCO = 0 atm (filled squares), 0.00015 atm (open squares), 0.00025 atm (open circles), and 0.0005 atm (filled circles). For panel B, each plot was determined in the presence of the following fixed level of CO: pCO = 0 atm (filled squares), 0.000025 atm (open squares), 0.000063 atm (filled circles), and 0.0001 atm (open circles).

from data presented in Figure 21. CO was found to be a much more potent inhibitor of acetylene reduction catalyzed by the α–195^{Gln} MoFe protein (Ki = 0.00004 atm) when compared to the wild–type MoFe protein (Ki = 0.00033 atm). Km values for acetylene binding calculated from these data (0.008 atm for the wild–type MoFe protein and 0.012 atm for the α–195^{Gln} MoFe protein, see Figure 22) are somewhat higher than calculated from the data shown in Figure 21. It should be noted that the Km values determined from N_2 inhibition of acetylene reduction (Figure 21) are probably more accurate than those determined from the CO–inhibition experiments (Figure 22) because the low level of CO used in the latter experiments required serial dilution of the stock gas, thus, introducing the possibility of errors in the estimation of CO in the reaction vessel. Nevertheless, all of the values fall within the range of published values (Dilworth, 1966; Hardy *et al.*, 1971; Hwang and Burris, 1972; Hwang *et al.*, 1973; Rivera–Ortiz and Burris, 1975; Schollhorn and Burris, 1967).

Discussion

Our results provide insight concerning the nature of the interaction of the substrates, N_2, acetylene and protons, and the inhibitor CO, with the nitrogenase substrate–reduction site. It has been known for many years that N_2 is a potent inhibitor of both proton and acetylene reduction catalyzed by wild–type nitrogenase (Rivera–Ortiz and Burris, 1975). However, because N_2 is also a substrate for nitrogenase, it was not known heretofore whether or not N_2 inhibits reduction of other substrates by binding at a separate site and then competing for the available reducing equivalents or by competing for occupancy of the same active site. The observation that N_2 is not reduced by the α–195^{Gln} MoFe protein but effectively

inhibits both proton reduction and acetylene reduction demonstrates that N_2 is able to compete with both acetylene and protons for active site occupancy. Although these results do not rule out the formal possibility that different substrates bind to the active site in different ways or bind at different subsites within the active site, the results do show that different substrates cannot bind at the active site at the same time. As only marginally different binding affinities for acetylene and N_2 are observed when the wild type and α–195^{Gln} MoFe proteins are compared, the ability of N_2 to inhibit proton and acetylene reduction exhibited by the α–195^{Gln} MoFe protein is probably mechanistically relevant.

Another interesting feature of the α–195^{Gln} MoFe protein is that it exhibits a marked increase in susceptibility to CO inhibition of acetylene reduction and N_2 binding compared to the wild type (see Figures 22 and 23, and Table VIII). Two different possibilities for the increased affinity of CO for the altered MoFe protein can be considered. The first possibility comes from a structural consideration where substitution of the α–195–histidine residue by a glutamine residue simply makes a potential CO binding site more accessible. Inspection of the polypeptide environment surrounding FeMo–cofactor shows that the α–195–histidine residue is positioned such that the ε nitrogen of its imidazole group is able to participate in forming an NH→S hydrogen bond with a bridging sulfide. In this arrangement, the imidazole ring is positioned so that a neighboring Fe within FeMo–cofactor (see Figure 16), designated Fe2 in the molecular models of both Kim & Rees (1992a) and Bolin *et al.* (1993), would normally be sterically protected. Consequently, the steric protection of this Fe might either make it inaccessible to attack by CO or force CO to bind in an unfavorable geometry. Thus, it might be considered that substitution of the α–195–histidine position by glutamine would still permit formation of an

NH→S hydrogen bond to the bridging sulfide, but Fe2 of FeMo–cofactor would no longer be sterically protected. This latter possibility has biochemical precedence in the case of CO reactivity with the heme Fe of hemoglobin (Collman, *et al.*, 1976). However, based on the available molecular model of the MoFe protein structure, it does not appear obvious that substitution of glutamine for the α–195–histidine residue would either make any Fe atom contained within FeMo–cofactor more accessible to attack by CO or result in a polypeptide environment that favors a geometry more suitable for stabilization of the metal–CO bond. Clearly a satisfactory structural explanation for the increased sensitivity of the α–195^{gln} MoFe protein to CO will require determination of the three–dimensional structure of the altered protein. Nevertheless, the present results, which show that certain substitutions can result in proton reduction that is partially sensitive to CO (Table VII), whereas a different substitution results in an altered MoFe protein having proton reduction insensitive to CO but exhibiting increased CO inhibition of acetylene reduction or N_2 binding (Figures 22 and 23), suggest that there is more than one CO binding site located on or near the FeMo–cofactor. Indeed, the available published data suggests that there are at least two different CO–binding sites located within the MoFe protein (Davis, *et al.*, 1979), yet neither of these sites has been pinpointed. In this regard, it is also noted that the absence of any appreciable effect of the α–195^{gln} substitution on the Km's for acetylene or N_2 binding suggests that their binding site is somewhat remote from CO, which is in line with the usual interpretation of CO's non–competitive pattern of inhibition.

An electronic argument might also be considered in an attempt to explain the higher level of CO sensitivity of the α–195^{gln} MoFe protein. Replacement of the NH→S hydrogen bond to the bridging sulfide provided by the α–195–histidine residue by a corresponding

NH→S hydrogen bond from the substituting glutamine residue is expected to shift the redox potential of FeMo–cofactor in a slightly negative direction. However, it is unlikely that a small shift in redox potential could have such a dramatic effect on the susceptibility of one or more of the metal sites to attack by CO. On the other hand, any change in the electronic properties of FeMo–cofactor caused by the glutamine substitution could have a profound effect on the ability of the α–195^{Gln} MoFe protein to reduce N_2 by rendering the MoFe protein incapable of sufficiently lowering the unfavorable activation energy of the initial electron transfer to N_2. In this context, it is noted that there is a considerable network of NH→S hydrogen bonds to the FeMo–cofactor sulfides and they have already been suggested as possible contributors toward stabilization of intermediates formed during substrate reduction (Kim and Rees, 1992b, Bolin *et al.* 1993). Because the α–195^{Gln} MoFe protein is able to effectively reduce protons and acetylene, both of which require only two electrons, we favor a model where the NH→S hydrogen bond provided by the α–195–histidine residue functions to stabilize an early, partially reduced intermediate, most likely a hydrazido or diazene species, that is likely formed during the course of the six–electron reduction of N_2.

During nitrogenase turnover, the Fe protein cycles between a 2+ and 1+ redox state where it sequentially delivers single electrons to the MoFe protein in a process that requires association and dissociation of the two component proteins and hydrolysis of probably two MgATP per electron transfer. Because multiple electrons are required for substrate reduction, the association and dissociation of the Fe protein and the various reduced forms of the MoFe protein must be coordinated so that electron flow occurs mainly in one direction. Several different features might contribute to this aspect of nitrogenase catalysis.

First, a switching mechanism has been proposed to operate where, following MgATP hydrolysis and intermolecular electron transfer, the MgADP–bound Fe protein assumes a conformation that helps prevent electron back–flow to the Fe protein (Wolle *et al.*, 1992). Second, the presence of two different redox–active centers within the MoFe protein might serve to achieve an intramolecular distribution of the accumulated electrons. Third, the substrate itself could assist in insuring the quasi–unidirectional flow of electrons by acting as a molecular sink.

Our results with the α–195^{gln} MoFe protein demonstrate that electron capture by the substrate during turnover does indeed play a critical role in controlling the direction of electron flow during nitrogenase catalysis. This conclusion is supported by the following properties of the α–195^{gln} MoFe protein: (i) N_2 is able to effectively bind at the active site; (ii) N_2 is not reduced; (iii) N_2 slows the rate of proton reduction; and (iv) N_2 uncouples MgATP hydrolysis from electron transfer without substantialy altering the overall rate of MgATP hydrolysis. A simple explanation for these results is that because N_2 occupies the substrate–reduction site, but cannot be reduced, electrons accumulated within the α–195^{gln} MoFe are ultimately back donated to an oxidized form of the Fe protein (see discussion by Orme–Johnson *et al.*, 1977). A related possibility is that, once the altered MoFe protein becomes saturated with electrons that cannot be sequestered by substrate reduction, the two components retain their ability to associate and effect MgATP hydrolysis but are unable to achieve intermolecular electron transfer. This possibility is supported by evidence that MgATP hydrolysis precedes intermolecular electron transfer (Thorneley *et al.*, 1989), although MgATP–dependent proton release appears to be slower than electron transfer (Mensink *et al.*, 1992). It is important to emphasize that N_2 did not appreciably slow the

rate of MgATP hydrolysis in these experiments, so it is unlikely that binding of N_2 to the α–195^{gln} MoFe protein has any effect on component–protein interaction.

The uncoupling of MgATP hydrolysis and electron transfer is a familiar feature of nitrogenase enzymology. For example, conditions of high or low pH, high or low temperature (Imam and Eady, 1980; Jeng *et al.*, 1970; Watt *et al.*, 1975), low electron flux resulting from high MoFe protein to Fe protein ratios (Eady and Postgate, 1974; Hageman and Burris, 1978), and certain amino–acid substitutions that alter component–protein interaction (Lowery *et al.*, 1989; Wolle *et al.*, 1992) have all been shown to uncouple MgATP hydrolysis and electron transfer. These phenomena have also been explained as manifestations of futile cycling of electrons. The key difference in the present study is that a small molecule, N_2, uncouples a system that otherwise exhibits relatively efficient coupling of MgATP hydrolysis and proton reduction. A similar situation is found in the cases of CH_3NC and HCN, which have also been shown to uncouple MgATP hydrolysis from electron flow in the wild–type MoFe protein (Li *et al.*, 1982; Rubinson *et al.*, 1983). Uncoupling of MgATP and electron flow caused by CH_3NC and HCN is somewhat more complicated, however, because these compounds are both nitrogenase substrates and inhibitors. However, it is important that such uncoupling caused by CH_3NC and HCN does not have a dramatic effect on the overall rate of MgATP hydrolysis. Thus, it appears that uncoupling of MgATP hydrolysis and electron flow caused by all of these small molecules is likely to be a consequence of blocking electron transfer to the electron sink.

A *structural* role for the α–195–histidine residue became evident from experiments where the N_2 susceptibilities of proton reduction catalyzed by the various mutant strains were compared. In these experiments, N_2 inhibition of proton–reduction activity is an

obvious indication that the active site retains the ability to bind N_2. Conversely, the inability of N_2 to inhibit proton reduction catalyzed by certain mutant strains is interpreted to indicate that the substrate–binding site has been modified such that effective N_2 binding is not possible. Thus, the data summarized in Table VII show that the α–195^{gln} MoFe protein is distinguished from the other altered MoFe proteins in retaining the ability to bind N_2. The significant structural difference observed when glutamine is compared to the other substituting amino acids is that only the glutamine substitution retains the potential to form a NH→S hydrogen bond through its amide–N to the appropriate bridging sulfide of FeMo–cofactor in a configuration similar to that normally provided by the α–195–histidine residue. This feature is illustrated in Figure 16, where the ε–nitrogen of the α–195–histidine residue is approximately 3.14 Å from the bridging sulfide. It is, therefore, likely that a NH→S hydrogen bond to the bridging sulfide provided by either a histidine or glutamine residue can function in positioning the FeMo–cofactor within the polypeptide pocket, such that the substrate–binding site retains affinity for N_2, whereas the other substituting amino–acids are unable to fulfill this role. It is also probable that small changes in the EPR lineshape and g values, as well as the ability to either reduce acetylene to ethane or exhibit CO–sensitive proton reduction as observed for certain of the altered MoFe proteins, are manifestations of a reorientation of FeMo–cofactor within the polypeptide pocket. Another important finding is that, while whole cells of both the wild–type and α–195^{gln} strain exhibit similar EPR intensities and, therefore, have similar complements of FeMo–cofactor, whole–cell EPR intensities of the other mutant strains are generally much lower. Such results indicate that MoFe proteins from these other mutant strains probably do not have a full complement of FeMo–cofactor. Thus, it appears that the

NH→S hydrogen bond provided by the α–histidine–195 residue is likely to function not only in correctly positioning FeMo–cofactor for substrate binding and reduction, but also assisting in binding FeMo–cofactor within the polypeptide.

Chapter II. HD formation without nitrogen fixation by an altered nitrogenase

Acknowledgements

I thank Kim Harich for performing mass spectrometry experiments.

Introduction

Biological nitrogen fixation, performed by many free-living and symbiotic microorganisms, occurs at room temperature and atmospheric pressure. Nitrogenase can reduce a great variety of substrates, however it is the mechanism of N_2 reduction that has attracted most attention. A working model for nitrogen reduction must take into consideration the known properties of nitrogenase. Thus it must explain why N_2 reduction is always accompanied by the evolution of H_2, even under 50 N_2 atmospheres (Simpson and Burris, 1984); it must explain N_2 stimulated HD formation; and it must also explain why H_2 specifically inhibits N_2 binding.

Dihydrogen is produced by nitrogenase in the absence or presence of reducible substrates. The rate of H_2 evolution varies depending on experimental conditions and the different types and concentrations of the substrates being reduced. The maximal rate is obtained when no other substrates are present and all electrons are directed toward the reduction of protons, which are derived from water. Nitrogenase catalysis of H_2 evolution has been extensively explored by the Sussex group (Lowe and Thorneley, 1984a, b). Their kinetic model describes the reaction steps for H_2 evolution which requires MoFe protein to be reduced by a certain number of electron equivalents. Another H_2 evolution

pathway occurs by H_2 displacement upon the binding of N_2 is also indicated in this model. The 2:1 stoichiometry of NH_3 production and H_2 evolution is observed at high electron flux and saturated N_2 concentration (Rivera-Ortiz and Burris, 1975; Burgess *et al.*, 1981; Guth and Burris, 1983). This condition is obtained by the displacement reaction of H_2 upon binding of N_2.

The N_2-dependent H_2 evolution was first observed when a significant amount of HD was formed from D_2 by soybean nodules in the presence of N_2 (Hoch *et al.*, 1960). The HD formation reaction of nitrogenase has been studied in many laboratories to gain insight into the mechanism of N_2-dependent H_2 evolution. The earlier evidence supported the speculation that HD formation occurs by a reversible exchange of D_2 with an enzyme-bound intermediate (Hoch *et al.*, 1960). However, the electron balance studies indicate that one electron is required for each HD formed if total electron flow through nitrogenase is assumed to remain constant under all conditions (Newton *et al.*, 1977; Guth and Burris, 1983). Further studies ruled out the reversible exchange mechanism with solvent for HD production by demonstrating that the rate of incorporation of tritium from T_2 into the aqueous phase was negligible (Burgess *et al.*, 1981).

H_2 is not only a product but also a specific inhibitor of N_2 reduction. Reduction of other nitrogenase substrates including proton, nitrous oxide, azide, acetylene, cyanide, methylisonitrile, and hydrazine are not inhibited by H_2 (Burns and Bulen, 1977; Hoch *et al.*, 1960; Hwang *et al.*, 1973; Burgess *et al.*, 1981). In addition, HD formation occurs at the expense of NH_3 formation in the presence of D_2 and N_2 (Burgess *et al.*, 1981). These observations by the Kettering group have led to a suggestion that H_2 inhibition of NH_3 production and HD formation under D_2/N_2 are different manifestations of the same

molecular process involving an enzyme-bound diazene-level (E-N_2H_2) intermediate (Wherland *et al.*, 1981; Burgess *et al.*, 1981). In this model (Figure 11), D_2 reacts with an enzyme-bound intermediate of N_2 fixation resulting in the release of an N_2 molecule, the production of two molecules of HD, and the net consumption of two electrons. Thus D_2 inhibits N_2 reduction by diverting nitrogenase from NH_3 formation to N_2-dependent HD formation and one electron is utilized per HD in this process. This model offers an explanation for N_2 dependent H_2-D_2 exchange, as replacement of H_2 with D_2 would yield HD as a product. It also explains the observation that N_2 dependent H_2-HD exchange does not yield D_2 as a product.

In an alternative model for HD formation proposed by Guth and Burris (1983), D_2 and N_2 compete for the same form of the enzyme (Fig.12). In this ordered sequential model, N_2 can also bind to the D_2-bound form of the enzyme. Thus, binding of N_2 to the enzyme can either proceed to NH_3 formation if D_2 is absent or it can proceed to HD formation with the concomitant release of an N_2 molecule in the presence of D_2. The major difference of this model from the Kettering model is that D_2 does not react with an enzyme-bound intermediate but only binds to free nitrogenase before binding of N_2. The N_2-independent HD formation is excluded in this model because they demonstrated that HD formation was almost completely eliminated (less than 1-2% of total electron flux) in the absence of N_2. It was reported that the apparent Km (N_2) for NH_3 formation was higher than the apparent Km (N_2) for HD formation (Burgess *et al.*, 1981; Turner and Bergersen, 1969; Bulen, 1976; Burris and Orme-Johnson, 1976; Li and Burris, 1983). According to the Kettering model, the non-identical Km (N_2) is due to the HD formation in the absence of N_2. In Guth and Burris model, Km's (N_2) for the formation of HD and NH_3 are different because

N_2 enhances HD formation on binding to E-D_2 and simultaneously inhibits HD formation by competing for E with D_2.

In the third model, which was suggested by Cleland (Figure 13), H_2 is released upon the binding of an N_2 molecule, this accounts for the stoichiometry of one H_2 evolved per N_2 fixed (Guth and Burris, 1983). The reversible exchange reaction (E-N_2 + D_2 $\leftrightarrow$ E-D_2 + N_2) is shifted toward the formation of E-D_2 species in the presence of D_2 and HD is formed. This mechanism implicates that N_2-dependent H_2 evolution, H_2 inhibition of N_2 fixation, and HD formation are caused by the same mechanism.

It has been proposed that HD formation occurs at the expense of NH_3 formation (Burgess *et al.*, 1981). Guth and Burris, (1983) supported this idea and suggested that under saturating pN_2 75% of the total electron flux, which would have gone to NH_3 production will be redirected to HD formation in the presence of infinite pD_2, the remaining 25% of the electron flux going to H_2 evolution. According to the Cleland model, however, a stoichiometric ratio of one H_2 produced per two HD's formed was expected under saturating pN_2 and pD_2. Thus, 50% each of the total electron flux must go to HD and H_2 formation under these conditions. Consequently, D_2 should enhance H_2 evolution and reduce the percentage of electron flux toward HD plus NH_3 formation. These expectations conflict with the proposal by Burgess *et al.* (1981) and Guth and Burris (1983). Most of the previous data showed no increase in H_2 evolution by D_2 (Newton *et al.*, 1977; Guth and Burris, 1983). However, Jensen and Burris (1985) reported the enhancement of H_2 evolution by D_2 at the expense of HD and NH_3. They further showed that the $2HD/H_2$ ratio extrapolated to one at saturating pN_2 and infinite pD_2. These results support the Cleland mechanism for HD formation.

The three models described above represent different enzyme forms that bind D_2 in the process of HD formation. In the present study, this argument was tested experimentally with the altered purified MoFe protein from a mutant strain (α-195^{gln}) of *Azotobacter vinelandii* .

Materials and Methods

Procedures for strain construction, cell growth conditions, nitrogenase depression, crude extract preparation, and component protein purification are described in Experimental Procedures section. Nitrogenase assays were performed in the high electron flux with 0.075 mg MoFe protein and 0.925mg Fe protein present in the reaction (molar Fe:MoFe ratio = 40:1). Reaction vials (9.25ml) were fitted with butyl rubber serum stoppers and aluminum seal caps. MoFe protein specific activity was calculated as nmols product per min and mg MoFe protein in the reaction.

Acetylene reduction - The assay was performed under three different gas atmospheres: 0.5% C_2H_2 / 99.5% Ar, 0.5% C_2H_2 / 60% N_2 / 39.5% Ar, and 0.5% C_2H_2 / 60% N_2 / 39.5% H_2. The desired gas atmospheres in the reaction vials were prepared by using the gas tight syringes from pre-purified and analyzed gas tanks: 100% Ar, 10% C_2H_2 / 90% Ar, 100% N_2 (Airco), and 100% D_2 (Matheson). The 1.0 ml reaction contained 38 mM TES, pH 7.4, 2.5 mM ATP, 5.0 mM $MgCl_2$, 30 mM creatine phosphate, 0.125 mg creatine phosphokinase, 20 mM $Na_2S_2O_4$ and a total of 1 mg protein. The reaction vial which contained ATP regeneration system and water was degassed on an automatic manifold system with 4 cycles of 100 sec evacuation and 20 sec gassing and filled with the desired gases. Dithionite and optimal amount of Fe protein were added using gas tight

Hamilton syringes to the reaction vial which was then incubated at 30°C for 5 min. The reaction was started by adding appropriate amount of MoFe protein and terminated after incubation at 30°C for 8 min by the addition of 0.25 ml 0.4 M EDTA, pH 8.0. The head space was analyzed for C_2H_4 using a chromatograph equipped with a FID detector (Shimatsu). Measured gasses were calibrated using the standard gases of 1 ppm C_2H_2 or 1% H_2 (Scottys).

Formation of H_2, HD, and NH_3 - All three products were measured in the same reaction vial. HEPES buffer (35mM, PH7.4) was used because TES buffer, used in C_2H_2 reduction assay, interfered with the NH_3 assay. To measure N_2 dependent HD formation, nitrogenase assays were performed under two different gas atmospheres as described (Burgess et al, 1981): 50% D_2 / 50% Ar and 50% D_2 / 40% N_2 / 10% Ar. The gas atmospheres in the reaction vials were prepared from pre-purified and analyzed gases of 100% Ar, 100% N_2 (Airco), or 100% D_2 (Matheson). The head space of the EDTA-stopped reaction vial was analyzed for the formation of H_2 and/or HD using a mass spectrometer (VG Analytical, Manchester, UK, Model 7070 E-HF). H_2, HD, and D_2 were detected at masses 2, 3, and 4, respectively. Small but measurable HD background in the absence of N_2 was subtracted from each HD measurement. Mass spectrometer units were converted to nmoles by using nmol/unit ratio obtained from standard gas injections (5% H_2 and 5% D_2). The nmol HD/unit ratio was obtained by taking the average values of nmol H_2/unit and nmol D_2/unit. Assays for NH_3 production and ATP hydrolysis are described in the Experimental Procedures.

Results and discussion

From our previous studies, we found that the α-195^{gln} MoFe protein reduced proton to yield H_2 at comparable rates to wild type but did not reduce N_2 (Kim *et al.*, 1993; Kim *et al.*, 1994). The altered MoFe protein, however, bound N_2 since H_2 evolution was inhibited by >65% in the presence of N_2. Our conclusion was that N_2 bound to the α-195^{gln} MoFe protein could not compete with protons for electrons but inhibited proton reduction by simple occupation of the catalytic site. Testing the α-195^{gln} MoFe protein with respect to H_2 inhibition of N_2 binding and HD formation can answer the question on the requirement of enzyme-bound intermediate for HD formation.

H_2 inhibition of N_2 binding on wild type and the α-195^{gln} MoFe protein is shown in Table IX. A decrease in C_2H_2 reduction in the presence of N_2 and recovery of C_2H_2 reduction by the addition of H_2 were monitored to demonstrate the binding of N_2 at the active site. Detailed conditions of the experiments are described in the legend. The rationale for this experiment was based on the fact that N_2 was a competitive inhibitor of C_2H_2 reduction in both wild type and the altered MoFe protein (see Figure 21). Under an atmosphere of 0.5% C_2H_2 / 99.5% Ar, wild type MoFe protein produced 504 nmoles C_2H_4 / (min x mg MoFe protein). Addition of 60% N_2 decreased the C_2H_2 reduction by 67% therefore indicating that N_2 partially replaced C_2H_2 at the active site. The C_2H_2 reduction activity was recovered to 65% of the original in the presence of 39.5% H_2 which indicated that H_2 partially prevented N_2 from binding at the active site thereby facilitating the binding and reduction of C_2H_2. These results are consistent with the previous demonstrations that H_2 is a significant inhibitor of N_2 reduction (Wilson and Umbreit, 1937). A similar pattern was observed for the α-195^{gln} MoFe protein. Namely, addition of 39.5% H_2 almost completely excluded the binding of N_2 at the active site and C_2H_2

Table IX. H_2 inhibition of N_2 binding by wild type and α-Gln-195 MoFe protein. The specific activity for C_2H_2 reduction (nmol C_2H_4 / min / mg) decreases upon binding of N_2. The suppresion of C_2H_2 reduction by N_2 is inhibited by H_2. Therefore, H_2 inhibition of N_2 binding may be demonstrated by an increase in C_2H_2 reduction by H_2 in the presence of N_2.

MoFe protein	Assay atmosphere[a]	Specific activity[b]	% Specific activity[c]
Wild type	C_2H_2 / Ar	504	100
	C_2H_2 / N_2 / Ar	165	33
	C_2H_2 / N_2 / H_2	328	65
α-Gln-195	C_2H_2 / Ar	306	100
	C_2H_2 / N_2 / Ar	168	55
	C_2H_2 / N_2 / H_2	297	97

[a] Assay atmospheres are: C_2H_2 / Ar = 0.5% / 99.5%, C_2H_2 / N_2 / Ar = 0.5% / 60% / 39.5%, C_2H_2 / N_2 / H_2 = 0.5% / 60% / 39.5%.
[b] Specific activity of C_2H_2 reduction is expressed as nmoles C_2H_4 produced per min x mg MoFe protein.
[c] Percentage of specific activity was determined as the specific activity divided by the specific activity under 0.5% C_2H_2 / 99.5% Ar.

reduction activity increased to almost that determined under N_2- and H_2-free conditions. Weaker inhibition of C_2H_2 reduction by N_2 and almost complete elimination of N_2 reduction by H_2 could be due to α-195^{Gln} MoFe protein having a lower binding affinity for N_2 and/or a higher binding affinity for H_2 (e.g. Ki (N_2) ≈ 0.357 atm compared to 0.219 atm of wild type) (Kim *et al.*, 1994). Inhibition of N_2 binding by H_2 in α-195^{Gln} MoFe protein implies that the diazene-level intermediate may not be involved in H_2 inhibition of N_2 reduction, a different manifestation of the HD formation mechanism.

The second experiment directly measured HD formation from wild type and the α-195^{Gln} MoFe protein. Table X compares H_2, NH_3 and HD formation by wild type and the altered MoFe protein under the atmospheres of D_2 / Ar and D_2 / N_2 / Ar. Under 50% D_2 / 50% Ar, the total activity of H_2 evolution by the α-195^{Gln} MoFe protein (2923 ± 33 nmoles) was comparable to that of wild type MoFe protein (2968 ± 257 nmoles). This indicated that D_2 was not a potent inhibitor of H_2 evolution in the altered MoFe protein. Under 50% D_2 / 40% N_2 / 10% Ar, 365 ± 14 nmoles of NH_3 were formed per assay by wild type MoFe protein in addition to the formation of H_2 (1523 ± 212 nmoles) and HD (1769 ± 336 nmoles). Approximately 49% of total electron flux was distributed to the formation of HD (30%) and NH_3 (19%) under this condition. About 51% of total electron flux remained going toward H_2 evolution. Under the same condition, 1299 ± 112 nmoles of HD were formed per assay by the α-195^{Gln} MoFe protein which represented 20% of electron flow toward HD formation. The remaining 80% of total electron flow was directed toward H_2 production (2542 ± 145 nmoles) under this condition. Total electron flux through nitrogenase remained constant under all conditions for both wild type and the α-195^{Gln} MoFe protein (approx. 7% increase in total electron flux by α-195^{Gln} MoFe

Table X. Formation of H_2, HD, and NH_3 by wild type and α-Gln-195 MoFe protein.

		Total activity[b]			% e- to[c]			
MoFe protein	Atmosphere[a]	H_2	HD	NH_3	H_2	HD	NH_3	ATP/2e-
WT	D_2/Ar	2968	0	0	100	0	0	4.28
	D_2/N_2/Ar	1523	1769	365	51	30	19	4.58
α-Gln-195	D_2/Ar	2923	0	0	100	0	0	3.88
	D_2/N_2/Ar	2542	1299	0	80	20	0	3.60

[a] Assay atmospheres are: D_2/Ar = 50%/50%, D_2/N_2/Ar = 50%/40%/10%.
[b] Total activity is expressed as total nmoles of H_2, HD, or NH_3 produced per assay.
[c] Percentage of electron flux was determined as the electron flux to each product divided by the total electron flux; Two, one, and three e- were allocated for H_2, HD, and NH_3 respectively.

protein under 50% D_2 / 40% N_2 / 10% Ar are within the range of experimental error). As described above, the α-195^{gln} MoFe protein could not reduce N_2 to any of the nitrogenous intermediates or NH_3. A lower but significant amount of HD formation by the α-195^{gln} MoFe protein is not consistent with the Kettering's mechanism for HD formation which represents the reaction of D_2 with the diazene-level intermediate during the reduction of N_2 to NH_3. It is therefore reasonable to speculate that binding of nitrogen to the enzyme is necessary but its reduction is not required for the formation of HD.

Another important aspect in studying the HD formation mechanism was ATP hydrolysis by α-195^{gln} MoFe protein under D_2 / N_2 atmosphere. It was demonstrated that ATP hydrolysis during turnover of α-195^{gln} MoFe protein was uncoupled from proton reduction in the presence of N_2 (≈23 ATP / 2e$^-$, Table VIII) (Kim *et al.*, 1994). The N_2-induced uncoupling of ATP hydrolysis from proton reduction was observed when a significant decrease in H_2 evolution was not accompanied by a significant decrease in ATP hydrolysis in the presence of N_2. One explanation is that the uncoupled ATP hydrolysis is due to the formation of E-N_2 complex. The enzyme-bound N_2 can not be reduced due to the kinetic barrier acquired by the α-195^{gln} MoFe protein and the barrier prevents the transferred electrons from being utilized for N_2 reduction thereby redonating the electrons to the Fe protein. The back-donation of transferred electrons to the Fe protein was originally suggested by Orme-Johnson *et al.*, and by Mclean *et al.*, from their observation on an altered nitrogenase from *Klebsiella pneumoniae nifV* mutants (Orme-Johnson *et al.*, 1977; Mclean *et al.*, 1983). The net result of this electron back donation from the MoFe protein to the oxidized Fe protein is the hydrolysis of 2 MgATP without the transfer of an electron to substrate i.e. futile hydrolysis of MgATP. Under 50% D_2 / 40% N_2 / 10% Ar,

total electron flow through the α-195^{gln} nitrogenase was not decreased when compared to that under 50% D_2 / 50% Ar so that ATP hydrolysis was normally coupled with the substrate reduction (ATP/2e$^-$ ≈ 4.0, Table X). Therefore, addition of D_2 in the presence of N_2 in the assay atmosphere relieved the uncoupling caused by the E-N_2 complex. The Guth and Burris model (Fig 12) requires total domination of reaction 1 (E + D_2 → E-D_2) over reaction 2 (E + N_2 → E-N_2) to explain the normal ATP hydrolysis under D_2 / N_2 / Ar. As indicated previously, the α-195^{gln} MoFe protein has a slightly lower binding affinity for N_2 (Ki (N_2) ≈ 0.357 atm compared to 0.219 atm of wild type). It was also indicated that the altered MoFe protein could bind D_2 (H_2) with a different affinity. For example, almost complete elimination of N_2 binding by H_2 (Table IX) and a greater amount of H_2 formation under D_2 / N_2 / Ar (Table X) could be due to the higher binding affinity for D_2 (H_2) of α-195^{gln} MoFe protein. Therefore, it is possible that the altered MoFe protein binds D_2 preferably to N_2 under 50% D_2 / 40% N_2 / 10% Ar and excludes the formation of E-N_2 complex thereby restoring the normal ATP hydrolysis. In the Cleland model (Figure 13), N_2-induced uncoupling of ATP hydrolysis from substrate reduction is relieved by the addition of D_2 because the enzyme-bound N_2 can be quickly replaced by D_2.

Less amount of HD formed by the α-195^{gln} MoFe protein (1299 ± 112 nmol/assay) than by wild type MoFe protein (1769 ± 336 nmol/assay) was unexpected because electrons could not be diverted to N_2 reduction by the altered protein and, therefore, should be redirected toward HD formation. This can be explained better in Cleland model (Figure 13). The altered MoFe protein reduced by two electrons and two protons would go back to its original state (E_0) evolving H_2 (1. H-E-H → H_2 + E_0, or 2. H-E-H + 2H$^+$ + 2e$^-$ → 2H_2 + E_0) due to a lower affinity for N_2 of the α-195^{gln} MoFe protein, rather than proceeding

to HD formation which requires N_2 binding. Consequently, larger production of H_2 over HD observed by the α-195^{gln} MoFe protein under D_2 / N_2 / Ar satisfies the expectation of Cleland model.

Chapter III. Stopped-flow spectroscopic analysis to probe redox changes in metalloclusters within the altered MoFe protein

Acknowledgements

I thank Karl Fisher for performing the stopped-flow spectroscopy experiments and for helpful discussions.

Introduction

Thorneley & Lowe (1985) have previously proposed two catalytic cycles to account for the pre-steady-state and steady-state kinetics of N_2 reduction by *K. pneumoniae* nitrogenase at 23°C. The first of these cycles, the Fe-protein oxidation-reduction cycle, describes the transfer of electrons from the Fe protein to the MoFe protein (see Fig. 9). The MoFe-protein cycle (Fig. 10) consists of a combination of eight Fe-protein cycles, providing the eight electrons required to reduce $N_2 + 8H^+$ to $2NH_3$ and H_2. Dinitrogen reduction requires that the MoFe protein first undergo a minimum of three single electron reduction steps each requiring completion of one Fe-protein cycle. N_2 can only bind to E_3H_3 or E_4H_4 with displacement of a H_2 molecule, possibly from a molybdenum hydride as suggested by Chatt (1980). Acetylene is postulated to bind to the MoFe protein in the E_1H or E_2H_2 states (Lowe *et al.*, 1989; Lowe *et al.*, 1990). These states represent less reduced forms of the protein complex than those required for N_2 reduction. The formation of state E_4 from E_3 is potentially the most interesting reaction as it is after this electron transfer that MoFe protein with N_2 bound becomes irreversibly committed to reducing N_2 (Thorneley & Lowe, 1984a). We have shown that the altered α-195^{Gln} MoFe protein binds

N_2 but unlike the wild type it is unable to reduce it to NH_3. This inability of the altered MoFe protein to reduce N_2 can be explained either by 1) the structural and/or electronic barrier at the active site or 2) that the E_4 state essential for N_2 reduction is not attained.

Results and discussion

We have tested the possibility that the E_4 level of MoFe protein is not reached with the altered protien by using the stopped-flow spectrophotometric strategy recently described by Lowe *et al.* (1993). Their study was concerned with the absorbance changes (430 nm) that occur after the primary electron transfer reaction in an attempt to examine the redox changes occurring on the metal clusters of the MoFe protein. They analyzed the absorbance changes over the first 500 ms as the altered protein is reduced from E_0 through to E_4 and correlated these changes with the computed concentrations (using the Lowe-Thorneley model) of the various species as they change with time, substrate and component protein ratio. The nature of the redox changes taking place in the metal clusters of the MoFe protein during substrate reduction was probed by complementary EPR experiments. Their pertinent stopped flow data will be described to facilitate the interpretation of the data obtained in this study. Figure 24 shows the absorbance changes occurring over the first second of reaction time in the presence of C_2H_2 and N_2 respectively. Under these conditions N_2 binds to species E_3 and E_4 and species E_5 to E_7 of the MoFe protein cycle (Figure 10) become populated as it is reduced to $2NH_3$. Lowe *et al* (1993) analyzed the absorbance changes in three time ranges (0-25 ms, 25-50 ms and 150-500 ms) at which different redox levels of the MoFe protein become populated. The analysis undertaken in their investigation showed that the metal centers of MoFe protein undergo complex redox

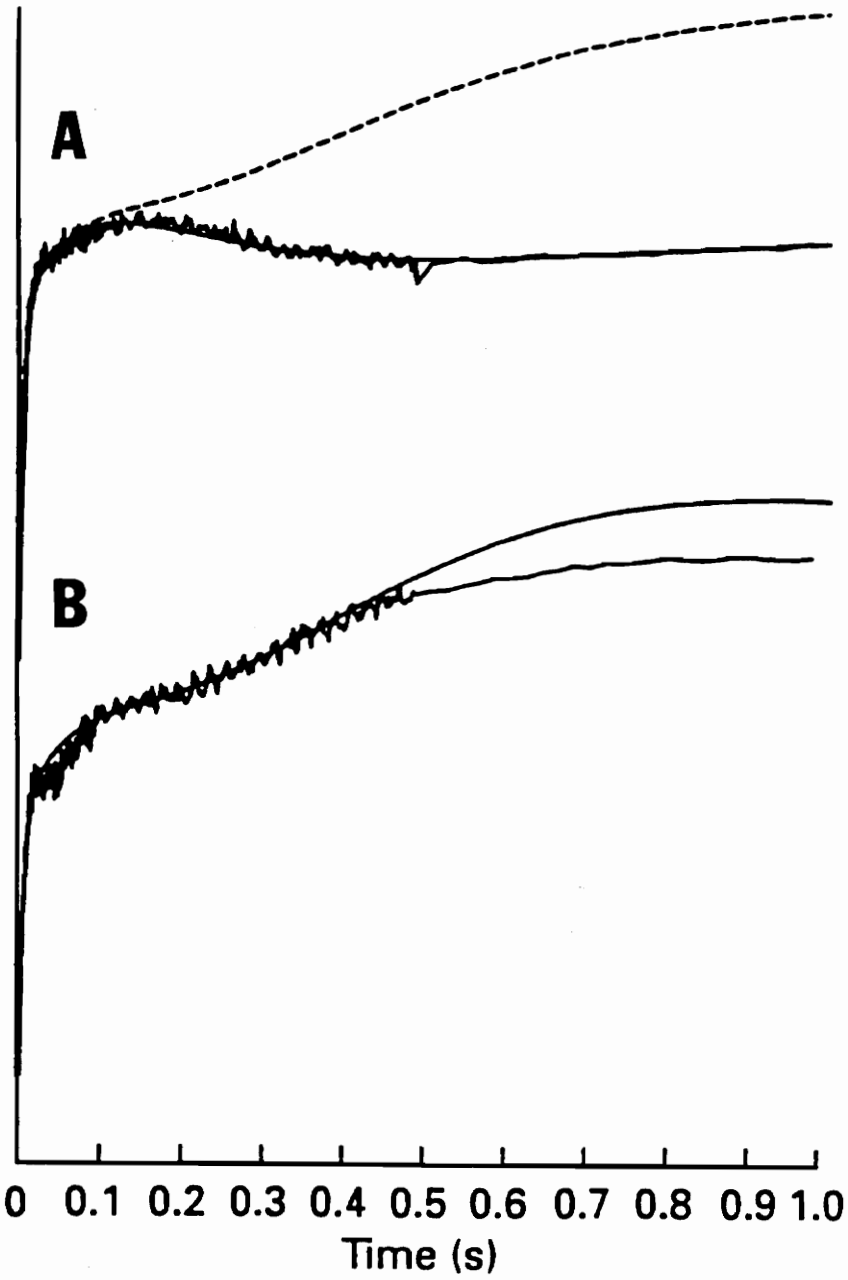

Figure 24. Absorbance changes during the first 1 s of reaction of Kp2 with Kp1 under C_2H_2 (A) and N_2 (B). The solid line is a good simulation of the experimental data, the rough line. The dashed line is the simulation obtained if the increase in absorbance on reduction of Kp1 from E_3 to E_4 is assumed (from Lowe et al., 1993).

changes as electrons are transferred from the Fe-protein. These changes have been shown not to correspond directly to the number of electrons that have been transferred from the Fe-protein. This suggests that electrons are transferred to other metal centers prior to the reduction of the FeMo-cofactor or the substrate bound to the FeMo-cofactor. The initial reduction over the first 25 ms, that generates E_1 from the E_0 dithionite reduced level, results in no significant change in absorbance, although the corresponding EPR signal of bound FeMo-cofactor is bleached. The previously reported change in the Mössbauer spectrum of MoFe protein is also consistent with a reduction of FeMo-cofactor (Smith & Lang, 1974; Münck *et al.*, 1975). Therefore the orbitals containing the unpaired electron(s) of FeMo-cofactor are not associated with any optical transitions contributing significantly to the A_{430}. An absorbance change associated with the second electron transfer to give E_2 from the E_1 level, corresponds to a reduction of a metal center. This implies that although E_2 has probably bound two protons and is capable of evolving H_2, the electron density remains on the metal center and not on bound protons or dihydrogen. No other optical changes were observed on the formation of E_3. Their investigation also shows by the optical changes detected that its reductive formation is associated with an oxidation of a cluster within the MoFe protein and furthermore by EPR that the metal centers oxidized are the P-clusters. It is hypothesized that attaining the E_4 level triggers a transfer of electron density from the P-clusters onto FeMo-cofactor and that this transfer of electron density generates an enhanced reducing power for substrate reduction. It is clear from Figure 24 (a) that in the presence of 100% C_2H_2 the oxidation that occurred as E_3 was reduced to E_4 under N_2 does not occur because according to Lowe *et al.* (1990) MoFe protein with C_2H_2 cannot be reduced below the E_3 level. The solid lines shown in Fig 24 (a) and (b) are the

simulations produced by multiplying the $\Delta\varepsilon_{430}$s obtained by the sum of the concentrations of all species in Lowe and Thorneley model (1984a, Figure 10). The dashed line shown in Fig 24 (a) is the simulation shown in Fig 24 (b) and serves to show the oxidation that is only present under N2 when the E4 state is reached.

We have been able to reproduce the absorbance changes observed under N_2 and C_2H_2 with wild type *A. vinelandii*, Fig 25 (a) and (b), by using exactly the same conditions as those employed by Lowe *et al.* (1993). The absorbance patterns are similar to those shown in Fig 24 (b) and (a), unfortunately it was beyond the scope of this investigation for us to perform the complex computer simulations on these spectra. Figure 26 (a) and (b) shows the result of the same experiment with the α-195^{Gln} MoFe protein. The amplitude and rate of the primary electron transfer reaction were the same for both the wild type and altered MoFe proteins under N_2 and C_2H_2 (data not shown). Absorbance changes over the 0-500 ms time range, under both N_2 and C_2H_2, were essentially the same as those observed with the wild type MoFe protein. This suggests that the electron transfer process occurring from the Fe protein to the altered MoFe protein is unlikely to be impaired up to attaining the E_4 level. More specifically the altered nitrogenase is likely to undergo similar redox changes involving the reduction and oxidation of P-clusters during this time period. Therefore it is possible to conclude that the reason for the altered MoFe protein being unable to reduce N_2 is not because it cannot reach the E_4 state. These results also suggest that the protonation that gives rise to the hydrazido(2-) intermediate and occurs because of the oxidation of P-clusters accompanied by an increase in electron density on N_2 bound to FeMo-cofactor is not the crucial and irreversible step for dinitrogen reduction in this altered protein. It is possible that this conclusion may also apply to wild type protein considering the similar

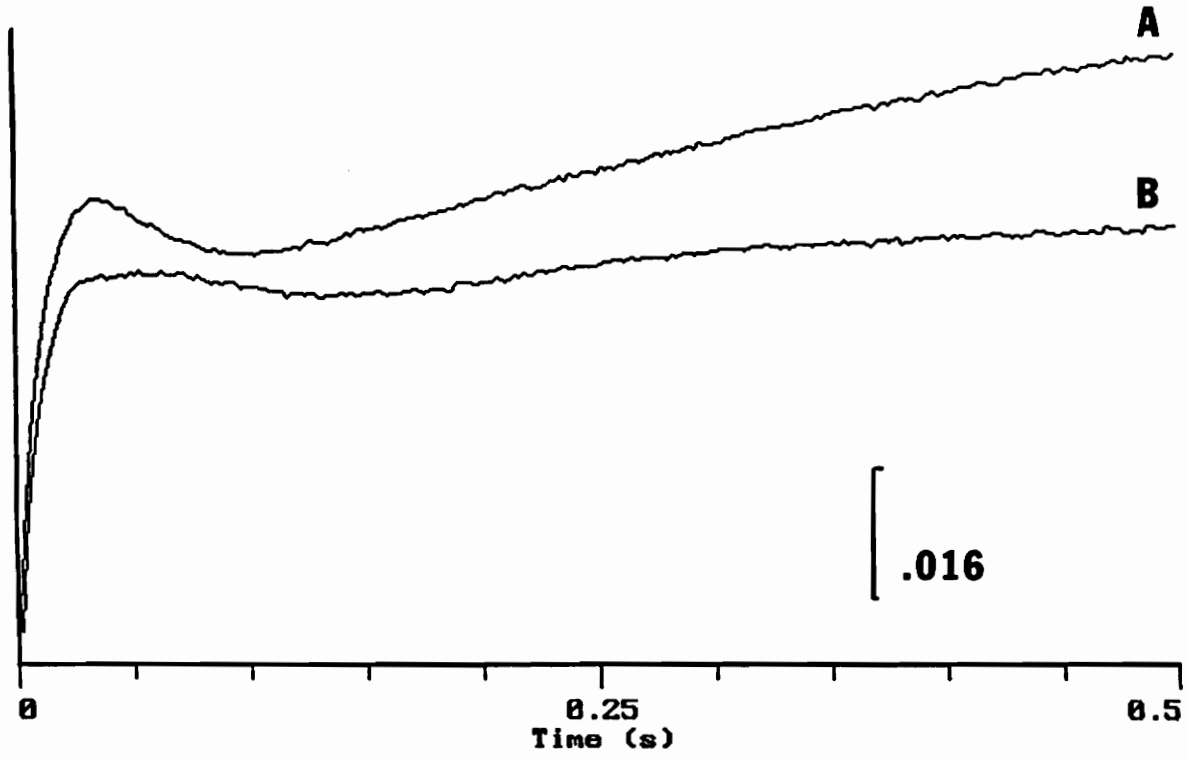

Figure 25. Absorbance changes during the first 500 ms of reaction of wild type Av2 with wild type Av1 under N_2 (A) and C_2H_2 (B).

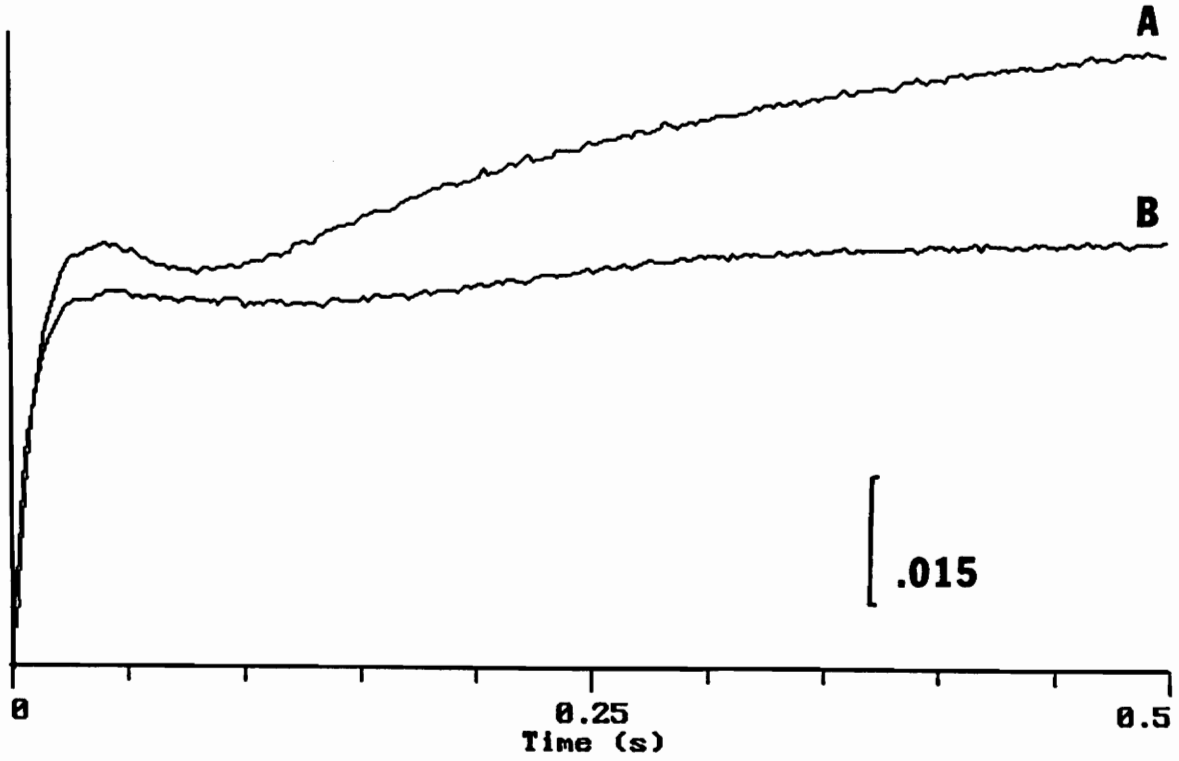

Figure 26. Absorbance changes during the first 500 ms of reaction of wild type Av2 with α-Gln-195 Av1 under N_2 (A) and C_2H_2 (B).

redox changes taking place in the metal centers of the wild type and the altered MoFe protein.

Chapter IV. Catalytic properties of altered Fe proteins containing single amino acid substitutions for the Arginine-100 residue

This chapter represents studies on the role of the Arg-100 residue by examining the mutant strains of *A. vinelandii* derived from the site-specific mutagenesis. This chapter describes the author's contribution to an already published work (Wolle, D., Kim, C-H., Dean, D. R., & Howard, J. B. 1992) including the activity data from *A. vinelandii* crude extracts and purified Fe proteins. The entire paper is attached in the Appendix. A description of the purification procedure used for the activity measurements is found in the Experimental Procedures section.

Introduction

During the Fe protein cycle in which an electron is transferred to the MoFe protein, the reduced Fe protein binds two MgATP molecules; takes a transition to a more open conformation in which the Fe-S cluster becomes more exposed and its redox potential lowered; associates with the MoFe protein; transfers one electron to the MoFe protein with the concomitant MgATP hydrolysis; and dissociates from the MoFe protein. Ionic interactions between the Fe protein and the MoFe protein are believed to be crucial in the whole process. For example, inhibition of the nitrogenase reaction by salt is believed to be due to masking of the charged residues located near the component binding site (Wolle et al., 1992).

One of the regulation mechanisms of the nitrogenase system involves disrupting the physical interaction between the two component proteins. This regulation occurs by the

reversible ADP-ribosylation of the Fe protein preventing formation of the Fe-MoFe protein complex and blocking the electron transfer (reviewed by Roberts and Ludden, 1992). This regulation mechanism has been studied extensively in the photosynthetic bacteria, *Rhodospirillum rubrum.* The enzymes involved in ADP-ribosylation (ADP-ribosyltransferase) and in removal of the ADP ribose (ADP-ribose glycohydrolase) have been purified from *R. rubrum* and characterized (Lowery and Ludden, 1988; Saari et al., 1984).

Studies on the regulation of nitrogenase activity by the ADP-ribosylation of the Fe protein provide some insight into the component protein interaction. The arginine-100 residue in the Fe protein is the site of the ADP-ribosylation, and is believed to be a residue involved in the ionic interaction between the Fe protein and the MoFe protein. The study of a mutant strain of *K. pneumoniae* having a histidine residue substituted for the arginine-100, has been reported previously (Lowery et al., 1989). Altered Fe protein from this mutant is incapable of catalyzing the reduction of protons or acetylene, under normal assay conditions. However, the 100^{his} Fe protein retains some properties characteristic of the normal Fe protein. For example, it contains a functional [4Fe-4S] cluster, undergoes MgATP-dependent conformational change, and catalyzes the hydrolysis of MgATP. These data suggest that the Arg-100 residue is required for the component interaction during electron transfer (Lowery et al., 1989).

Results and discussion

The *A. vinelandii* mutant strains studied have a single amino acid substitution at the Arg-100 site with several other residues including Ala, Asn, Gln, His, Leu, Lys, Phe, Trp, and

Tyr. Only three mutant strains, DJ275 (100^{leu}), DJ285 (100^{tyr}) and DJ359 (100^{phe}), had diazotrophic growth capabilities, whereas the other strains exhibited no detectable diazotrophic growth. Crude extracts were prepared from these three strains and the Fe protein activities were determined as described in Experimental Procedures. The acetylene reduction activity of the Fe protein was measured in the presence of an optimum amount of supplementing wild type MoFe protein (Table XI). The Fe proteins in crude extracts of DJ285 (100^{tyr}) and DJ359 (100^{phe}) exhibited very low acetylene reduction activity compared to that of the wild type Fe protein. DJ275 (100^{leu}) had no detectable crude extract activity. The Fe proteins were purified from the wild type and three Nif(+) mutant strains using Q-Sepharose ion exchange chromatography. The acetylene reduction specific activity of each purified Fe protein was determined at variable electron flux by titrating the Fe protein with the separately purified wild type MoFe protein (Table XII). The purified wild type Fe protein exhibited a maximum acetylene reduction activity of 1269 nmol / (min x mg) when assayed at a molar Fe:MoFe ratio of 1:3. The 100^{leu} Fe protein had only a minimal detectable level of activity. On the other hand, 100^{tyr} and 100^{phe} Fe proteins exhibited about 33% and 12% of wild type activity, respectively. The optimum molar Fe:MoFe ratio giving the maximum Fe protein activity was different in each Fe protein preparation because each sample had a different level of purity. The activity data from the purified Fe proteins of the wild type and mutant strains were generally in good agreement with their crude extract Fe protein activities. However, the altered Fe protein activities measured in crude extracts are relatively lower than the activities measured from the purified proteins. For example, 100^{tyr} Fe protein in a crude extract has ≈16% of the wild type crude extract Fe protein activity, whereas the purified 100^{tyr} Fe protein has ≈33% of

Table XI. Fe protein activities in crude extracts from wild type and mutant strains.

Strain	Residue at 100	Specific activity[a]
Wild Type	Arg	30.0
DJ275	Leu	0
DJ285	Tyr	4.8
DJ359	Phe	0.9

[a] Crude extract specific activity is expressed as nmoles C_2H_4 produced / (min x mg total extract protein).

Table XII. Specific activities of the purified wild type and altered Fe proteins.

Strain	Residue at 100	Specific Activity[a]	Molar Fe:MoFe Ratio
Wild type	Arg	1269	1 : 3
DJ275	Leu	14	4 : 1
DJ285	Tyr	425	1 : 1
DJ359	Phe	155	1 : 1

[a] specific activity is expressed as nmoles of C_2H_4 produced / (min x mg Fe protein).

the purified wild type Fe protein activity. It appears that the nitrogenase activities of these mutant strains are more sensitive to unknown inhibitory factor(s) present in crude extracts.

Chapter V. Intermolecular electron transfer and substrate reduction properties of MoFe proteins altered by site-specific amino acid substitution

This chapter represents a publication (Kim, C-H., Zheng, L., Newton, W. E., & Dean, D. R. 1993) which combined Limin Zheng's work on intermolecular electron transfer and the author's work on altered substrate reduction properties. We are particularly grateful to Jeff Bolin, Steve Muchmore and Nino Campobasso for providing details of their structure of the *C. pasteurianum* MoFe protein prior to publication.

Introduction

Biological nitrogen fixation is catalyzed by nitrogenase a two–component metalloprotein comprised of the Fe protein and the MoFe protein. The Fe protein is the obligate electron donor to the MoFe protein upon which is located the site of substrate reduction. During catalysis electrons are delivered one at a time from the Fe protein to the MoFe protein in a gated process involving the association–dissociation of the component proteins and hydrolysis of 2 MgATP for each electron transfer. Although electrons are delivered to the MoFe only one at a time, six electrons are required for reduction of dinitrogen to yield 2 molecules of ammonia. Thus, major challenges in the biochemical process of nitrogen reduction involve accomplishing the unidirectional delivery of electrons to the substrate reduction site and subsequent capture of those electrons by nitrogen or one of its semi–reduced intermediates. In its simplest terms the electron pathway can be considered in three stages: intermolecular delivery of electrons from the Fe protein to the MoFe protein, intramolecular delivery of electrons to the substrate reduction site, and reduction of

the substrate. Ongoing work in several laboratories has endeavored to dissect these processes by placing amino acid substitutions within the Fe protein and MoFe protein. Recent advances in determination of the structures of the nitrogenase component proteins and their complementary metalloclusters (Georgiadis et al., 1992; Kim and Rees, 1992) now provide a basis for interpreting some of the biochemical changes associated with such amino acid substitutions and also provide insight for designing new amino acid substitution strategies. In this brief review our recent results on characterization of altered MoFe proteins which are affected in either the intermolecular delivery of electrons to the MoFe protein or in substrate reduction are presented and discussed.

Altering intermolecular electron transfer

The Fe protein is a homodimer which has a single redox–active [4Fe–4S] cluster bridged between its identical subunits. Transfer of an electron from the Fe protein to the MoFe Protein requires that the two component proteins dock such that the Fe protein's [4Fe–4S] cluster is brought into reasonable proximity with a complementary redox site located on the MoFe protein. This site on the MoFe protein is believed to be occupied by the so called "P–clusters". The P–clusters are organized into two [8Fe–8S] clusters (hereafter referred to as 8Fe–clusters) each of which is symmetrically bridged between an α–β unit of the MoFe protein. How do the component proteins communicate to accomplish electron transfer? Inspection of the component protein structures reveals that simple face–to–face contact between them would not necessarily bring the respective clusters in close proximity. Namely, the Fe protein's [4Fe–4S] cluster is probably located at or very near the polypeptide surface in its MgATP–bound form but the MoFe protein's

8Fe–cluster is not. Thus, one must consider that either the MoFe protein polypeptide itself provides an adequate path for cluster–to–cluster electron transfer, or the MoFe protein undergoes a conformational change when it interacts with the Fe protein such that its cluster becomes more accessible to the Fe protein's cluster. This latter possibility makes sense in light of a gating mechanism which could help enforce unidirectionality of the electron path.

What are the residues that could participate in such a process? Previous work on the Fe protein has shown that substitutions placed at the Arg–100 position (Lowery et al., 1989; Wolle et al., 1992) a near neighbor of the cluster coordinating Cys–98 residue, can affect intermolecular electron transfer. This is manifested in the His–100 Fe protein which exhibits electron transfer that is substantially uncoupled to MgATP hydrolysis (18 ATP equivalents consumed per electron transfer) and catalytic activity that is hypersensitive to salt concentration. In a related study, initiated before the present structures were available, we attempted to identify analogous residues located on the MoFe protein which might have complementary functions in coupling MgATP hydrolysis and intermolecular electron transfer. Because the Fe protein's [4Fe–4S] cluster is bridged between identical subunits and the MoFe protein's 8Fe clusters are bridged between non–identical subunits we expected that the Fe protein would interact at a MoFe protein α–subunit: β–subunit interface which exhibits pseudo–twofold symmetry. The other possibility we considered is that component protein docking could involve charged residues capable of ionic interaction. Particular emphasis was, therefore, placed on negatively charged residues which, theoretically, could interact with the Arg–100 residues from the Fe protein. Thus, two pairs of tandem aspartate residues located 7 and 8 residues downstream from the MoFe protein 8Fe–cluster coordinating residues α–154 and β–153, respectively, were targeted for

substitution.

In a series of site–directed mutagenesis experiments the α–subunit Asp–161 and Asp–162 positions and the corresponding β–subunit Asp–160 and Asp–161 positions were substituted by Glu, singly and in various combinations. Although certain of these mutants had slightly lowered diazotrophic growth rates, none of them exhibited a Nif– phenotype. In a different set of experiments the same four residues were substituted by Asn, again singly and in various combinations. Results of these experiments showed that substitution of Asn at the α–subunit Asp–161 position, and only at that position, resulted in a strictly Nif– phenotype. The altered α–subunit Asn–161 MoFe protein was purified to homogeneity and characterized. The purified α–subunit Asn–161 MoFe protein activity has remarkable similarity to the Fe protein His–100 protein because it exhibits electron transfer that is substantially uncoupled to MgATP hydrolysis (18 ATP equivalents consumed per electron transfer). Also, component protein mixing experiments were used to show that the altered MoFe protein remains capable of specific interaction with the Fe protein. Namely, the altered MoFe protein can effectively compete *in vitro* with wild type MoFe protein for the available Fe protein. Thus, the α–Asn–161 MoFe protein can dock with the Fe protein but it is defective in the intermolecular delivery of electrons to the 8Fe–cluster.

These results can now be placed in the context of the available MoFe protein structure. Examination of the MoFe protein structure reveals a pseudo–twofold symmetry between domains which encompass the α–subunit Asp–161: Asp–162 residues and the corresponding β–subunit Asp–160: Asp–161 residues (Figure 27). Furthermore, α–Asp–162 and the analogous β–Asp–161 are solvent exposed and are located at opposite

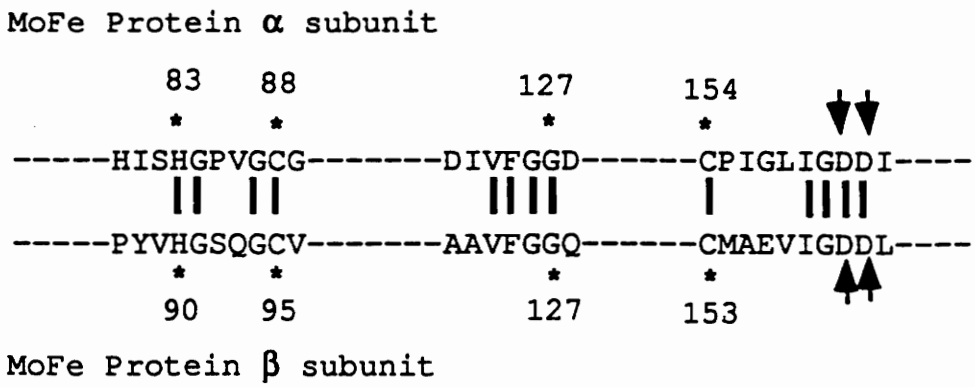

Figure 27. Comparison of the *Azotobacter vinelandii* MoFe protein α- and β-subunits in regions proposed to be involved in intermolecular electron transfer. Arrowheads indicate Asp residues that were substituted by Glu or Asn. The single letter code for amino acids is used in the figure.

sides near an α–subunit: β–subunit interface cleft which approaches the 8Fe–cluster. At the present state of refinement it also appears that the carboxylate group of α–Asp–161 interacts with α–His–83 and α–Gly–127. Similarly, the analogous carboxylate group of β–160 appears to interact with β–His–90 and β–Gly–127 (Bolin, J. unpublished data). This arrangement is interesting because it allows one to consider potential communication between solvent exposed residues which are candidates for participation in component protein docking (for example, α–Asp–162, β–Asp–161, α–Phe–125, and β–Phe–125 [see also, Lowe et al., 1993]) and the 8Fe–coordinating ligands α–Cys–88, α–Cys–154, β–Cys–95, and β–Cys–153. Thus, component protein association and dissociation could effect movement (or accessibility) of the MoFe protein's 8Fe–cluster towards and away from the Fe protein's [4Fe–4S] cluster. If such a mechanism exists it is likely to be coupled to MgATP hydrolysis, which requires component protein association, and could facilitate a unidirectional electron path. Our present results show that α–Asp–161 plays an essential, and perhaps a dominant, role in coupling intermolecular electron transfer and MgATP hydrolysis. Based on the available structural information and biochemical data, we wonder if α–Asp–161 and β–Asp–160 participate in forming a productive electron transfer pathway by transducing conformational changes within the MoFe protein during component protein association and dissociation. This possibility and the potential participation of other residues in the process of intermolecular electron transfer are now being tested by further amino acid substitution experiments (also see Mortenson et al., 1993).

Altering the substrate reduction site

The substrate reduction site for nitrogenase is located on another metallocluster contained within the MoFe protein called FeMo–cofactor (Fe_6S_9Mo–Homocitrate). Evidence for this was provided by a series of studies which ultimately demonstrated that substitution of citrate for homocitrate within FeMo–cofactor changes the substrate reduction properties and inhibitor susceptibilities of the altered nitrogenase (Liang et al, 1990; McLean et al. 1983). More recently these studies were extended by eliciting specific alterations in the substrate reduction properties of nitrogenase using diastereomers of FeMo–cofactor which contain 1–fluorohomocitrate (Madden et al. 1990). A complementary approach that we have used involves altering the substrate reduction properties of nitrogenase by placing amino acid substitutions within the FeMo–cofactor polypeptide environment (Scott et al. 1990; Scott et al. 1992). Prior to the availability of a structure, such strategies relied on primary amino acid sequence comparisons, FeMo–cofactor extrusion properties, and consideration of the path for FeMo–cofactor biosynthesis. Although this approach was successful, it clearly did not identify the entire FeMo–cofactor environment as revealed by the structures. In particular, neither the close approach of certain β–subunit residues toward the FeMo–cofactor nor the N–coordination to the Mo–site by α–His–442 was anticipated. Residues which appear to be within the immediate FeMo–cofactor environment are shown in Figure 28.

Studies on the polypeptide environment in the region which encompasses the α–subunit residues 183 to 199 are discussed here because they are our most advanced. The original hypothesis for the involvement of this region in FeMo–cofactor binding was based on comparison of the MoFe protein α–subunit primary sequence to the product of the FeMo–cofactor biosynthetic gene *nifE*, which, together with *nifN*, forms a heterotetramer

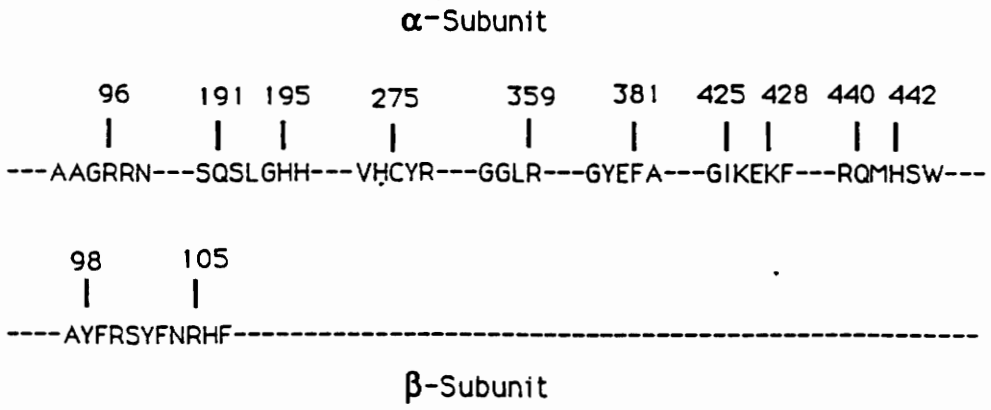

Figure 28. Residues within the *Azotobacter vinelandii* MoFe protein α- and β-subunits which are probably located near the FeMo-cofactor.

analogous to the MoFe protein. This approach provided a method for selecting specific residues for substitution and a strategy for choosing the appropriate substituting amino acid. In this way the *A. vinelandii* MoFe protein α–Gln–191 residue was chosen for substitution by Lys which results in a strict Nif– phenotype (Scott et al. 1990). The purified α–Lys–191 MoFe exhibits remarkable similarity to MoFe protein produced in *nifV* mutants from *K. pneumoniae* (i.e., hydrogen evolution sensitive to CO). Because the FeMo–cofactor from *K. pneumoniae nifV* mutants contains citrate rather than homocitrate it was proposed that α–Gln–191 might interact with homocitrate in the wild type protein (Scott et al. 1992). Structural analysis of the MoFe protein has now shown that α–Gln–191 does indeed interact with the α–carboxylate of homocitrate. More recently, Klipp and coworkers have shown that a *nifV* mutant from *R. capsulatus* is able to reduce acetylene by 2 and 4 electrons to yield both ethylene and ethane. This feature is also exhibited by the *A. vinelandii* α–191–Lys MoFe protein. Taken together these and previous results show that homocitrate and its polypeptide environment play an important role in directing substrate reduction.

In a separate set of experiments the α–His–195 position was substituted by Asn, which also results in a Nif– phenotype. This altered MoFe protein was purified and found to reduce protons and acetylene at moderate rates but was unable to reduce nitrogen. Another interesting feature of the α–Asn–195 MoFe protein is that it does not exhibit the ESEEM signal characteristic of N–coordination to FeMo–cofactor (Thomann et al. 1991). This observation led us to suggest that α–His–195 is directly ligated to FeMo–cofactor. However, inspection of the MoFe protein structure shows that α–His–195 is close to the FeMo–cofactor but not close enough for direct ligation (at least in the crystal form at its

present state of refinement, Kim and Rees 1992). Nevertheless, the fact that the α–Asn–195 MoFe protein can reduce protons and acetylene but not nitrogen indicated that this position plays an integral role, either electronic or structural, in the catalytic mechanism of nitrogenase. These possibilities were explored further by substituting other amino acids at the α–His–195 position.

The most interesting phenotype observed among those MoFe proteins which have substitutions at the α–195 position was exhibited by the α–Gln–195 MoFe protein. This altered protein was purified and shown to have proton reduction and acetylene reduction specific activities only slightly lower than purified wild type MoFe protein. Although nitrogen could not be reduced by the α–Gln–195 MoFe protein, nitrogen was able to inhibit both acetylene reduction and proton reduction. This pattern of inhibition was almost identical to nitrogen inhibition of acetylene reduction and proton reduction catalyzed by the wild type MoFe protein. Nitrogen inhibition of acetylene reduction catalyzed by the α–Gln–195 MoFe protein was shown to be competitive ($K_i \approx 0.359$ atm) and completely reversible. These results can be explained in two possible ways. One possibility is that nitrogen bound to the α–Gln–195 MoFe protein can compete with protons or acetylene for electrons to yield some product other than ammonia. The other possibility is that nitrogen bound to the α–Gln–195 MoFe protein inhibits proton and acetylene reduction by simple occupation of the catalytic site. This latter possibility turned out to be the correct one as it was demonstrated that proton reduction catalyzed by the α–Gln–195 MoFe protein becomes uncoupled from ATP hydrolysis by the addition of nitrogen (11.5 ATP equivalents per electron transfer in the presence of nitrogen). This feature was demonstrated by measuring the amount of product (hydrogen evolution) under conditions

of limiting ATP or limiting reductant under argon or nitrogen atmospheres.

An important observation from the α–His–195 substitution studies is that histidine at this position is not *absolutely* required for nitrogen binding but is essential for nitrogen reduction. Thus, it appears that α–His–195 is likely to function either in electronic fine tuning the substrate reduction site or properly positioning substrate nitrogen within the active site. These possibilities are not mutually exclusive. The fact that both acetylene and protons are reduced by the α–Gln–195 MoFe protein at rates comparable to the wild type protein argues that this residue is unlikely to function as a proton donor during catalysis. Another feature that emerged is that the α–Gln–195 MoFe protein is able to bind nitrogen but the α–Asn–195 MoFe protein is not. Nitrogen binding in these experiments was assessed by its ability to inhibit proton reduction. This observation is interesting in light of the MoFe protein structure, which at its present refinement, shows the δ1 and ε2 nitrogens of the imidazole ring of α–His–195 respectively positioned away and toward the FeMo–cofactor. The δ1 and ε2 nitrogens of the α–His–195 imidazole ring can theoretically occupy positions equivalent to the δ1 and ε2 amide nitrogens in α–Asn–195 and α–Gln–195, respectively. Thus, if α–His–195 does have a role in positioning substrate nitrogen within the reduction site, it appears the ε2 nitrogen of the imidazole ring is the functional player in this process.

Summary

Recent elucidation of the three dimensional structures of the nitrogenase component proteins and their associated metalloclusters places new emphasis on site–directed amino acid substitution studies aimed at determining functional aspects of individual residues

within nitrogenase. Concerning the MoFe protein, major challenges that remain include elucidation of the details of component protein docking, identification of the electron path between the 8Fe–cluster and FeMo–cofactor, and participation of individual amino acid residues in the catalytic mechanism. Work described here and ongoing elsewhere (see Mortenson et al., 1993) demonstrates the feasibility of dissecting specific functional aspects of individual amino acid residues within the nitrogenase component proteins by using the amino acid substitution approach.

Summary

In this dissertation, the role of MoFe protein α-195-histidine residue in nitrogenase catalysis has been investigated. Biochemical and spectroscopic observations using the α-His-195 mutant strains of *Azotobacter vinelandii* with further characterizations of the altered purified α-Gln-195 MoFe protein are included in Chapters I and III.

Six major conclusions resulted from these studies. First, the α-Gln-195 MoFe protein is able to bind, but can not reduce N_2. Second, α-Gln-195 MoFe protein is likely to undergo the same kind of redox changes as the wild type protein, involving the reduction and oxidation of P-clusters up to the E_4 redox state, which was proposed by Thorneley and Lowe (1984a) to be the essential step for N_2 reduction. Therefore, the reason for the altered MoFe protein being unable to reduce N_2 is not because the MoFe protein can not reach the redox state necessary for N_2 reduction. Third, N_2 is able to inhibit acetylene reduction and proton reduction catalyzed by the α-Gln-195 MoFe protein without competing for the available reducing equivalents, which suggests that N_2 inhibits both acetylene and proton reduction by simple occupation of a common substrate-binding site. Fourth, although the binding of N_2 to the α-Gln-195 MoFe protein uncouples MgATP hydrolysis from proton reduction, it does not affect the overall rate of MgATP hydrolysis. This result provides evidence that the substrate ordinarily plays a significant role in controlling the direction of electron flow during nitrogenase turnover by serving as an effective electron sink and, thereby, avoiding the futile cycling of MgATP hydrolysis. Fifth, replacement of the α-195-histidine residue by glutamine results in a dramatic increase in the apparent affinity for CO by the altered protein. Although the most reasonable interpretation of this result is that the imidazole group of the α-195-histidine residue might normally protect the Fe2 atom of the FeMo-cofactor from attack by CO, molecular

modeling of the α-195^{Gln} MoFe protein does not provide compelling support for this hypothesis. Finally, comparison of the altered substrate binding, spectroscopic, and catalytic properties of MoFe proteins from various mutant strains provides evidence that a NH→S hydrogen bond, donated by the ε-nitrogen of the α-195-histidine residue, has a structural role in correctly positioning FeMo-cofactor within the polypeptide matrix and a catalytic role in fine tuning the electronic properties of the substrate binding and reduction site.

Proposed mechanisms for N_2-dependent HD formation have been tested by examining the catalytic properties of the α-Gln-195 MoFe protein, and the results are described in Chapter II. H_2 inhibition of N_2 binding and HD formation in the presence of N_2 and D_2 by the α-Gln-195 MoFe protein, are not consistent with the proposal of the Kettering Institute that the interaction between an enzyme-bound diazene intermediate and D_2 is required for HD formation. N_2-induced uncoupling of ATP hydrolysis from substrate reduction by the α-Gln-195 MoFe protein is reversed by the addition of D_2 in the assay atmosphere. This observation can successfully be explained in Guth & Burris model and Cleland model (Guth and Burris, 1983) if the binding affinity of the altered MoFe protein for D_2 is assumed to be much greater than for N_2. It is also proposed that a larger portion of the α-Gln-195 MoFe protein population could be reduced by two electrons and go back to its original state evolving H_2 instead of reacting with N_2 because of the lower affinity of the altered protein for nitrogen.

Studies on component-protein interactions and intermolecular electron transfer were addressed in Chapter IV and Chapter V.

References

Arnold, W., Rump, A., Klipp, W., Priefer, U. B., & Puhler, A. (1988) Nucleotide sequence of a 24,206-base-pair DNA fragment carrying the entire nitrogen fixation gene cluster of *Klebsiella pneumoniae*. *J. Molec. Biol.* **203**, 715-738.

Ashby, G. A., Dilworth, M. J., & Thorneley, R. N. F. (1987) *Klebsiella pneumoniae* nitrogenase: Inhibition of hydrogen evolution by ethylene and the reduction of ethylene to ethane. *Biochem. J.* **247**, 547-554.

Benemann, J. R., Yoch, D. C., Valentine, R. C., & Arnon, D. I. (1969) The electron transport system in nitrogen fixation by *Azotobacter*. I. Azotoflavin as an electron carrier. *Proc. Natl. Acad. Sci.USA* **64**, 1079-1086.

Bennett, L. T., Cannon, F., & Dean, D. R. (1988) Nucleotide sequence and mutagenesis of the *nifA* gene from *Azotobacter vinelandii*. *Molec. Microbiol.* **2**, 315-321.

Bishop, P. E. & Premakumar, R. (1992) Alternative nitrogen fixation systems. *Biological nitrogen fixation.* (Stacey, G., Burris, R. H., & Evans, H. J. eds.) Chapman & Hall, New York and London. pp. 736-762.

Bolin, J. T., Campobasso, N., Muchmore, S.W., Morgan, T. V., & Mortenson, L. E. (1993) Structure and environment of metal clusters in the nitrogenase molybdenum-iron

protein from *Clostridium pasteurianum. Molybdenum enzymes, cofactors, and model systems* (Stiefel, E. I., Coucouvanis, D., and Newton, W. E. eds.) American Chemical Society, Washington D.C. pp. 186-195.

Bolin, J. T., Ronco, A. E., Mortenson, L. E., Morgan, T. V., Williamson, M., & Xuong, N. -H. (1990) Structure of the nitrogenase MoFe protein: Spatial distribution of the intrinsic metal atoms determined by X-ray anomalous scattering. *Nitrogen fixation: Achievements and objectives.* (Grasshoff, P. M., Roth, L. E., Stacey, G., & Newton, W. E. eds.) Chapman & Hall, New York and London. pp. 117-124.

Brigle, K. E., Newton, W. E., & Dean, D. R. (1985) Complete nucleotide sequence of the *Azotobacter vinelandii* nitrogenase structural gene cluster. *Gene* **37**, 37-44.

Brigle, K. E., Setterquist, R. A., Dean, D. R., Cantwell, J. S., Weiss, M. C., & Newton, W. E. (1987a) Site-directed mutagenesis of the nitrogenase MoFe protein of *Azotobacter vinelandii. Proc.Natl. Acad. Sci. USA.* **84**, 7066-7069.

Brigle, K. E., Weiss, M. C., Newton, W. E., & Dean, D. R. (1987b) Products of the iron-molybdenum cofactor-specific biosynthetic genes, *nifE* and *nifN*, are structurally homologous to the products of the nitrogenase molybdenum-iron protein genes, *nifD* and *nifK. J. Bact.* **169**, 1547-1553.

Bulen, W. A. (1976) Nitrogenase from *Azotobacter vinelandii* and reactions affecting

mechanistic interpretations. *Proc. 1st Int. Symp. Nitrogen fixation.* Pullman, Washington. Washington State University Press. pp. 177-186.

Bulen, W. A., Burns, R. C., LeComte, J. R., & Hinkson, J. (1965) in *Non–Heme Iron Proteins: Role in Energy Conversion.* (San Pietro, A. eds.) Antioch Press, Yellow Springs, OH. pp. 261–274.

Burgess, B. K., Stiefel, E. I., & Newton, W. E. (1980) Oxidation-reduction properties and complexation reactions of the iron-molybdenum cofactor of nitrogenase. *J. Biol. Chem.* **255**, 353-356.

Burgess, B. K., Wherland, S., Newton, W. E., & Stiefel, E. I. (1981) Nitrogenase reactivity: insight into the nitrogen-fixing process through hydrogen-inhibition and HD-forming reactions. *Biochemistry* **20**, 5140-5146.

Burns, R. C., & Bulen, W. A. (1965) ATP-dependent hydrogen evolution by cell-free preparations of *Azotobacter vinelandii. Biochim. Biophys. Acta* **105**, 437-445.

Burris, R. H. (1976) Nitrogen fixation. *Plant Biochemistry* 3rd ed. (Bonner, J. & Varner, J. E. eds.) Academic Press. New York. pp. 887-908.

Burris, R. H. (1991) Nitrogenases. *J. Biol. Chem.* **266**, 9339–9342.

Burris, R. H., & Orme-Johnson, W. H. (1976) Mechanism of biological N_2 fixation. *Proceedings of the first international symposium on nitrogen fixation* (Newton, W. E., & Nyman, C. J. eds.) Washington State University Press, Pullman. **1**, pp. 208-233.

Chan, M. K., Kim, J., & Rees, D. C. (1993) The nitrogenase FeMo-cofactor and P-cluster pair: 2.2 Å resolution structures. *Science* **260**, 792-794.

Chaney, A. L., & Marbach, E. P. (1962) Modified reagents for determination of urea and ammonia. *Clin. Chem.* **8**, 130–132.

Chatt, J. (1980) Chemistry relevant to the biological fixation of nitrogen. *Nitrogen fixation.* (Stewart, W. D. P., Gallon, J. R. eds.) Academic press, inc. London. pp. 1-18.

Collman, J. P., Brauman, J. I., Halbert, T. R., & Suslick, K. S. (1976) Nature of O_2 and CO binding to metalloporphyrins and heme proteins. *Proc. Natl. Acad. Sci.* **73**, 3333–3337.

Conradson, S. D., Burgess, B. K., Vaughn, S. A., Roe, A. L., Hedman, B., Hodgson, K. G., & Holm, R. H. (1989) Cyanide and methylisocyanide binding to the isolated iron-molybdenum cofactor of nitrogenase. *J. Biol. Chem.* **264**, 15967-15974.

Davis, L. C., Henzl, M. T., Burris, R. H., & Orme-Johnson, W. H. (1979) Iron-Sulfur clusters in the Molybdenum-iron protein component of nitrogenase: Electron paramagnetic

resonance of the carbon monoxide inhibited state. *Biochemistry* **18**, 4860-4869.

Dean, D. R., Bolin, J. T., & Zheng, L. (1993) Nitrogenase metalloclusters: Structures, organization, and synthesis. *J. Bact.* **175**, 6737-6744.

Dean, D. R., & Jacobson M. R. (1992) Biochemical genetics of nitrogenase.*Biological nitrogen fixation.* (Stacey, G., Burris, R. H., & Evans, H. J. eds.) Chapman & Hall, New York and London. pp. 763-834.

Dean, D. R., Scott, D. J., & Newton, W. E. (1990a) Identification of FeMo-co domains within the nitrogenase MoFe protein. *Nitrogen fixation: Achievements and objectives.* (Grasshoff, P. M., Roth, L. E., Stacey, G., & Newton, W. E. eds.) Chapman & Hall, New York and London. pp. 95-102.

Dean, D. R., Setterquist, R. A., Brigle, K. E., Scott, D. J., Laird, N. F., & Newton, W. E. (1990b) Evidence that conserved residues Cys-62 and Cys-154 within the *Azotobacter vinelandii* nitrogenase MoFe protein α-subunit are essential for nitrogenase activity but conserved residues His-83 and Cys-88 are not. *Molecular Microbiology* **4**, 1505-1512.

Dilworth, M. J. (1966) Acetylene reduction by nitrogen-fixing preparations from *Clostridium pasteurianum. Biochim. Biophys. Acta* 127, 285–294.

Dilworth, M. J., Eady, R. R. (1991) Hydrazine is a product of dinitrogen reduction by the

vanadium-nitrogenase from *Azotobacter chroococcum. Biochem. J.* **277**, 465–468.

Dilworth, M. J., Eady, R. R., Robson, R. L., & Miller, R. W. (1987) Ethane formation from acetylene as a potential test for vanadium nitrogenase *in vivo*. *Nature* **327**, 167-168.

Dilworth, M. J., Eldridge, M. E., & Eady, R. R. (1992) Correction for creatine interference with the direct indophenol measurement of NH_3 in steady-state nitrogenase assays. *Analytical Biochemistry* **207**, 6-10.

Dilworth, M. J. & Thorneley, R. N. F. (1981) Nitrogenase of *Klebsiella pneumoniae*: hydrazine is a product of azide reduction. *Biochem. J.* **193**, 971-983.

Eady, R. R., Lowe, D. J., & Thorneley, R. N. F. (1978) Nitrogenase of *Klebsiella pneumoniae* : A pre-steady-state burst of ATP hydrolysis is coupled to electron transfer between the component proteins. *FEBS Lett.* **95**, 211-213.

Eady, R. R. & Postgate J. R. (1974) Nitrogenase. *Nature* **249**, 804–910.

Ennor, A. H. (1957) Determination and preparation of N-phosphates of biological origin. *Methods in Enzymol.* **3**, 850–856.

Filler, W. A., Kemp, R. M., Hawkes, Ng, J. C., Hawkes, T. R., Dixon, R. A., & Smith, B. E. (1986) The *nifH* gene product is required for the synthesis or stability of the

iron-molybdenum cofactor of nitrogenase from *Klebsiella pneumoniae*. *Eur. J. Biochem.* **160**, 371-377.

Fisher, K., Lowe, D. J., & Thorneley, R. N. F. (1991) *Klebsiella pnemoniae* nitrogenase. The pre-steady-state kinetics of MoFe-protein reduction and hydrogen evolution under conditions of limiting electron flux show that the rates of association with the Fe protein and electron transfer are independent of the oxidation level of the MoFe-protein. *Biochem. J.* **279**, 81-85.

Fisher, K., Thorneley, R. N. F., Lowe, D. J. (1990) Nitrogenase of *Klebsiella pneumoniae* : mechanism of acetylene reduction. *Biochem. J.* **272**, 621-625.

Gavini, N., & Burgess, B. K. (1992) FeMo-cofactor synthesis by a *nifH* mutant with altered MgATP reactivity. *J. Biol. Chem.* **267**, 21179-21186.

Gemoets, J. P., Bravo, J., McKenna, C. E., Leigh, G. J., & Smith, B. E. (1989) Reduction of cyclopropene by NifV- and wild type nitrogenases from *Klebsiella pneumoniae*. *Biochem. J.* **258**, 487-491.

Georgiadis, M. M., Komiya, H., Chakrabarti, P., Woo, D., Kornuc, J. J., & Rees, D. C. (1992) Crystallographic structure of the nitrogenase iron protein from *Azotobacter vinelandii*. Science **257**, 1653-1659.

Guth, J. H., & Burris, R. H. (1983) Inhibition of nitrogenase-catalyzed NH_3 formation by H_2. *Biochemistry* **22**, 5111-5122.

Hageman, R. V., & Burris, R. H. (1978) Kinetic studies on electron transfer and interaction between nitrogenase components from *Azotobacter vinelandii. Biochemistry* **17**, 4117-4124.

Hageman, R. V., Orme-Johnson, W. H., & Burris, R. H. (1980) Role of magnesium adenosine 5'-triphosphate in the hydrogen evolution reaction catalyzed by nitrogenase from *Azotobacter vinelandii. Biochemistry* **19**, 2333-2342.

Hagen, W. R., Wassink, H., Eady, R. R., Smith, B. E., & Haaker, H. (1987) Quantitative EPR of an S = 7/2 system in thionine-oxidized MoFe proteins of nitrogenase: A redefinition of the P-cluster concept. *Eur. J. Biochem.* **169**, 457-465.

Hardy, R. W. F., Burns, R. C., & Parshall, G. W. (1971) The biochemistry of N_2 fixation. *Bioorganic Chemistry* (Gould, R. F. eds.) American Chemical Society, Washington D.C. pp. 219–247.

Hardy, R. W. F. & Knight, E. (1966) Reduction of N_2O by biological N_2-fixing systems. *Biochem. Biophys. Res. Commun.* **23**, 409-414.

Hardy, R. W. F., Knight, Jr., E., & D'Eustachio, A. J. (1965) An energy-dependent

hydrogen-evolution from dithionite in nitrogen-fixing extracts of *Clostridium pasteurianum*. *Biochem. Biophys. Res. Commun.* **20**, 539–544.

Hawkes, T. R., McLean, P. A., & Smith, B. E. (1984) Nitrogenase of *nifV* mutants of *Klebsiella pneumoniae* contains an altered form of the iron-molybdenum cofactor. *Biochem. J.* **217**, 317-321.

Hawkes, T. R., & Smith, B. E. (1983) Purification and characterization of the inactive MoFe protein (NifB-Kp1) of the nitrogenase from *nifB* mutants of *Klebsiella pneumoniae*. *Biochem. J.* **209**, 43-50.

Howard, J. B. (1993) Protein component complex formation and adenosine triphosphate hydrolysis in nitrogenase. *Molybdenum enzymes, cofactors, and model systems* (Stiefel, E. I., Coucouvanis, D., and Newton, W. E. eds.) American Chemical Society, Washington D.C. pp. 271-289.

Hoch, G. E., Little, H. N., & Burris, R. H. (1957) Hydrogen evolution from soybean nodules. *Nature*. **179**, 430-431.

Hoch, G. E., Schneider, K. C., & Burris, R. H. (1960) Hydrogen evolution and exchange, and conversion of N_2O to N_2 by soybean root nodules. *Biochim. Biophys. Acta* **37**, 273-279.

Hoover, T. R., Imperial, J., Ludden, P. W., & Shah, V. K. (1989) Homocitrate is a component of the iron-molybdenum cofactor of nitrogenase. *Biochemistry USA.* **28**, 2768-2771.

Hwang, J. C., & Burris, R. H. (1972) Nitrogenase-catalyzed reactions. *Biochim. Biophys. Acta* **283**, 339–350.

Hwang, J. C., Chen, C. H., & Burris, R. H. (1973) Inhibition of nitrogenase-catalyzed reductions. *Biochim. Biophys. Acta.* **292**, 256-270.

Imam, S. & Eady, R. R. (1980) Nitrogenase of *Klebsiella pneumoniae* : Reductant-independent ATP hydrolysis and the effect of pH on the efficiency of coupling of ATP hydrolysis to substrate reduction. *FEBS Lett.* **110**, 35–38.

Jacobson, M. R., Brigle, K. E., Bennett, L. T., Setterquist, R. A., Wilson, M. S., Cash, V. L., Beynon, I., Newton, W. E., & Dean, D. R. (1989) Physical and genetic map of the major *nif* gene cluster from *Azotobacter vinelandii. J. Bact.* **171**, 1017-1027.

Jacobson, M. R., Cash, V. L., Weiss, M. C., Laird, N. F., Newton, W. E., & Dean, D. R. (1989) Biochemical and genetic analysis of the *nifUSVWZM* cluster from *Azotobacter vinelandii. Mol. Gen. Genet.* **219**, 49–57.

Jeng, D. Y., Morris, J. A., & Mortenson, L. E. (1970) The effect of reductant in

inorganic phosphate release from adenosine 5'triphosphate by purified nitrogenase of *Clostridium pasteurianum*. *J. Biol. Chem.* **245**, 2809–2813.

Jensen, B. B., & Burris, R. H. (1985) Effect of high pN_2 and high pD_2 on NH_3 production, H_2 evolution, and HD formation by nitrogenases. *Biochemistry* **24**, 1141-1147.

Jensen, B. B., & Burris, R. H. (1986) N_2O as a substrate and as a competitive inhibitorof nitrogenase. *Biochemistry* **25**, 1083-1088.

Joerger, R. D., & Bishop, P. E. (1988) Nucleotide sequence and genetic analysis of the *nifB-nifQ* region from *Azotobacter vinelandii*. *J. Bacteriol.* **170**, 1475-1487.

Kelly, M., Postgate, J. R., & Richards, R. L. (1967) Reduction of cyanide and isocyanide by nitrogenase of *Azotobacter chroococcum*. *Biochem. J.* **102**, 1c-3c.

Kennedy, C., Eady, R. R., Kondorosi, E., & Rekosh, D. K. (1976) The molybdenum-iron protein of *Klebsiella pneumoniae*. *Biochem. J.* **155**, 383-389.

Kent, H. M., Ioannidis, I., Gormal, C., Smith, B. E., & Buck, M. (1989) Site-directed mutagenesis of the *Klebsiella pneumoniae*. *Biochem. J.* **264**, 257-264.

Kent, H. M., Bainea, M., Gormal, C., Smith, B. E., & Buck, M. (1990) Analysis of

site-directed mutations in the α- and β-subunits of *Klebsiella pneumoniae* nitrogenase. *Molec. Microbiol.* **4**, 1497-1504.

Kim, C.-H., Newton, W. E., & Dean, D. R. (1994) Studies on the role of the MoFe protein α-subunit histidine-195 residue in FeMo-cofactor binding and nitrogenase catalysis. *Biochemistry* (submitted).

Kim, C.-H., Zheng, L., Newton, W. E., & Dean, D. R. (1993) Intermolecular electron transfer and substrate reduction properties of MoFe proteins altered by site-specific amino acid substitution. *New horizons in nitrogen fixation.* (Palacios, R., Mora, J., & Newton, W. E. eds.) Kluwer Academic Publishers, Norwell, Mass. pp. 105-110.

Kim, J., & Rees, D. C. (1992a) Crystallographic structure and functional implications of the nitrogenase molybdenum-iron protein from *Azotobacter vinelandii. Nature* **360**, 553-560.

Kim, J., & Rees, D. C. (1992b) Structural Models for the metal centers in the nitrogenase molybdenum-iron protein. *Science* **257**, 1677-1682.

Kim, J., Woo, D., & Rees, D. C. (1993) X-ray crystal structure of the nitrogenase molybdenum-iron protein from *Clostridium pasteurianum* at 3.0-Å resolution. *Biochemistry* **32**, 7104-7115.

Kim, J., & Rees, D. C. (1994) Nitrogenase and biological nitrogen fixation. *Biochemistry* **33**, 389-397.

Kraulis, P. (1991) MOLSCRIPT: a program to produce both detailed and schematic plots of protein structures. *J. Appl. Cryst.* **24**, 946–950.

Kurtz, D. M. Jr., McMillan, R. S., Burgess, B. K., Mortenson, L. E., & Holm, R. M. (1979) Identification of iron-sulfur centers in the iron-molybdenum proteins of nitrogenase. *Proc. Natl. Acad. Sci. USA* **76**, 4986-4989.

Laemmli, U. K. (1970) Cleavage of structural proteins during the assembly of the head of bacteriophage T_4. *Nature* **227**, 680-685.

Li, J.–G., Burgess, B. K., & Corbin, J. L. (1982) Nitrogenase reactivity: Cyanide as a substrate and inhibitor. *Biochemistry* **21**, 4393–4402.

Li, J., & Burris, R. H. (1983) Influence of pN_2 on HD formation by various nitrogenases. *Biochemistry* **22**, 4472-4480.

Liang, J., & Burris, R. H. (1988) Interactions among N_2, N_2O, and C_2H_2 as substrates and inhibitors of nitrogenase from *Azotobacter vinelandii* . *Biochemistry* **27**, 6726-6732.

Liang, J., & Burris, R. H. (1989) N_2O reduction and HD formation by nitrogenase from a

NifV- mutant of *Klebsiella pneumoniae*. *J. Bact.* **171**, 3176-3180.

Liang, J., Madden, M., Shah, V. K., & Burris, R. H. (1990) Citrate substitutes for homocitrate in nitrogenase of a *nifV* mutant of *Klebsiella pneumoniae*. Biochemistry **29**, 8577-8581.

Lowe, D. J., Eady, R. R., & Thorneley, R. N. F. (1978) Electron paramagnetic studies on the nitrogenase of *Klebsiella pneumoniae* : Evidence for acetylene and ethylene-nitrogenase transient complexes. *Biochem. J.* **173**, 277-290.

Lowe, D. J., Fisher, K., Pau, R. N., & Thorneley, R. N. F. (1993) Kinetics and mechanism of nitrogenase - a role for 'P' centers in dinitrogen reduction. *New horizons in nitrogen fixation.* (Palacios, R., Mora, J., & Newton, W. E. eds.) Kluwer Academic Publishers, Norwell, Mass. pp. 95-100.

Lowe, D. J., Fisher, K., Thorneley, R. N. F. (1990) *Klebsiella pneumoniae* nitrogenase: Mechanism of acetylene reduction and its inhibition by carbon monoxide. *Biochem. J.* **272**, 621-625.

Lowe, D. J., Fisher, K., Thorneley, R. N. F. (1993) *Klebsiella pneumoniae* nitrogenase: Pre-steady-state absorbance changes show that redox changes occur in the MoFe protein that depend on substrate and component protein ratio; a role for P-centers in reducing dinitrogen? *Biochem. J.* **292**, 93-98.

Lowe, D. J., Fisher, K., Thorneley, R. N. F., Vaughn, S. W., & Burgess, B. K. (1989) Kinetics and mechanism of the reaction of cyanide with molybdenum nitrogenase from *Azotobacter vinelandii. Biochemistry* **28**, 8460-8466.

Lowe, D. J., & Thorneley, R. N. F. (1984a) The mechanism of *Klebsiella pneumoniae* nitrogenase action: Pre-steady-state kinetics of H_2 formation. *Biochem. J.* **224**, 877-886.

Lowe, D. J., & Thorneley, R. N. F. (1984b) The mechanism of *Klebsiella pneumoniae* nitrogenase action: The determination of rate constants required for the simulation of the kinetics of N_2 reduction and H_2 evolution. *Biochem. J.* **224**, 895-901.

Lowe, D. J., Thorneley, R. N. F., & Smith, B. E. (1985) Nitrogenase. *Metalloproteins. Part 1: Metal proteins with redox roles* (Harrison, P. ed.) Verlag-Chemie, Basel. pp. 207-249.

Lowery, R. G., Chang, C. L., Davis, L. C., McKenna, M. C., Stephens, P. J., & Ludden, P. W. (1989) Substitution of histidine for arginine-101 of dinitrogenase reductase disrupts electron transfer to dinitrogenase. *Biochemistry* **28**, 1206-1212.

Lowery, R. G. & Ludden, P. W. (1988) Purification and properties of dinitrogenase reductase ADP-ribosyltransferase from the photosynthetic bacterium *Rhodospirillum rubrum. J. Biol. Chem.* **263**, 16714-16719.

Lundell, D. J., & Howard, J. B. (1978) Isolation and partial characterization of two different subunits of the molybdenum-iron protein of *Azotobacter vinelandii* nitrogenase. *J. Biol. Chem.* **253**, 3422-3426.

Madden, M. S., Kindon, N. D., Ludden, P. W., & Shah, V. K. (1990) Diastereomer-dependent substrate reduction properties of a dinitrogenase containing 1-fluorohomocitrate in the iron-molybdenum cofactor. *Proc. Natl. Acad. Sci. USA* **87**, 6517-6521.

McKenna, C. E., Huang, C. W., Jones, J. B., McKenna, M-C, Nakajima, T., & Nguyen, H. T. (1980) Cyclopropenes: new chemical probes of nitrogenase active site interactions. *Nitrogen fixation Vol. 1.* (Newton, W. E. & Orme-Johnson, W. H. eds.) University Park Press. Baltimore. pp. 223-235.

McKenna, C. E., Stephens, P. J., Eran, H., Luo, G. M., Zhang, F. X., Ding, M., Nguyen, H. T. (1984) Substrate interactions with nitrogenase and its FeMo-cofactor: Chemical and spectroscopic investigations. *Advances in nitrogen fixation research..* (Veeger, C. & Newton, W. E. eds.) pp. 115.

McLean, P. A., & Dixon, R. A. (1981) Requirement of *nifV* gene for production of wild type nitrogenase enzyme in *Klebsiella pneumoniae. Nature* **292**, 655-656.

McLean, P. A., Papaefthymiou, V., Orme-Johnson, W. H., & Munck, E. (1987) Isotopic hybrids of nitrogenase: Mossbauer study of MoFe protein with selective ^{57}Fe enrichment

of the P-cluster. *J. Biol. Chem.* **262**, 12900-12903.

McLean, P. A., Smith, B. E., & Dixon, R. A. (1983) Nitrogenase of *Klebsiella pneumoniae nifV* mutants. *Biochem. J.* **211**, 589-597.

McNary, J. E., & Burris, R. H. (1962) Energy requirements for nitrogen fixation by cell-free preparations from *Clostridium pasteurianum. J. Bacteriol.* **84**, 598-599.

Menon, A. L., Stults, L. W., Robson, R. L., & Mortenson, L. E. (1990) Cloning, sequencing and characterization of the [NiFe] hydrogenase-encoding structural genes (*hoxK* and *hoxG*) from *Azotobacter vinelandii. Gene* **96**, 67–74.

Mensink, R. E., Wassink, H., & Haaker, H. (1992) A reinvestigation of the pre-steady-state ATPase activity of the nitrogenase from *Azotobacter vinelandii. Eur. J. Biochem.* **208**, 289-294.

Miller, R. W., & Eady, R. R. (1988) Cyanamide: A new substrate for nitrogenase. *Biochim. Biophys. Acta* **952**, 290-296.

Mortenson L. E. (1963) Nitrogen fixation: Role of ferredoxin in anaerobic metabolism. *Ann. Rev. Microbiol.* **17**, 115-138.

Mortenson, L. E., Morgan, T. V., & Seefeldt, L. C. (1993) Use of Fe protein altered at

specific amino acid positions to probe its function in nitrogenase catalysis. *New horizons in nitrogen fixation.* (Palacios, R., Mora, J., & Newton, W. E. eds.) Kluwer Academic Publishers, Norwell, Mass. pp. 111-116.

Mozen, M. M., & Burris, R. H. (1954) The incorporation of ^{15}N-labeled nitrous oxide by nitrogen fixing agents. *Biochim. Biophys. Acta* **14**, 577-578.

Munck, E., Rhodes, H., Orme-Johnson, W. H., Davis, L. C., Brill, W. J., & Shah, V. K. (1975) Nitrogenase. VIII. Mossbauer and EPR spectroscopy. *Biochim. Biophys. Acta* **400**, 32-53.

Nagatani, H. H., Shah, V. K., & Brill, W. J. (1974) Activation of inactive nitrogenase by acid-treated component I. J. Bact. **120**, 697-701.

Newton, W. E. (1993) Nitrogenases: distribution, composition, structure and function. *New horizons in nitrogen fixation.* (Palacios, R., Mora, J., & Newton, W. E. eds.) Kluwer Academic Publishers, Norwell, Mass. pp. 5-18.

Newton, W. E., Bulen, W. A., Hadfield, K. L., Stiefel, E. I., & Watt, G. D. (1977) HD formation as a probe for intermediates in N_2 reduction. *Recent developments in nitrogen fixation.* (Newton, W. E., Postgate, J. R., & Rodriguez-Barrueco, C. eds.) Academic Press. London. New York. San francisco. pp. 119-130.

Newton, W. E., & Dean, D. R. (1993) Role of the iron-molybdenum cofactor polypeptide environment in *Azotobacter vinelandii* molybdenum-nitrogenase catalysis.*Molybdenum enzymes, cofactors, and model systems* (Stiefel, E. I., Coucouvanis, D., and Newton, W. E. eds.) American Chemical Society, Washington D.C. pp. 216-230.

Novak, R., Wilson, P. W. (1948) The utilization of nitrogen in hydroxylamine and oximes by *Azotobacter vinelandii. J. Bact.* **55**, 517–524.

Orme-Johnson, W. H. (1992) Nitrogenase structure: Where to now? *Science* **257**, 1639-1640.

Orme–Johnson, W. H., Davis, L. C., Henzl, M. T., Averill, B. A., Orme–Johnson, N. R., Munck, E., & Zimmerman, R. (1977) Components and pathways in biological nitrogen fixation. *Recent Developments In Nitrogen Fixation.* (Newton, W. E., Postgate, J. R., & Rodriguez–Barrueco, C. eds.) Academic Press, London, New York, and San Francisco. pp. 131–178.

Orme-Johnson, W. H., Hamilton, W. D., Ljones, T., T'so, M. Y. W., Burris, R. H., Shah, V. K., Brill, W. J. (1972) Electron paramagnetic resonance of nitrogenase and nitrogenase components from *Clostridium pasteurianum* W5 and *Azotobacter vinelandii* O.P. *Proc. Natl. Acad. Sci. USA* **69**, 3142-3145.

Orme-Johnson, W. H., Lindahl, P., Meade, J., Warren, W., Nelson, M., Groh, S.,

Orme-Johnson, N. R., Munck, E., Huynh, B. H., Emptage, M., Rawlings, J., Smith, J., Roberts, J., Hoffmann, B., & Mims, W. B. (1981) Nitrogenase: prosthetic groups and their reactivities. *Current perspectives in nitrogen fixation.* (Gibson, A. H. Newton, W. E. eds.) Aust. Acad. Sci. Canberra. pp. 79-83.

Paustian, T. D., Shah, V. K., & Roberts, G. P. (1989) Purification and characterization of the *nifN* and *nifE* gene products from *Azotobacter vinelandii* mutant UW45. *Proc. Natl. Acad. Sci. U.S.A.* **86**, 6082-6086.

Paustian, T. D., Shah, V. K., & Roberts, G. P. (1990) Apodinitrogenase: Purification, association with a 20-kilodalton protein, and activation by the iron-molybdenum cofactor in the absence of dinitrogenase reductase. *Biochemistry* **29**, 3515-3522.

Rawlings, J., Shah, V. K., Chisnell, J. R., Brill, W. J., Zimmermann, R., Munck, E., & Orme-Johnson, W. H. (1978) Novel metal cluster in the Iron-Molybdenum cofactor of nitrogenase. *J. Biol. Chem.* **253**, 1001-1004.

Rivera-Ortiz, J. M., & Burris, R. H. (1975) Interactions among substrates and inhibitors of nitrogenase. *J. Bact.* **123**, 537-545.

Roberts, G. P. & Ludden, P. W. (1992) Nitrogen fixation by photosynthetic bacteria. *Biological nitrogen fixation.* (Stacey, G., Burris, R. H., & Evans, H. J. eds.) Chapman & Hall, New York and London. pp. 135-165.

Roberts, G. P., MacNeil, T., MacNeil, D., & Brill, W. J. (1978) Regulation and characterization of protein products coded by the *nif* (nitrogen fixation) genes of *Klebsiella pneumoniae*. *J. Bacteriol.* **136**, 267-279.

Robinson, A. C., Burgess, B. K., & Dean, D. R. (1986) Activity, reconstitution, and accumulation of nitrogenase components in *Azotobacter vinelandii* mutant strains containing defined deletions within the nitrogenase structural gene cluster. *J. Bact.* **166**, 180-186.

Robinson, A. C., Chun, T. W., Li, J-G., Burgess, B. K. (1989) Iron-molybdenum cofactor insertion into the apo-MoFe protein of nitrogenase involves the iron protein-MgATP complex. *J. Biol. Chem.* **264**, 10088-10095.

Rubinson, J. F., Burgess, B. K., Corbin, J. L., & Dilworth, M. J. (1985) Nitrogenase activity: Azide reduction. *Biochemstry* **24**, 273-283.

Rubinson, J. F., Corbin, J. L., & Burgess, B. K. (1983) Nitrogenase reactivity: Methyl isocyanide as a substrate and inhibitor. *Biochemistry*. **22**, 6260-6268.

Saari, L. L., Triplett, E. W., & Ludden, P. W. (1984) Purification and properties of the activating enzyme for iron protein of nitrogenase from the photosynthetic bacterium *Rhodospirillum rubrum*. *J. Biol. Chem.* **259**, 15502-15508.

Schollhorn, R., & Burris, R. H. (1967a) Reduction of azide by the N_2-fixing enzyme system. *Proc. Natl. Acad. Sci. U.S.A.* **57**, 1317-1323.

Schollhorn, R., & Burris, R. H. (1967b) Acetylene as a competitive inhibitor of N_2 fixation. *Proc. Natl. Acad. Sci. U.S.A.* **58**, 213–216.

Scott, D. J., Dean, D. R., & Newton, W. E. (1992) Nitrogenase-catalyzed ethane production and CO-sensitive hydrogen evolution from MoFe proteins having amino acid substitutions in an α-subunit FeMo cofactor-binding domain. *J. Biol. Chem.* **267**, 20002-20010.

Scott, D. J., May, H. D., Newton, W. E., Brigle, K. E., & Dean, D. R. (1990) Role for the nitrogenase MoFe protein α-subunit in FeMo-cofactor binding and catalysis. *Nature* **343**, 188-190.

Shah, V. K., & Brill, W. J. (1977) Isolation of an iron-molybdenum cofactor from nitrogenase. *Proc. Natl. Acad. Sci. USA* **74**, 3249-3253.

Simpson, F. B., & Burris, R. H. (1984) A nitrogen pressure of 50 atmospheres does not prevent evolution of hydrogen by nitrogenase. *Science* **224**, 1095-1097.

Smith, B. E., Buck, M., Eady, R. R., Lowe, D. J., Thorneley, R. N. F., Ashby, G., Deistung, J., Eldridge, M., Fisher, K., Gormal, C., Ioannidis, I., Kent, H., Arber, J.,

Flood, A., Garner, C. D., Hasnain, S., & Miller, R. (1988) Recent studies on the structure and function of molybdenum nitrogenase. *Nitrogen fixation: Hundred years after.* (Bothe, H., de Bruijn, F. J., & Newton, W. E. eds.) Stuttgart: Gustav Fischer. pp. 91-100.

Smith, E. D., Eady, R. R., Lowe, D. J., & Gormal, C. (1988) The vanadium-iron protein of vanadium nitrogenase from *Azotobacter chroococcum* contains an iron-vanadium cofactor. *Biochem. J.* **250**, 299-302.

Smith, B. E., & Lang, G. (1974) Mossbauer spectroscopy of the nitrogenase proteins from *Klebsiella pneumoniae* : Structural assignments and mechanistic conclusions. *Biochem. J.* **137**, 169-180.

Smith, B. E., Lowe, D. J., & Bray, R. C. (1973) Studies by electron paramagnetic resonance on the catalytic machanism of nitrogenase of *Klebsiella pneumoniae. Biochem. J.* **135**, 331-341.

Swisher, R. H., Landt, M. L., & Reithel, F. J. (1977) The molecular weight of, and evidence for two types of subunits in, the molybdenum-iron protein of *Azotobacter vinelandii* nitrogenase. *Biochem. J.* **163**, 427-432.

Thomann, H., Bernardo, M., Newton, W. E., & Dean, D. R. (1991) N coordination of FeMo-cofactor requires His-195 of the MoFe protein α subunit and is essential for

biological nitrogen fixation. *Proc. Natl. Acad. Sci.* **88**, 6620–6623.

Thomann, H., Morgan, T. V., Jin, H., Burgmayer, S. J. N., Bare, R. E., & Stiefel, E. I. (1987) Protein nitrogen coordination to the FeMo center of nitrogenase from *Clostridium pasteurianum. J. Am. Chem. Soc.* **109**, 7913-7914.

Thorneley, R. N. F. (1975) Nitrogenase of *Klebsiella pneumoniae* : A stopped-flow study of magnesium-adenosine triphosphate-induced electron transfer between the component proteins. *Biochem. J.* **145**, 391-396.

Thorneley, R. N. F., Ashby, G. A., Howarth, J. V., Millar, N. C., & Gutfreund, H. (1989) A transient kinetic study of the nitrogenase of *Klebsiella pneumoniae* by stopped-flow calorimetry. *Biochem. J.* **264**, 657-661.

Thorneley, R. N. F., Chatt, J., Eady, R. R., Lowe, D. J., O'Donnell, M. J., Postgate, J. R., Richards, R. L., & Smith, B. E. (1980) The mechanism of biological nitrogen fixation: Transient complexes in catalytic cycles. *Nitrogen fixation* (Newton, W. E., & Orme-Johnson, W. H. eds.) University Park Press. Baltimore. pp. 171-193.

Thorneley, R. N. F., Eady, R. R., Lowe, D. J. (1978) Biological nitrogen fixation by way of an enzyme-bound dinitrogen-hydride intermediate. *Nature* **272**, 557-558.

Thorneley, R. N. F., Eady, R. R., & Yates, M. G. (1975) Nitrogenases of *Klebsiella*

pneumoniae and *Azotobacter chroococcum* : Complex formation between the component proteins. *Biochim. Biophys. Acta* **403**, 269-284.

Thorneley, R. N. F., & Lowe, D. J. (1983) Nitrogenase of *Klebsiella pneumoniae* . Kinetics of the dissociation of oxidized iron protein from molybdenum-iron protein: Identification of the rate-limiting step for substrate reduction. *Biochem. J.* **215**-393-403.

Thorneley, R. N. F., & Lowe, D. J. (1985) Kinetics and mechanism of the nitrogenase enzyme system. *Molybdenum enzymes*. (Spiro, T. G. ed.) Wiley, New York. pp. 222-284.

Thorneley, R. N. F., & Lowe, D. J. (1984a) The mechanism of *Klebsiella pneumoniae* nitrogenase action: Pre-steady-state kinetics of an enzyme-bound intermediate in N_2 reduction and of NH_3 formation. *Biochem. J.* **224**, 887-894.

Thorneley, R. N. F., & Lowe, D. J. (1984b) The mechanism of *Klebsiella pneumoniae* nitrogenase action: Simulation of the dependence of the H_2 evolution rate on component-protein concentration and ratio and sodium dithionite concentration. *Biochem. J.* **224**, 903-909.

Thorneley, R. N. F., Yates, M. G., & Lowe, D. J. (1976) Nitrogenase of *Azotobacter chroococcum* : Kinetics of the reduction of oxidized iron-protein by sodium dithionite. *Biochem. J.* **155**, 137-144.

Turner, G. L., & Bergersen, F. J. (1969) The relationship between nitrogen fixation and the production of HD from D_2 by cell-free extracts of soya-bean nodule bacteroids. *Biochem. J.* **115**, 529-535.

Vaughn, S. A., & Burgess, B. K. (1989) Nitrite, a new substrate for nitrogenase. *Biochemistry* **28**, 419-424.

Watt, D. G., Bulen, W A., Burns, A., & Hadfield, K. L. (1975) Stoichiometry, ATP/2e values, and energy requirements for reactions catalyzed by nitrogenase from *Azotobacter vinelandii*. *Biochemistry* **14**, 4266–4272.

Wherland, S., Burgess, B. K., Stiefel, E. I., & Newton, W. E. (1981) Nitrogenase Reactivity: Effects of component ratio on electron flow and distribution during nitrogen fixation. *Biochemistry* 20, 5132-5140.

Willing, A. H., Georgiadis, M. M., Rees, D. C., & Howard, J. B. (1989) Crosslinking of nitrogenase components: Structure and activity of the covalent complex. *J. Biol. Chem.* **264**, 8499-8503.

Wilson, P. W., & Umbreit, W. W. (1937) Symbiotic nitrogen fixation. III. Hydrogen as a specific inhibitor. *Arch. Mikrobiol.* **8**, 440–457.

Wolle, D., Kim, C. -H., Dean, D. R., & Howard, J. B. (1992) Ionic interactions in the

nitrogenase complex. *J. Biol. Chem.* **267**, 3667-3673.

Yates, M. G. (1992) The enzymology of molybdenum-dependent nitrogen fixation. *Biological nitrogen fixation.* (Stacey, G., Burris, R. H., & Evans, H. J. eds.) Chapman & Hall, New York and London. pp. 685-735.

Zimmerman, R., Munck, E., Brill, W. J., Shah, V. K., Henzl, M. T., Rawlings, J., & Orme-Johnson, W. H. (1978) Nitrogenase X: Mossbauer and EPR studies on reversibly oxidized MoFe protein from *Azotobacter vinelandii* O.P. Nature of the iron centers. *Biochim. Biophys. Acta* **537**, 185-207.

Zumft, W. G., Mortenson, L. E., & Palmer, G. (1974) Electron paramagnetic resonance studies on nitrogenase: Investigation of the oxidation reduction behaviour of azoferredoxin and molybdoferredoxin with potentiometric and rapid-freeze techniques. *Eur. J. Biochem.* **46**, 525-535.

APPENDIX

THE JOURNAL OF BIOLOGICAL CHEMISTRY
1992 by The American Society for Biochemistry and Molecular Biology, Inc.

Vol. 267, No. 6, Issue of February 25, pp. 3667-3673, 1992
Printed in U.S.A.

Ionic Interactions in the Nitrogenase Complex

PROPERTIES OF Fe-PROTEIN CONTAINING SUBSTITUTIONS FOR Arg-100*

(Received for publication, August 16, 1991)

Dana Wolle‡, ChulHwan Kim§, Dennis Dean§, and James Bryant Howard‡

From the ‡Department of Biochemistry, University of Minnesota, Minneapolis, Minnesota 55455 and the §Department of Anaerobic Microbiology, Virginia Polytechnic Institute and State University, Blacksburg, Virginia 24061

A series of *Azotobacter vinelandii* strains have been constructed in which the nitrogenase Fe-protein (Av2) was altered by substitutions for Arg-100. This invariant residue is a likely partner in a salt bridge with the MoFe-protein and, in some species, is the site of reversible regulation by ADP-ribosylation (Pope, M. R., Murrell, S. A., and Ludden, P. W. (1985) *Proc. Natl. Acad. Sci. U. S. A.* 82, 3173–3177). Although we find that arginine is the optimum amino acid, other residues in this position could support diazotrophic growth. These results were surprising because *Klebsiella pneumoniae* Fe-protein substituted by His-100 had been reported to be inactive (Lowery, R. G., Chang, C. L., Davis, L. C., McKenna, M.-C., Stevens, P. J., and Ludden, P. W. (1989) *Biochemistry* 28, 1206–1212). Two altered Fe-proteins (Av2-R100Y, the tyrosyl form, and Av2-R100H, the histidyl form) were isolated and, in contrast to this earlier report, we found that both had some activity in acetylene reduction. However, both altered proteins exhibited a decreased maximum velocity (35 and 3% of wild type, respectively) and were strongly inhibited by excess MoFe-protein. These adverse activity parameters were also manifest in the increased sensitivity of the altered proteins to inhibition by salts. Indeed, the salt sensitivity of Av2-R100H is so significant that its activity is masked in the normal assay and is easily missed. In addition, for Av2-R100H, substrate reduction is substantially uncoupled from MgATP hydrolysis. These results suggest that substitutions for Arg-100 may decrease the affinity of the Fe-protein for the MoFe-protein prior to electron transfer but increase affinity after electron transfer. Hence, the role of Arg-100 may be to provide the optimum balance in stabilities of these two complexes for maximum efficiency in substrate reduction.

Biological reduction of dinitrogen to ammonia is catalyzed by the nitrogenase complex. This highly conserved and widely distributed enzyme consists of two components: the MoFe-protein,[1] where dinitrogen reduction occurs, and the Fe-protein, which is the unique electron donor for substrate reduction. The Fe-protein has one redox active 4Fe:4S cluster that bridges symmetrically the two identical protein subunits (1), while the MoFe-protein is an $\alpha_2\beta_2$ tetramer thought to contain four 4Fe:4S clusters and two Fe_{5-7}:Mo:S_{8-9}:homocitrate cofactors (2, 3). An abbreviated version of the reaction path is shown in Scheme 1 (adapted from Refs. 4–6). The prominent features of the mechanism are the initial formation of a complex (Complex I) between the components, the electron transfer coupled to the hydrolysis of two MgATP (formation of Complex II), and the dissociation of Complex II. Because the complex must dissociate after each electron transfer step, several cycles of component interaction and complex turnover must occur before substrates are reduced on the MoFe-protein (4, 5). The dissociation of Complex II is rate-determining when reduced Fe-protein is in excess (5).

The physical interactions that lead to the productive complexes shown in Scheme 1 are unknown. However, some clues are provided by the effects that salts have on the physical and catalytic properties of nitrogenase (7–17). For example, *Azotobacter vinelandii* nitrogenase is substantially inhibited by various salts in excess of 100–200 mM (6, 9). The inhibition can be accounted for by a simple modification of the model as shown in Scheme 1, namely the salt is treated as a dead-end inhibitor which binds to the Fe-protein (6).[2] One explanation for this phenomenon is that salt ions mask charged residues located in or near the component binding site(s), thereby preventing the interactions necessary for complex formation. At least two residues involved in a putative salt bridge have been identified by chemical cross-linking (17, 18). The highly specific reaction mediated by 1-ethyl-3-(3-dimethylaminopropyl)carbodiimide results in the formation of an isopeptide between Lys-399 of Av1 α-subunit and Glu-112 of Av2. The cross-linking reaction was inhibited by NaCl with a pattern similar to inhibition of substrate reduction. More recently, we have found that Glu-112 is part of a cation binding pocket formed by a patch of acidic residues.[3]

* This work was supported by Grant GM 34321 from the National Institutes of Health (to J. B. H.) and Grants DMB 88-86920 (to J. B. H.) and DMB 89-17171 (to D. D.) from the National Science Foundation. The costs of publication of this article were defrayed in part by the payment of page charges. This article must therefore be hereby marked "*advertisement*" in accordance with 18 U.S.C. Section 1734 solely to indicate this fact.

[1] The abbreviations and nomenclature used were: Av2, Fe-protein or dinitrogenase reductase from *A. vinelandii*; Av1, MoFe-protein or dinitrogenase from *A. vinelandii*; Av2-WT, wild type Fe-protein from *A. vinelandii*; Av1-WT, wild type MoFe-protein from *A. vinelandii*; Av2-R100Y, Fe-protein from *A. vinelandii* substituted by tyrosine at position 100; Av2-R100H, Fe-protein from *A. vinelandii* substituted by histidine at position 100; K_{Av2}, the dissociation constant for Av1 and nucleotide-containing Av2; K_{ATP}, the K_m of Av2 for ATP; Av2(2ATP)', one electron reduced Av2 containing two bound molecules of MgATP; and Av2(2ADP)°, oxidized Av2 containing two bound molecules of MgADP.

[2] A more complex model in which salts interact with both the Fe-protein and MoFe-protein is kinetically equivalent to the simpler version of Scheme 1.

[3] A. Willing and J. B. Howard, manuscript in preparation.

Glu-112 has been identified in the three-dimensional structure of Av2 and is on the same surface of the protein as the Fe:S cluster (19). Also on this face of Av2 and neighboring the cluster is the invariant cationic residue, Arg-100. In some species, Arg-100 is reversibly ADP-ribosylated in a process that regulates the nitrogenase activity (20–22). Although ADP-ribosylation probably inactivates nitrogenase turnover by steric interference between the components (23), the normal functional role of Arg-100 is more likely as a partner in an ionic interaction at the complex interface. An altered form of Fe-protein generated by random mutagenesis in *Klebsiella pneumoniae* has been isolated in which Arg-100 is replaced by histidine (24). This protein was reported to be inactive in substrate reduction yet could participate in the turnover of ATP. Thus, Arg-100 appears to be a promising residue to examine by site-specific amino acid substitution in order to further evaluate elements of the productive protein-protein interactions.

MATERIALS AND METHODS

Mutations in the Av2 gene (*nifH*) were generated by the oligonucleotide-directed mutagenesis method of Zoller and Smith (25) as previously described (26, 27). Template DNA was a 2577-base pair fragment from the *PstI* digestion of plasmid pDB6 (28) and contained the entire *A. vinelandii nifH*. The oligonucleotides used for mutagenesis (30 bases long) were synthesized with a mixture of all four bases in the positions corresponding to the codon for amino acid residue-100. Plasmids containing mutant *nifH* were isolated with either a histidyl (CAT), lysyl (AAG), asparaginyl (AAC), glutaminyl (CAG), alanyl (GCC), leucyl (TTG), phenylalanyl (TTC), or tyrosyl (TAT) codon at position 100. *A. vinelandii* strains were constructed by homologous recombination and were isolated as described by Dean *et al.* (28). The genetic stability of strains DJ230 (R100H) and DJ284 (R100Y) were established by several cycles of growth and re-isolation before the altered Fe-proteins were purified. All strains were maintained on agar plates of Burk's medium with NH_4^+.

Cells were grown in 40-liter carboys of Burk's medium containing limiting, 1 mM NH_4^+. The nitrogenase components are expressed upon exhaustion of NH_4^+. Two hours after the initial detection of *in vivo* nitrogenase activity or the onset of stationary phase, the cells were harvested and used immediately for protein purification. The whole cell acetylene reduction was measured by incubating 1 ml of cells for 20 min at 30 °C in septum-sealed, 9-ml vials containing 10% acetylene, 90% air. Ethylene was quantified by gas chromatography. The manipulation of all buffers, reagents, and proteins was performed under anaerobic conditions provided by a Schlenk manifold system with argon and vacuum lines. The purification scheme for altered Fe-proteins was a modification of previously published procedures (29, 30). These modifications were as follows. 1) The heat treatment of the crude extract was omitted. 2) The ion exchange chromatography step utilized a 1.6 × 50-cm DEAE-Sepharose column and a 0.1–0.35 M NaCl gradient. 3) The final step was gel chromatography on Sepharose S-200 in 50 mM Tris-HCl buffer, pH 8.0. Purified Fe-proteins were stored as 1-ml samples in liquid nitrogen. No change in activity was detected after 2 months in low temperature storage. Each Fe-protein was >95% a single component as judged by gel electrophoresis.

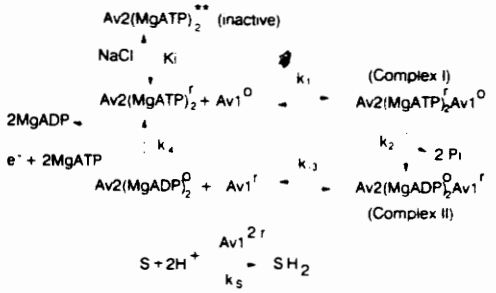

SCHEME 1. **The Fe-protein oxidation-reduction cycle, based on the models of Hageman and Burris (4) and Thorneley and Lowe (5), as modified by Deits and Howard (6).** Shown are the different redox states (r = 1 electron reduced, o = oxidized) of the Fe-protein (Av 2) and the MoFe-protein (Av1) from A. vinelandii. The presence of 2 bound nucleotide molecules (MgATP or MgADP) on Av2 is also denoted. The form of Av2 inhibited by bound salt is indicated in the upper left-hand corner. K_i is the inhibition constant for salt. S denotes the substrates (acetylene, protons, etc.) which are reduced by the 2 electron reduced form of Av1.

Carboxymethylation, trypsin digestion, and peptide mapping of the Fe-proteins were as described by Hausinger and Howard (1). Each altered Av2 was carboxymethylated with 2-[^{14}C]iodoacetic acid, while Av2-WT was carboxymethylated with 2-[^{3}H]iodoacetic acid. For peptide maps, ^{14}C-labeled, altered Av2 was mixed with ^{3}H-labeled Av2-WT and digested with 2% trypsin for 2 h at 30 °C. The tryptic peptides were applied to a 1 × 50-cm column of DEAE-Sepharose Cl-6B equilibrated in 100 mM Tris-HCl, 5% *n*-propanol, pH 8.0. The peptides were eluted by a 0–0.75 M NaCl gradient, and the radioactive peaks were quantified by liquid scintillation counting.

Nitrogenase activity was detected by acetylene or proton reduction using a modification of methods previously described (8, 31). Reactions were performed in 9-ml serum vials containing 2 mM ATP, 2.5 mM $MgCl_2$, 6 mM creatine phosphate, 0.125 mg/ml creatine phosphokinase, 10 mM sodium dithionite, and 25 mM Tris-HCl buffer, pH 8.0, in a total volume of 1 ml. The NaCl concentration in the assay was adjusted by the addition of 1 M NaCl in 25 mM Tris-HCl buffer, pH 8.0. For the acetylene reduction assay, the gas phase was 11% acetylene in argon. Acetylene, ethylene, and hydrogen were quantified by gas chromatography.

The ratio of ATP hydrolyzed to acetylene reduced was determined using a limiting number of ATP equivalents (ATP plus creatine phosphate) and excess dithionite as described previously (6). Assay vials containing nitrogenase components and a known number of ATP equivalents were incubated at 30 °C. At specified times, the amount of product formed was determined by gas chromatography. Exhaustion of the ATP equivalents was assumed when no additional product was formed. The end point was verified by introducing new dithionite and active wild type nitrogenase; if no further product formation occurred, the exhaustion of ATP equivalents was confirmed. The ratio was calculated from the known initial amount of ATP equivalents and the amount of product formed. The amount of ATP consumed at any time before its exhaustion could be calculated from the difference in amount of product before and after adding a large excess of wild type nitrogenase and the known efficiency for wild type nitrogenase (4.1 mol of ATP/mol of acetylene reduced, the experimentally determined value).

Protein concentrations were determined by amino acid analyses. Active Av2 concentration was measured by MgATP-dependent Fe chelation using the chelator *o*-bathophenanthroline disulfonate (32). The rates of Fe chelation by 2,2′-bipyridyl were determined as described by Deits and Howard (31). Absorbance data were collected at 30 °C and were analyzed by nonlinear regression (31).

RESULTS AND DISCUSSION

Growth curves for *A. vinelandii* wild type (strain DJ-WT) and strains with Av2 substituted at position 100 are shown in Fig. 1. All strains had nearly identical growth rates in medium containing ammonia. However, when ammonia was exhausted, a range of growth rates was exhibited from no detectable growth in the strains having the histidyl, lysyl, asparaginyl, glutaminyl, or alanyl substitution to near wild type growth for the strain with Av2-R100Y (the tyrosyl substitution). Strains incapable of diazotrophic growth also lacked detectable whole-cell substrate reduction activity, while those strains that grew had enzyme activity levels commensurate with the cell growth rate. These initial results clearly indicated that the previously proposed, exclusive role for arginine at residue 100 must be re-evaluated (24).

In an effort to understand why arginine is the "best" residue at position 100, two altered Fe-proteins were purified and characterized. Av2-R100Y was chosen because it supports a moderate level of substrate reduction activity, and hence, a number of kinetic parameters could be readily obtained. Av2-

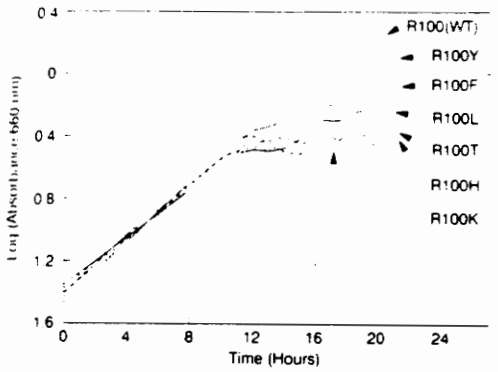

FIG. 1. **Growth curves for selected mutants of *A. vinelandii*, containing Fe-proteins altered at position 100.** Each mutant was grown at 30 °C, in 100 ml of Burks' media containing 0.8 mM NH_4Cl. Absorbance (660 nm) values and *in vivo* acetylene reduction activities were measured at 1-h intervals. Expression of the various nitrogenase proteins was detected by the *in vivo* acetylene reduction assay. The doubling time for wild type *A. vinelandii* was approximately 2.7 h, while the doubling time for the *A. vinelandii* strain containing Av2-R100Y was 4 h, and the doubling time for the strain containing Av2-R100L was 6 h. Not shown are growth curves for strains of *A. vinelandii* with glutamine, asparagine, or alanine substituted for Arg-100. These strains have growth curves and acetylene reduction activities similar to the strains containing Av2-R100H or Av2-R100K.

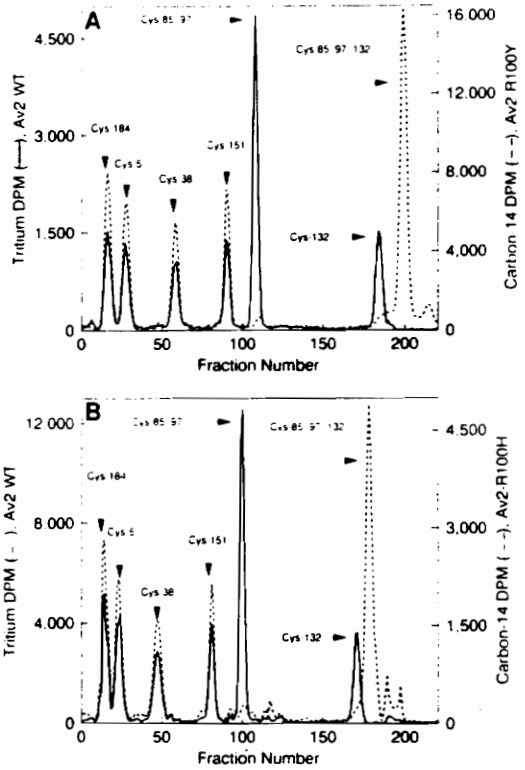

FIG. 2. **Elution patterns of tryptic peptides derived from Av2-WT, Av2-R100Y, and Av2-R100H, radiolabeled by carboxymethylation of their cysteines.** Peptides were separated by chromatography on DEAE-Sepharose Cl-6B in 50 mM Tris-HCl, pH 8.0, using a NaCl gradient from 0.0 to 1.0 M NaCl. Undigested protein eluted in a small peak or set of peaks at the end of the chromatogram. *A*, Radioactive elution profile of Av2-WT (——) *versus* Av2-R100Y (- - -). *B*, Radioactive elution profile of Av2-WT (——) *versus* Av2-R100H (- - -).

R100H was chosen because it did not support growth and, although previously it had been considered to be inactive (24), the nature of the nonproductive complex might be evaluated. To demonstrate that the mutations were expressed as amino acid substitutions in the isolated proteins, two methods of chemical characterization were used. Amino acid analyses of Av2-R100Y and Av2-R100H indicated 1 less arginine (per subunit), while Av2-R100Y had 1 more tyrosine and Av2-R100H had 1 more histidine. A second, more definitive demonstration of the amino acid substitution was the use of peptide maps. Fortuitously, replacement of Arg-100 by histidine or tyrosine removes a trypsin cleavage site resulting in the fusion of two tryptic peptides containing Cys-85, -97, and -132. Thus, the distinction between Av2-WT and the altered proteins is readily discerned by the change in the elution positions of cysteinyl peptides. The results are shown in Fig. 2 and include the peptides from Av2-WT for comparison. As anticipated for the altered proteins, two of the cysteinyl tryptic peptides were no longer present and a new peptide containing the radioactivity equivalent to three carboxymethylated cysteines appeared. On this basis, we estimate that both isolated, altered proteins are >95% substituted at position 100.

An important characteristic of functional Av2-WT is the effect that MgATP binding has on the properties of the Fe:S cluster (summarized in Ref. 2). The most dramatic of these effects is the requirement for MgATP binding in order to chelate the iron (31–33). This phenomenon is usually ascribed to an ATP-induced conformational change which exposes the Fe:S cluster. Both Av2-R100H and Av2-R100Y retained this property; no iron was chelated except in the presence of MgATP, and the full complement of iron was removed (data not shown). A similar result was found previously for the *K. pneumoniae* Fe-protein-R100H (24). As for Av2-WT, irreversible oxygen damage to the altered proteins resulted in the loss of the MgATP requirement for iron chelation. Preliminary studies indicated that, compared with Av2-WT, the rate of chelation was approximately 30% for Av2-R100Y and 15% for Av2-R100H.[4] The chelation rates may reflect subtle changes in access to the cluster which should have some effect on electron transfer. However, this difference is not sufficient to account for the observed decrease in substrate reduction activity (see below). Hence, the rate of ATP-dependent iron chelation does not appear to be a valid indicator of the relative specific activities.

Both Av2-R100Y and Av2-R100H had readily detectable activity with Av1 in the proton or acetylene reduction assays. Because the *A. vinelandii* strain containing Av2-R100Y had good diazotrophic growth and whole-cell acetylene reduction activity, the high specific activity of this protein was expected. However, the low but definite activity of Av2-R100H from a strain with no growth or *in vivo* activity was unanticipated. A complication in detecting the low activity of purified Av2-R100H is the substantial inhibition by the salt concentration of the standard assay mixture; undoubtedly this is why the activity was not observed in earlier investigations (24). Indeed, the intracellular ionic strength may be sufficient to decrease the Av2-R100H activity below the threshold for it to

[4] D. Wolle and J. B. Howard, unpublished results.

support growth or for it to be detected by the *in vivo* assay. To maximize the low activities of Av2-R100H, a modified assay was devised to balance between the inhibition by ionic strength and the need for acceptable concentrations of sodium dithionite, MgATP, and creatine phosphate. Although the observed Av2-R100H activity might have arisen from small amounts of contaminating Av2-WT, this possibility can be discounted because of the substantial differences between Av2-WT and Av2-R100H in both the shapes of their titration curves and their sensitivity to salt (see below for a more complete description of these effects).

The ability of these altered proteins to participate in substrate reduction with wild type Av1 was assessed by titrating a fixed amount of Av1-WT with varying amounts of Av2. As shown in Figs. 3 and 4, both Av2-R100Y and Av2-R100H have lower activity than Av2-WT even when the altered Fe-protein is at a high (saturating) ratio (note the difference in scales between the two figures). Likewise, compared with Av2-WT, both altered proteins require much higher concentrations to obtain their maximum velocities. From the activity data, Av2-R100Y is estimated to be 35% as active as Av2-WT and Av2-R100H is 3% as active (see Table I for a summary of kinetic parameters). The titration curve for Av2-R100Y closely resembles the hyperbolic curve for Av2-WT, yet the curve for Av2-R100H clearly has a significant lag in activity. A possible origin for this sigmoidal-shaped curve is discussed below.

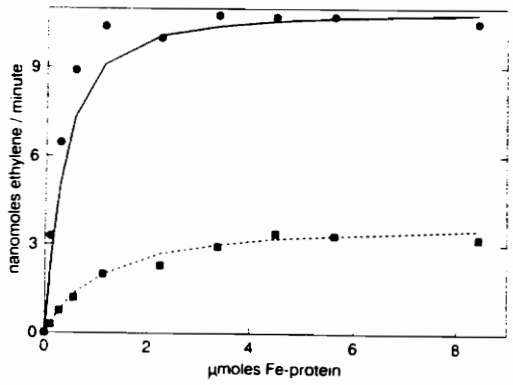

FIG. 3. **Nitrogenase-catalyzed acetylene reduction.** 0.256 μmol of Av1-WT was titrated with increasing amounts of either Av2-WT (●), or Av2-R100Y (■). The low salt assay conditions used were as described under "Materials and Methods." The *lines* indicate values obtained by fitting the data points to the Deits-Howard treatment of Scheme 1 (6), which yielded a K_{Av2} of 0.2 μM for Av2-WT and 0.8 μM for Av2-R100Y.

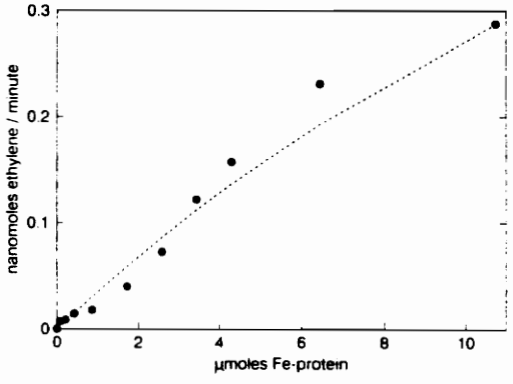

FIG. 4. **Nitrogenase-catalyzed acetylene reduction.** 0.256 μmol of Av1-WT was titrated with increasing amounts of Av2-R100H (●). Low salt assay conditions were as described under "Materials and Methods." The *line* indicates values obtained from the "best fit" of the data set to the Deits-Howard treatment of Scheme 1 (6), with a K_{Av2} of >25 μM, and a V_{max} of ~1.1 nmol of ethylene/min. Saturating levels of Av2-R100H were not experimentally obtained; the highest observed value was 0.3 nmol of ethylene/min.

The specific activity of Fe-protein is usually reported as the maximum activity obtained by titration of a fixed amount of the Fe-protein with MoFe-protein as shown in Fig. 5. There are a number of caveats when attempting to assign a definitive specific activity by this method because the Fe-protein is partially inhibited by high MoFe-protein concentrations. The results shown in Fig. 5 indicate that the inhibition by Av1 was significantly enhanced for Av2-R100Y compared with Av2-WT. For example, the maximum activity of Av2-R100Y is decreased by approximately 4-fold for an Av1-WT concentration range that only minimally depresses Av2-WT activity (compare the activity of the two proteins at 1.5 and 7.8 μmol of Av1 in Fig. 5). The extent of the inhibition is further noted by comparing the ratio of maximum activities for Av2-WT and Av2-R100Y. In Fig. 3, Av2-R100Y has ~35% of Av2-WT activity when the Fe-proteins are in excess, while Av2-R100Y

TABLE I

Summary of kinetic parameters

The following parameters were obtained by the rapid equilibrium treatment of Scheme 1 as described by Deits and Howard (6).

Enzyme	V_{max}[a]	K_{Av2}	K_{ATP}	K_i	Exp[b]	[ATP/e⁻][c]
	nmol ethylene/min	*μM*	*μM*	*mM*		
Av2-WT	10.8	0.2	105	55	3.5	2.1
Av2-R100Y	3.4	0.8	185	55	1.95	2.2
Av2-R100H	0.3[d]	>25[e]	800	55	1.95	18

[a] Value obtained for saturating Av2, at 0.256 μM Av1.

[b] The exponent for salt molecularity, denoting cooperativity in inhibition of activity.

[c] The ratio of ATP hydrolyzed per electron transferred to substrate.

[d] The highest velocity observed; saturating levels were not experimentally obtained (see Fig. 4).

[e] Estimate based on 50% of the maximum observed velocity.

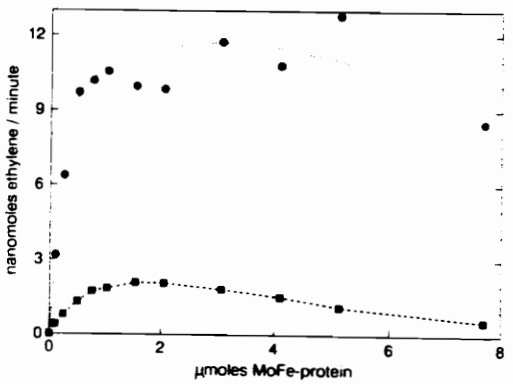

FIG. 5. **Nitrogenase-catalyzed acetylene reduction. 0.281 μmol of Av2-WT (●) and 0.273 μmol of Av2-R100Y (■) were titrated with increasing amounts of Av1-WT.** Low salt assay conditions were used, as described under "Materials and Methods." The *lines* through the two data sets were free-hand approximations. The Deits-Howard treatment (6) is inappropriate for conditions of high Av1/Av2 ratio.

has only ~15% of wild type activity when Av1-WT is in excess. Thus, Av1-WT is a more potent inhibitor of Av2-R100Y than of Av2-WT. In addition, the observed specific activity of Av2-R100Y is likely to be lower than its intrinsic activity and the 35% value should be considered a minimum. A similar systematic comparison between Av2-WT and Av2-R100H was precluded by the very low activity of this altered form when Av1 is in excess (see Table I for the kinetic parameters).

The K_m for ATP in the substrate reduction activity was investigated as a potential source of difference between the altered proteins and Av2-WT. It should be remembered that the K_m in the nitrogenase reaction is not a thermodynamic binding constant but is a kinetically determined constant encompassing all forms of nucleotide bound Av2. Hence, a shift in the apparent K_m has numerous potential interpretations *in lieu* of more detailed analysis. Nevertheless, determination of the K_m is a useful parameter for a preliminary comparison of the altered enzymes. The results are shown in Fig. 6. The activity dependence on ATP is slightly shifted to higher concentrations for Av2-R100Y, yet both Av2-WT and Av2-R100Y are saturated at 2 mM MgATP, the concentration that was used for the titration curves in Figs. 3–5. From the data shown in Fig. 6 and based upon our simplified treatment of Scheme 1 (6), a K_m of 185 μM was calculated for Av2-R100Y which is approximately twice that for Av2-WT (105 μM). In contrast, at 2 mM MgATP, Av2-R100H has only approximately 80% of the activity at 5 mM ATP. Moreover, 5 mM MgATP cannot be considered a saturating value because of the profound effects of ionic strength on the activity (see below). With these reservations, there is at least a 5–8-fold increase in the MgATP concentration required by Av2-R100H for maximal activity.

The electron transfer between components (conversion of Complex I to Complex II in Scheme 1) is tightly coupled to MgATP hydrolysis. For the wild type nitrogenase system, the coupling is most efficient at saturating concentrations of MgATP and Fe-protein and has an optimum value of ~2 ATP/e^- or ~4 ATP/acetylene reduced (35–38). This value can be conveniently ascertained by measuring the amount of substrate reduced during the consumption of a specific, limiting amount of MgATP (including ATP equivalents in the form of creatine phosphate) (31). The ratio of ATP/acetylene reduced (or ATP/e^-) was 4.2 (2.1) for Av2-WT and 4.4 (2.2) for Av2-R100Y. Thus, at saturating concentrations of Av2-R100Y, the 35% activity of the altered protein cannot be a consequence of uncoupling of electron transfer. In striking contrast, Av2-R100H was significantly uncoupled with a ratio for ATP/acetylene reduced of ~36 (~18 ATP/e^-). Under these conditions, Av2-R100H is turning over ATP at ~20% of the rate of Av2-WT yet only a small portion of the electrons go to substrate reduction. Similarly high levels of uncoupling have been reported in heterologous nitrogenase assays (assays using Fe-protein from a different source than the MoFe-protein) (35, 39).

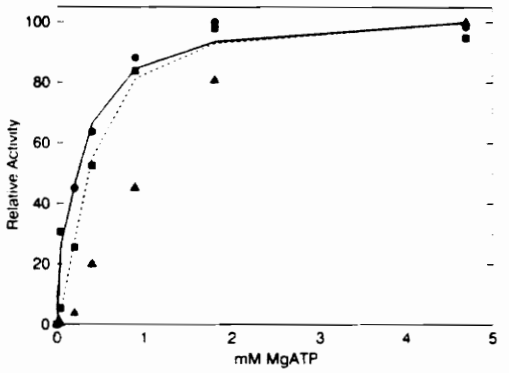

FIG. 6. **Effect of MgATP on the acetylene reduction activity of Av2-WT (●), Av2-R100Y (■), and Av2-R100H (▲).** 0.27 μmol of Av1-WT was incubated with either 1.34 μmol of Av2-WT, 1.34 μmol of Av2-R100H, or 0.72 μmol of Av2-R100Y and increasing amounts of MgATP. The activities in each data set were normalized to the highest value in that set. MgATP concentration was calculated from the concentration of added ATP and $MgCl_2$ using $[Mg^{2+}][ATP]/[MgATP] = 5.01 \times 10^4\ M^{-1}$ (34). *Lines* through the data sets were generated from the Deits-Howard treatment of Scheme 1 (6).

In an attempt to understand the role of Arg-100 in the nitrogenase mechanism, we have evaluated our studies in terms of Scheme 1. Because the same wild type Av1 was used with all three forms of Av2 (Av2-WT, Av2-R100H, and Av2-R100Y), the difference in maximum activity cannot be due to the rate of substrate reduction by Av1 (k_r in Scheme 1). Rather the lower V_{max} and increased apparent K_m (for Av2) must reside in altered steps prior to substrate reduction, most likely in the rate determining redox cycle between components. The net effect of the altered redox cycle is to decrease the steady state concentration of free, twice-reduced Av1, the earliest state which can reduce substrates (5). Thorneley and Lowe (5, 11) have determined the fundamental rate constants of the principal steps in Scheme 1 for wild type *K. pneumoniae* nitrogenase. At saturation by Fe-protein, k_{-3} is limiting while ratios k_1/k_{-1} and k_3/k_{-3} dictate the overall rate away from saturation. The ATP dependent electron transfer rate is >50-fold larger than other potential rate-determining steps, *e.g.* k_{-3} or k_4 at low dithionite concentration. Hence, an order of magnitude change in k_2 still will not make it rate-determining and under our conditions of activity measurements, the lower V_{max} undoubtedly arises from a decreased k_{-3}.

Clearly, both Av2-R100Y and Av2-R100H have altered V_{max} and K_m values (see Figs. 3–5). The changes are most simply interpreted by assuming the principal effect of the amino acid substitution is to influence the stability of Complexes I and II. For Av2-R100Y, whose titration curves, ATP dependence, and ATP coupling resembles Av2-WT, our simplified, rapid equilibrium treatment of Scheme 1 can be applied (6). As shown in Fig. 3, only a ~4-fold increase in the K_{Av2} (the K_m of Av1 for Av2 in the rapid equilibrium model) is needed to fit the titration curve. Although the K_{Av2} for wild type *A. vinelandii* nitrogenase approximates the dissociation constant (~0.2 μM (5, 11)), it is actually a measure of the relative stabilities of all Av1-Av2 complexes and not a thermodynamic constant. If the rate-determining step at saturating Fe-protein is k_{-3} (11), then the increased K_{Av2} and decreased V_{max} represent a decreased affinity in the formation of Complex I and an increased stability of Complex II (or subsequent complexes involving oxidized Av2). Indeed, the pronounced inhibition of Av2-R100Y by excess Av1 is consistent with the increased stability of Complex II (see Fig. 5 and relevant discussion in text).

Although our simplified mathematical treatment does not predict the lag in activity (see Fig. 4), the properties of Av2-R100H can be explained by a qualitative evaluation using Scheme 1. Clearly, the concentration for Av2-R100H needed for half-maximal velocity is >10-fold the value for Av2-WT (the hypothetical line in Fig. 4 is 100 × K_{Av2} of wild type). Equally important is the 30-fold decrease in V_{max} that we interpret to mean a decrease in k_{-3}. Together the changes in V_{max} and K_{Av2} are consistent with an increased dominance of

Complex II which leads to sequestering of Av1 in a nonproductive complex (only *free*, reduced Av1 can reduce substrate). There are two manifestations of the shift to a tight Complex II. First, Av2(2ATP)^r competes with Av2(2ADP)^o for singly reduced Av1 (Av1' in Scheme 1), and only at higher concentrations of total Av2-R100H will the second reduction proceed. Thus, the sigmoidal shape of the curve is the result of the relative stabilities of Complex I and II. Second, because Complex II is more stable and has a longer lifetime, the transfer of the electron back to Av2 without productive substrate reduction can occur. Hence, the electron transfer becomes uncoupled from ATP hydrolysis.

Perhaps the most intriguing aspect of these altered Fe-proteins is their response to NaCl. As shown in Figs. 7 and 8, both Av2-R100Y and Av2-R100H are acutely sensitive to increase in salt concentration. For example, at 50 mM NaCl, Av2-R100H is only 20% active while Av2-WT is fully active. Besides the change in salt concentration needed to effect inhibition, the shape of the salt inhibition appears much less sigmoidal compared with Av2-WT. The dramatically increased sensitivity to ionic strength seems to be counter-intuitive; replacing a charged arginyl residue by a neutral residue seemingly would decrease the sensitivity to salts. The paradox can be explained if Complex I involves several ionic interactions, including Arg-100. Replacing Arg-100 removes a dominant interaction resulting in lower overall affinity (observed decrease in K_{Av2}). However, the remaining, weaker ionic interactions should be more sensitive to ionic strength as is observed. Thus, the weaker the affinity between protein components, the larger the ionic strength effect. This argument is supported by the results for Av2-R100H which has the weakest apparent affinity and is the most inhibited by salt.

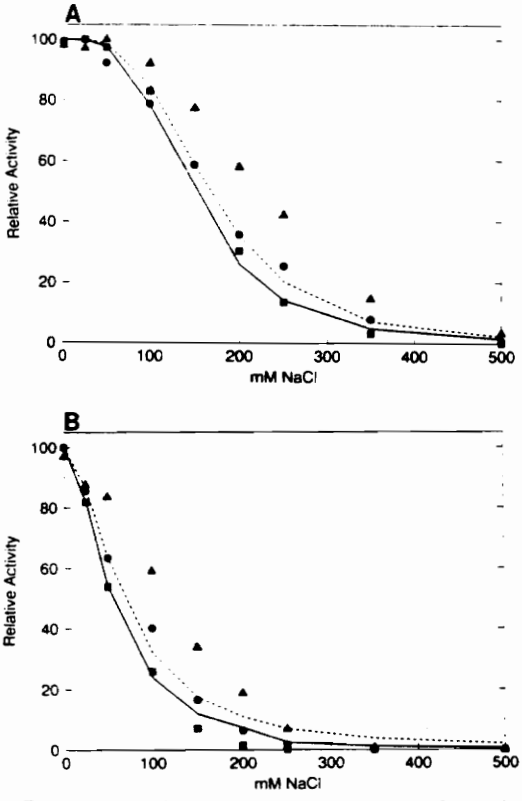

FIG. 7. **The inhibition of nitrogenase-catalyzed acetylene reduction by NaCl.** *A*, assay of 0.216 μmol of Av1-WT with 0.48 μmol (■), 1.32 μmol (●), and 4.33 μmol (▲) of Av2-WT, at increasing [NaCl]. *B*, assay of 0.216 μmol of Av1-WT with 0.44 μmol (■), 1.27 μmol (●), and 4.4 μmol (▲) of Av2-R100Y, at increasing [NaCl]. The activities in each data set were normalized to the highest value in that set. *Lines* through the data sets were generated from the Deits-Howard treatment of Scheme 1 (6).

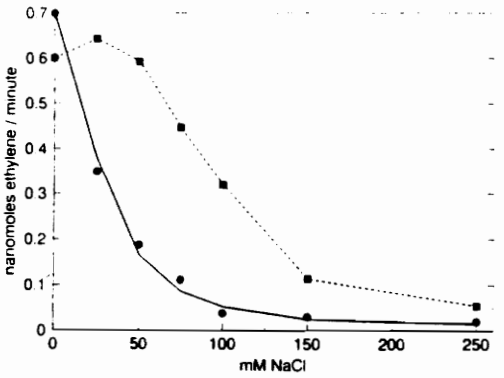

FIG. 8. **The inhibition of nitrogenase-catalyzed acetylene reduction by NaCl.** 0.256 μmol of Av1-WT was assayed with either 0.024 μmol of Av2-WT (■) or 22.17 μmol of Av2-R100H (●) at increasing concentrations of NaCl. The *line* through the Av2-R100H data set was generated using the Deits-Howard equations (6). The *line* through the Av2-WT data set was a free-hand approximation, because the Deits-Howard treatment is not applicable at high ratios of Av1/Av2. This ratio for wild type nitrogenase was required here so that comparable activity for both Av2-WT and Av2-R100H could be obtained with the same concentration of Av1-WT.

Recently, we adapted the general scheme of the nitrogenase cycle to account for the salt inhibition of wild type nitrogenase (see Scheme 1) (6). The principal addition to the model is that salt interacts with the Fe-protein as a dead-end inhibitor preventing the formation of Complex I. The sigmoidal shape of inhibition reflects the multiple sites for the salt interaction. The most conclusive test of this hypothesis was to demonstrate a competition between either component and salt. A typical result for wild type nitrogenase is shown in Fig. 7*A*, where the apparent K_i increases as the ratio of Av2/Av1 increases. That is, Av1 and NaCl compete for Av2. This result places the salt inhibition primarily on complex formation not electron transfer or substrate reduction. However, it is still not possible to localize how salts prevent complex formation.

The salt data for the altered proteins were also fit to the model using appropriate K_{Av2} and K_{ATP} obtained from the titration curves. Keeping the salt K_i for Av2-WT (~55 mM), the only significant parameter changed was the exponent in the salt cooperativity which had to be adjusted from ~3.5 for Av2-WT to ~1.9 for both Av2-R100Y and Av2-R100H. This parameter, which is equivalent to the Hill coefficient, should not be considered the number of physical binding sites but the number of effective sites. Nevertheless, it is tempting to correlate the decrease of ~1.6 in the exponent to the removal of two charges from the Av2 surface (1 arginine/subunit). As indicated in the more qualitative discussion above, the increased sensitivity to salts was primarily the reflection of the K_{Av2} of the altered proteins. The validity of this conclusion was tested by varying the Fe-protein concentration. As for Av2-WT, the salt inhibition of Av2-R100Y could be partially

overcome by increasing the ratio of the components, *e.g.* the salt concentration for 50% inhibition increased from ~60 to ~130 mM as the component ratio was increased 10-fold. Although we can only crudely approximate a K_{Av2} for Av2-R100H, the model was well fit by the salt data. For larger K_{Av2}, the salt so effectively competes with Av1 that uncertainty in the K_{Av2} is not important and there is only minimal effect of the component ratio on the apparent K_i. These results strongly support the hypothesis that the Arg-100 substitutions are mainly altering the stability of the Av1-Av2 complexes.

The major conclusion from this study is that arginine is *not* an obligate residue for position 100. Substitutions at this site appear to decrease the affinity for the MoFe-protein in Complex I formation and increase the stability after electron transfer. This is manifest in the decreased V_{max}, increased K_{Av2}, and increased potency of salts as inhibitors. Thus, Arg-100 interactions appear to dominate the complex stability, yet other ionic residues, perhaps the "glutamic acid patch" at residues 110–116, contribute in a secondary role. In contrast to previous suggestions (24), clearly Fe-protein with substitutions for Arg-100 are able to form active complexes. Furthermore, because residues as diverse as phenylalanine, tyrosine, or leucine adequately substitute for arginine, it is unlikely that this residue participates directly in the electron transfer pathway between redox centers.

Enigmatic questions remain: what is the special role of arginine that makes it the preferred residue: and why is tyrosine so much more acceptable than histidine (or the isoionic lysine)? At the present state of refinement, the x-ray diffraction structure provides little insight except to show the location of residue 100 near the cluster and at the amino terminus of an α-helix that extends to the Glu-112 (19). Unfortunately, the electron density does not show the complete Arg-100 side chain; however, model building indicates that the η nitrogen of Arg-100 or the phenolic oxygen of Tyr-100 could extend to the cluster and that shorter residues cannot reach.[5] Although the two amino acid substitutions do not disrupt the immediate environment of the cluster ligands as monitored by proton NMR,[6] it is possible that the helix may have been partially disrupted. For example, Dao-pin *et al.* (40) found that histidyl substitutions could destabilize α helices even when the histidine is favorably positioned to form a salt bridge. We believe the explanation for arginine as the optimum residue may lie in the structures of Complex I and Complex II. We postulate that the role of Arg-100 is to stabilize Complex I and to destabilize Complex II; this could be accomplished by different interactions in the two complexes and would suppose a conformational change in going from one complex to the other.

[5] D. C. Rees, personal communication of atomic coordinates.

[6] J. B. Howard, D. Wolle, and G. LaMar, unpublished results.

REFERENCES

1. Hausinger, R. P., and Howard J. B. (1983) *J. Biol. Chem.* **258**, 13486–13492
2. Orme-Johnson, W. (1985) *Annu. Rev. Biophys. Biophys. Chem.* **14**, 419–459
3. Hoover, T. R., Imperial, J., Ludden, P. W., and Shah, V. K. (1988) *Biofactors* **1**, 199–205
4. Hageman, R. V., and Burris, R. H. (1978) *Proc. Natl. Acad. Sci. U. S. A.* **75**, 2699–2702
5. Lowe, D., and Thorneley, R. (1984) in *Molybdenum Enzymes* (Spiro, T. G., ed) pp. 222–284, John Wiley & Sons, New York
6. Deits, T. L., and Howard, J. B. (1990) *J. Biol. Chem.* **265**, 3859–3867
7. Bulen, W. A. and LeComte, J. R. (1966) *Proc. Natl. Acad. Sci. U. S. A.* **57**, 979–986
8. Shah, V. K., Davis, L. C., and Brill, W. J. (1972) *Biochim. Biophys. Acta* **256**, 498–511
9. Burns, A., Watt, G. D., and Wang, Z. C. (1985) *Biochemistry* **24**, 3932–3936
10. Guth, J. H., and Burris, R. H. (1983) *Biochem. J.* **213**, 741–749
11. Thorneley, R. N. F., and Lowe, D. J. (1983) *Biochem. J.* **215**, 393–403
12. Eady, R. R. (1980) *Methods Enzymol.* **69**, 753–778
13. Watt, G. D., Burns, A., Lough, S., and Tennent, D. L. (1980) *Biochemistry* **19**, 4926–4932
14. Saari, L. L., Triplett, E. W., and Ludden, P. W. (1984) *J. Biol. Chem.* **259**, 15502–15508
15. Lowery, R. G., and Ludden, P. W. (1988) *J. Biol. Chem.* **263**, 16714–16719
16. Lindahl, P., Goerlich, N. J., Munck, E., and Orme-Johnson, W. H. (1987) *J. Biol. Chem.* **262**, 14945–14953
17. Willing, A. H., Georgiadis, M. M., Rees, D. C., and Howard, J. B. (1989) *J. Biol. Chem.* **264**, 8499–8503
18. Willing, A. H., and Howard, J. B. (1990) *J. Biol. Chem.* **265**, 6596–6599
19. Georgiadis, M. M., Chakrabarti, P., and Rees, D. C. (1990) in *Nitrogen Fixation: Achievements and Objectives* (Gresshoff, P. M., Roth, E., Stacy, G., and Newton, W. E., eds) pp. 111–116, Chapman & Hall, New York
20. Pope, M. R., Murrell, S. A., and Ludden, P. W. (1985) *Proc. Natl. Acad Sci. U. S. A.* **82**, 3173–3177
21. Gotto, J. W., and Yoch, D. C. (1985) *Arch. Microbiol.* **141**, 40–43
22. Lowery, R. G., Saari, L. L., and Ludden, P. W. (1986) *J. Bacteriol.* **186**, 513–518
23. Murrell, S. A., Lowery, R. G., and Ludden, P. W. (1988) *Biochem. J.* **251**, 609–612
24. Lowery, R. G., Chang, C. L., Davis, L. C., McKenna, M.-C., Stevens, P. J., and Ludden, P. W. (1989) *Biochemistry* **28**, 1206–1212
25. Zoller, M. J., and Smith, M. (1983) *Methods Enzymol.* **100**, 468–500
26. Brigle, K. B., Setterquist, R. A., Dean, D. R., Cantwell, J. S., Weiss, M. C., and Newton, W. E. (1987) *Proc. Natl. Acad. Sci. U. S. A.* **84**, 7066–7069
27. Howard, J. B., Davis, R., Moldenhauer, B., Cash, V. L., and Dean, D. R (1989) *J. Biol. Chem.* **264**, 11270–11274
28. Jacobson, M., Brigle, K. E., Bennett, L. T., Setterquist, R. A., Wilson, M. S., Cash, V. L., Beynon, J., Newton, W. E., and Dean, D. R. (1989) *J. Bacteriol.* **171**, 1017–1027
29. Burgess, B. K., Jacobs, D. B., and Stiefel, E. I. (1980) *Biochim. Biophys. Acta* **614**, 196–209
30. Anderson, G. L., and Howard, J. B. (1984) *Biochemistry* **23**, 2118–2122
31. Deits, T. L., and Howard, J. B. (1989) *J. Biol. Chem.* **264**, 6619–6628
32. Ljones, T., and Burris, R. H. (1978) *Biochemistry* **17**, 1866–1872
33. Walker, G. A., and Mortenson, L. E. (1974) *Biochemistry* **13**, 2382–2388
34. Pecoraro, V. L., Hermes, J. D., and Cleland, W. W. (1984) *Biochemistry* **23**, 5262–5271
35. Emerich, D. W., and Burris, R. H. (1978) *J. Bacteriol.* **134**, 936–947
36. Li, J., Burgess, B. K., and Corbin, J. L. (1982) *Biochemistry* **21**, 4393–4402
37. Rubinson, J. F., Corbin, J. L., and Burgess, B. K. (1983) *Biochemistry* **22**, 6260–6269
38. Thorneley, R. N. F., and Lowe, D. J. (1984) *Biochem. J.* **224**, 903–909
39. Smith, B. E., Thorneley, R. N. F., Eady, R. R., and Mortenson, L. E. (1976) *Biochem. J.* **157**, 439–447
40. Dao-pin, S., Sauer, U., Nicholson, H., and Matthews, B. W. (1991) *Biochemistry* **30**, 7142–7153

VITA

ChulHwan Kim was born on Aug 20, 1962, in Seoul, Korea. He graduated from Yonsei University in Seoul with a Bachelor of Engineering in Food Engineering in 1987. He received his Master of Science degree in Biochemistry from Virginia Polytechnic Institute and State University in 1990. Subsequently he entered a doctoral program in the Department of Anaerobic Microbiology which was later merged together with Biochemistry into the Department of Biochemistry and Anaerobic Microbiology. He completed the requirements for the Ph.D. in July of 1994.